STATE OF THE CLIMATE IN 2019

REGIONAL CLIMATES

P. Bissolli, C. Ganter, T. Li, A. Mekonnen, and A. Sánchez-Lugo, Eds.

Special Online Supplement to the *Bulletin of the American Meteorological Society,* Vol.101, No. 8, August, 2020

https://doi.org/10.1175/2020BAMSStateoftheClimate_Chapter7.1

Corresponding authors:
North America: Ahira Sánchez-Lugo / Ahira.Sanchez-Lugo@noaa.gov.
Central America and the Caribbean: Ahira Sánchez-Lugo / Ahira.Sanchez-Lugo@noaa.gov
South America: Ahira Sánchez-Lugo / Ahira.Sanchez-Lugo@noaa.gov
Africa: Ademe Mekonnen / amekonne@ncat.edu
Europe: Peter Bissolli / Peter.Bissolli@dwd.de
Asia: Tim Li / timli@hawaii.edu
Oceania: Catherine Ganter / Catherine.Ganter@bom.gov.au

STATE OF THE CLIMATE IN 2019

Regional Climates

Editors

Jessica Blunden
Derek S. Arndt

Chapter Editors

Peter Bissolli
Howard J. Diamond
Matthew L. Druckenmiller
Robert J. H. Dunn
Catherine Ganter
Nadine Gobron
Rick Lumpkin
Jacqueline A. Richter-Menge
Tim Li
Ademe Mekonnen
Ahira Sánchez-Lugo
Ted A. Scambos
Carl J. Schreck III
Sharon Stammerjohn
Diane M. Stanitski
Kate M. Willett

Technical Editor

Andrea Andersen

BAMS Special Editor for Climate

Richard Rosen

American Meteorological Society

Cover credit:
Front: © Lynnebeclu/Royalty-free/iStock / Getty Images Plus
Horizontal landscape of burnt, scorched and blackened coastal forest trees and ash-scattered sandy ground after bushfires ravaged the coastal landscape near Yamba, New South Wales Australia in 2019.

Regional Climates is one chapter from the *State of the Climate in 2019* annual report. Compiled by NOAA's National Centers for Environmental Information, *State of the Climate in 2019* is based on contributions from scientists from around the world. It provides a detailed update on global climate indicators, notable weather events, and other data collected by environmental monitoring stations and instruments located on land, water, ice, and in space. The full report is available from https://doi.org/10.1175/2020BAMSStateoftheClimate.1.

How to cite this document:

Citing the complete report:
Blunden, J. and D. S. Arndt, Eds., 2020: State of the Climate in 2019. *Bull. Amer. Meteor. Soc.*, **101** (8), Si–S429, https://doi.org/10.1175/2020BAMSStateoftheClimate.1.

Citing this chapter:
Bissolli, P., C. Ganter, T. Li, A. Mekonnen, and A. Sánchez-Lugo, Eds., 2020: Regional Climates [in "State of the Climate in 2019"]. *Bull. Amer. Meteor.* Soc., **101** (8), S321–S420, https://doi.org/10.1175/2020BAMSStateoftheClimate_Chapter7.1.

Citing a section (example):
Amador, J. A., H. G. Hidalgo, E. J. Alfaro, B. Calderón, and N. Mora, 2020: Central America [in "State of the Climate in 2019"]. *Bull. Amer. Meteor. Soc.*, **101** (8), S338–S339, https://doi.org/10.1175/2020BAMSStateoftheClimate_Chapter7.1.

Editor and Author Affiliations (alphabetical by name)

Abida, Abdallah, Agence Nationale de l'Aviation Civile et de la Météorologie de l'Union des Comores, Moroni, Comoros
Aldeco, Laura S., Servicio Meteorológico Nacional, Buenos Aires, Argentina
Alfaro, Eric J., Center for Geophysical Research and School of Physics, University of Costa Rica, San José, Costa Rica
Alves, Lincoln M., Centro de Ciencia do Sistema Terrestre/Instituto Nacional de Pesquisas Espaciais, São Paulo, Brazil
Amador, Jorge A., Center for Geophysical Research and School of Physics, University of Costa Rica, San José, Costa Rica
Andrade, B., Seychelles Meteorological Authority, Mahe, Seychelles
Baez, Julian, Universidad Católica Nuestra Senora de la Asunción, Asunción, Paraguay
Bardin, M. Yu., Yu. A. Izrael Institute of Global Climate and Ecology, and Institute of Geography, Russian Academy of Sciences, Moscow, Russia
Bekele, Endalkachew, NOAA/NWS Climate Prediction Center, College Park, Maryland
Bissolli, Peter, Deutscher Wetterdienst, WMO RA VI Regional Climate Centre Network, Offenbach, Germany
Broedel, Elisangela, Centro Nacional de Monitoramento e Alertas de Desastres Naturais CEMADEN, São Paulo, Brazil
Bukunt, Brandon, NOAA/NWS Weather Forecast Office, Guam
Calderón, Blanca, Center for Geophysical Research, University of Costa Rica, San José, Costa Rica
Campbell, Jayaka D., Department of Physics, The University of the West Indies, Jamaica
Campos Diaz, Diego A., Dirección Meteorológica de Chile, Santiago de Chile, Chile
Carvajal, Gilma, Instituto Nacional de Meteorología e Hidrología de Ecuador (INAMHI), Quito, Ecuador
Chandler, Elise, Bureau of Meteorology, Melbourne, Victoria, Australia
Cheng, Vincent. Y. S., Environment and Climate Change Canada, Toronto, Ontario, Canada
Choi, Chulwoon, Climate Prediction Division, Korea Meteorological Administration, South Korea
Clarke, Leonardo A., Department of Physics, The University of the West Indies, Jamaica
Correa, Kris, Servicio Nacional de Meteorología e Hidrología del Perú, Lima, Perú
Costa, Felipe, Centro Internacional para la Investigación del Fenómeno El Niño (CIIFEN), Guayaquil, Ecuador
Cunha, A. P., Centro Nacional de Monitoramento e Alertas de Desastres Naturais CEMADEN, São Paulo, Brazil
Demircan, Mesut, Turkish State Meteorological Service, Ankara, Turkey
Dhurmea, R., Mauritius Meteorological Service, Vacoas, Mauritius
Díaz, Eliecer A., Instituto de Hidrología de Meteorología y Estudios Ambientales de Colombia (IDEAM), Bogotá, Colombia
ElKharrim, M., Direction de la Météorologie Nationale Maroc, Rabat, Morocco
Enyew, Bantwale D., Department of Physics, North Carolina A & T State University, Greensboro, North Carolina
Espinoza, Jhan C., Instituto Geofisico del Perú, Lima, Perú, and Université Grenoble Alpes, Grenoble, France
Fazl-Kazem, Amin, National Center for Drought Monitoring and Crisis Management, Islamic Republic of Iranian Meteorological Organization, Tehran, Iran
Fedaeff, Nava, National Institute of Water and Atmospheric Research, Ltd. (NIWA), Auckland, New Zealand
Feng, Z., Atmospheric Sciences and Global Change Division, Pacific Northwest National Laboratory, Richland, Washington
Fenimore, Chris, NOAA/NESDIS National Centers for Environmental Information, Asheville, North Carolina
Francis, S. D., National Weather Forecasting and Climate Research Centre, Nigerian Meteorological Agency, Abuja, Nigeria
Ganter, Catherine, Bureau of Meteorology, Melbourne, Victoria, Australia
Gleason, Karin, NOAA/NESDIS National Centers for Environmental Information, Asheville, North Carolina
Guard, Charles "Chip" P., Tropical Weather Sciences, Sinajana, Guam
Gustari, Indra, Climate Variability Analysis Division, Center for Climate Change Information, BMKG, Indonesia
Hagos, S., Atmospheric Sciences and Global Change Division, Pacific Northwest National Laboratory, Richland, Washington
Heim, Jr., Richard R., NOAA/NESDIS National Centers for Environmental Information, Asheville, North Carolina
Hernández, Rafael, Instituto Nacional de Meteorología e Hidrología de Venezuela (INAMEH), Caracas, Venezuela
Hidalgo, Hugo G., Center for Geophysical Research and School of Physics, University of Costa Rica, San José, Costa Rica
Ijampy, J. A., Nigerian Meteorological Agency, Abuja, Nigeria
Joseph, Annie C., Dominica Meteorological Service, Canefield Airport, Canefield, Dominica
Jumaux, Guillaume, Météo France, Direction Interrégionale pour l'Océan Indien, Réunion
Kabidi, Khadija, Direction de la Météorologie Nationale Maroc, Rabat, Morocco
Kaiser, Johannes W., Deutscher Wetterdienst, Satellite-Based Climate Monitoring Division, Offenbach, Germany
Kamsu-Tamo, Pierre-Honore, NOAA/NWS Climate Prediction Center, College Park, Maryland
Kennedy, John, Met Office Hadley Centre, Exeter, United Kingdom
Khan, Valentina, Hydrometcenter of Russia, WMO North EurAsia Climate Center, Moscow, Russia
Khiem, Mai Van, Viet Nam National Center of Hydro-Meteorology Forecasting, Viet Nam Meteorology Hydrology Administration, Ha Noi, Viet Nam
Kokosadze, Khatuna, National Environmental Agency, Tbilisi, Georgia
Korshunova, Natalia N., All-Russian Research Institute of Hydrometeorological Information - World Data Center, Obninsk, Russia
Kruger Andries C., South African Weather Service, Pretoria, South Africa
Kutaladze, Nato, National Environmental Agency, Tbilisi, Georgia
Labbé, L., Météo France, Direction Interrégionale pour l'Océan Indien, Réunion
Lakatos, Mónika, Climatology Unit, Hungarian Meteorological Service, Budapest, Hungary
Lam, Hoang Phuc, Viet Nam National Center of Hydro-Meteorology Forecasting, Viet Nam Meteorology Hydrology Administration, Ha Noi, Viet Nam
Lander, Mark A., University of Guam, Mangilao, Guam
Lavado-Casimiro, Waldo, Servicio Nacional de Meteorología e Hidrología del Perú, Lima, Perú
Lee, T. C., Hong Kong Observatory, Hong Kong, China
Leung, Kinson H. Y., Environment and Climate Change Canada, Toronto, Ontario, Canada
Li, Tim, Department of Atmospheric Sciences, University of Hawai'i, Honolulu, Hawai'i, USA
Magee, Andrew D., Centre for Water, Climate and Land, School of Environmental and Life Sciences, University of Newcastle, Callaghan, NSW, Australia
Mamen, Jostein, Climate Division, Norwegian Meteorological Institute, Oslo, Norway
Marengo, José A., Centro Nacional de Monitoramento e Alertas aos Desastres Naturais, Cachoeira Paulista, São Paulo, Brazil
Marín, Dora, Servicio Nacional de Meteorología e Hidrología (SENAMHI), Lima, Perú

McBride, Charlotte, South African Weather Service, Pretoria, South Africa
Megrelidze, Lia, National Environmental Agency, Tbilisi, Georgia
Mekonnen, Ademe, Department of Physics, North Carolina A & T State University, Greensboro, North Carolina
Misevicius, Noelia, Instituto Uruguayo de Meteorología, Montevideo, Uruguay
Mochizuki, Y., Tokyo Climate Center, Japan Meteorological Agency, Japan
Moise, Aurel, Centre for Climate Research Singapore, Meteorological Service, Singapore
Molina-Carpio, Jorge, Universidad Mayor de San Andrés, La Paz, Bolivia
Mora, Natali, Center for Geophysical Research and School of Physics, University of Costa Rica, San José, Costa Rica
Mostafa, Awatif E., Department of Seasonal Forecast and Climate Research, Cairo Numerical Weather Prediction, Egyptian Meteorological Authority, Cairo, Egypt
Nieto, Juan José, Centro Internacional para la Investigación del Fenómeno El Niño (CIIFEN), Guayaquil, Ecuador
Oyunjargal, Lamjav, National Agency for Meteorology, Hydrology and Environmental Monitoring, Ulaanbaatar, Mongolia
Pascual Ramírez, Reynaldo, National Meteorological Service of Mexico, Mexico
Pastor Saavedra, Maria Asuncion, Agencia Estatal de Meteorología, Madrid, Spain
Pfeifroth, Uwe, Deutscher Wetterdienst, Satellite-Based Climate Monitoring Division, Offenbach, Germany
Phillips, David, Environment and Climate Change Canada, Toronto, Ontario, Canada
Rajeevan, Madhavan, Earth System Science Organization, Ministry of Earth Sciences, New Delhi, India
Ramos, Andrea M., Instituto Nacional de Meteorologia, Brasilia, Brazil
Revadekar, Jayashree V., Indian Institute of Tropical Meteorology, Pune, India
Robjhon, Miliaritiana, NOAA/NWS Climate Prediction Center, College Park, Maryland
Rodriguez Camino, **Ernesto**, Agencia Estatal de Meteorología, Madrid, Spain
Rodriguez Guisado, **Esteban**, Agencia Estatal de Meteorología, Madrid, Spain
Ronchail, Josyane, Université Paris Diderot/Laboratoire LOCEAN-IPSL, Paris, France
Rösner, Benjamin, Laboratory for Climatology and Remote Sensing, Faculty of Geography, University of Marburg, Marburg, Germany
Salinas, Roberto, Dirección de Meteorología e Hidrología/Dirección Nacional de Aeronáutica Civil, Asunción, Paraguay
Sánchez-Lugo, Ahira, NOAA/NESDIS National Centers for Environmental Information, Asheville, North Carolina
Sayouri, Amal, Direction de la Météorologie Nationale Maroc, Rabat, Morocco
Schreck III, Carl J., North Carolina State University, Cooperative Institute for Climate and Satellites – North Carolina (CICS-NC), Asheville, North Carolina
Sensoy, Serhat, Turkish State Meteorological Service, Ankara, Turkey
Shimpo, A., Tokyo Climate Center, Japan Meteorological Agency, Tokyo, Japan
Sima, Fatou, Division of Meteorology, Department of Water Resources, Banjul, The Gambia
Smith, Adam, NOAA/NESDIS National Centers for Environmental Information, Asheville, North Carolina
Spence, Jacqueline, Meteorological Service, Kingston, Jamaica
Spillane, Sandra, Met Éireann, Irish Meteorological Service, Dublin, Ireland
Spitzer, Arne, Deutscher Wetterdienst, Satellite-Based Climate Monitoring Division, Offenbach, Germany
Srivastava, A. K., India Meteorological Department, Pune, India
Stella, José L., Servicio Meteorológico Nacional, Buenos Aires, Argentina
Stephenson, Kimberly A., Department of Life Sciences, The University of the West Indies, Jamaica
Stephenson, Tannecia S., Department of Physics, The University of the West Indies, Jamaica
Taylor, Michael A., Department of Physics, The University of the West Indies, Jamaica
Thiaw, Wassila, NOAA/NWS Climate Prediction Center, College Park, Maryland
Tobin, Skie, Bureau of Meteorology, Melbourne, Victoria, Australia
Todey, Dennis, Agricultural Research Service, USDA Midwest Climate Hub, Ames, Iowa
Trachte, Katja, Brandenburg University of Technology (BTU), Cottbus, Germany
Trotman, Adrian R., Caribbean Institute for Meteorology and Hydrology, Bridgetown, Barbados
van der Schrier, Gerard, Royal Netherlands Meteorological Institute (KNMI), De Bilt, Netherlands
Van Meerbeeck, Cedric J., Caribbean Institute for Meteorology and Hydrology, Bridgetown, Barbados
Vazifeh, Ahad, National Center for Drought Monitoring and Crisis Management, Islamic Republic of Iranian Meteorological Organization, Tehran, Iran
Vicencio Veloso, José, Dirección Meteorológica de Chile, Santiago de Chile, Chile
Wang, Wei, Minhang Meteorological Bureau, Shanghai, China
Xin, Fei, Shanghai Climate Center, Shanghai, China
Zhang, Peiqun, Beijing Climate Center, Beijing, China
Zhu, Zhiwei, Nanjing University of Information Science and Technology, China
Zucule, Jonas, Mozambique National Institute of Meteorology, Maputo, Mozambique

Editorial and Production Team

Andersen, Andrea, Technical Editor, Innovative Consulting Management Services, LLC, NOAA/NESDIS National Centers for Environmental Information, Asheville, North Carolina
Griffin, Jessicca, Graphics Support, Cooperative Institute for Satellite Earth System Studies, North Carolina State University, Asheville, North Carolina
Hammer, Gregory, Content Team Lead, Communications and Outreach, NOAA/NESDIS National Centers for Environmental Information, Asheville, North Carolina
Love-Brotak, S. Elizabeth, Lead Graphics Production, NOAA/NESDIS National Centers for Environmental Information, Asheville, North Carolina
Misch, Deborah J., Graphics Support, Innovative Consulting Management Services, LLC, NOAA/NESDIS National Centers for Environmental Information, Asheville, North Carolina
Riddle, Deborah B., Graphics Support, NOAA/NESDIS National Centers for Environmental Information, Asheville, North Carolina
Veasey, Sara W., Visual Communications Team Lead, Communications and Outreach, NOAA/NESDIS National Centers for Environmental Information, Asheville, North Carolina

7. Table of Contents

***Please refer to Chapter 8 (Relevant datasets and sources) for a list of all climate variables and datasets used in this chapter for analyses, along with their websites for more information and access to the data.**

7. REGIONAL CLIMATES

P. Bissolli, C. Ganter, T. Li, A. Mekonnen, and A. Sánchez-Lugo, Eds.

a. Overview

This chapter provides summaries of the 2019 temperature and precipitation conditions across seven broad regions: North America, Central America and the Caribbean, South America, Africa, Europe, Asia, and Oceania. In most cases, summaries of notable weather events are also included. Local scientists provided the annual summary for their respective regions and, unless otherwise noted, the source of the data used is typically the agency affiliated with the authors. The primary base period used for these analyses is 1981–2010. However, please note that on occasion different nations, even within the same section, may use unique periods to define their normals. Section introductions typically define the prevailing practices for that section, and exceptions will be noted within the text. In a similar way, many contributing authors use languages other than English as their primary professional language. To minimize additional loss of fidelity through re-interpretation after translation, editors have been conservative and careful to preserve the voice of the author. In some cases, this may result in abrupt transitions in style from section to section.

b. North America—A. Sánchez-Lugo, Ed.

This section is divided into three subsections: Canada, the United States, and Mexico. Unless otherwise noted, the reference period is 1981–2010. The meteorological seasons follow Northern Hemisphere (NH) midlatitude conventions, such as December–February for winter, March–May for spring.

Above-average temperatures were present across much of northern Canada, the southeastern and mid-Atlantic United States, and Mexico during 2019, while much of central North America had near- to below-average temperatures. Canada observed its 15th warmest year, the United States its 34th warmest, and Mexico its second warmest for their respective historical records. The United States observed its second-wettest year on record, while Mexico experienced its 19th driest. Notable events across the region include spring floods across parts of Canada and the contiguous United States, Hurricane Dorian impacts on parts of the United States and Canada, and the lack of tropical storms affecting southern Mexico.

1) Canada—K. H. Y. Leung, V. Y. S. Cheng, and D. Phillips

In 2019, mean annual temperatures were above the 1981–2010 average across most of northern Canada (north of 60°N) and below average over most of southern Canada (south of 60°N). The mean temperatures were much higher than average in northwestern Canada during winter and spring, and in northeastern Canada (closer to 80°N) during summer and autumn. The Canadian Prairies consistently experienced below-average temperatures during all four seasons; portions of northwestern Canada experienced below-average temperatures during summer as well.

(I) TEMPERATURE

The 2019 annual average temperature for Canada was 0.2°C above the 1981–2010 national average and the 15th warmest year since nationwide records began in 1948 (Fig. 7.1). Four of the 10 warmest years have occurred during the last decade, with 2010 experiencing all-time record warmth (+2.2°C). The national annual average temperature has increased 1.7°C over the past 72 years (updated from Vincent et al. 2015). Spatially, annual temperature departures above +1.5°C

were recorded in the north and northwest, whereas annual departures below –1°C were experienced across Canada's southern border from British Columbia's interior eastward through to New Brunswick (Fig. 7.2). Three provinces/territories experienced an average annual temperature that ranked among their 10 highest since 1948: Yukon (third highest), Nunavut (fifth highest), and Northwest Territories (seventh highest).

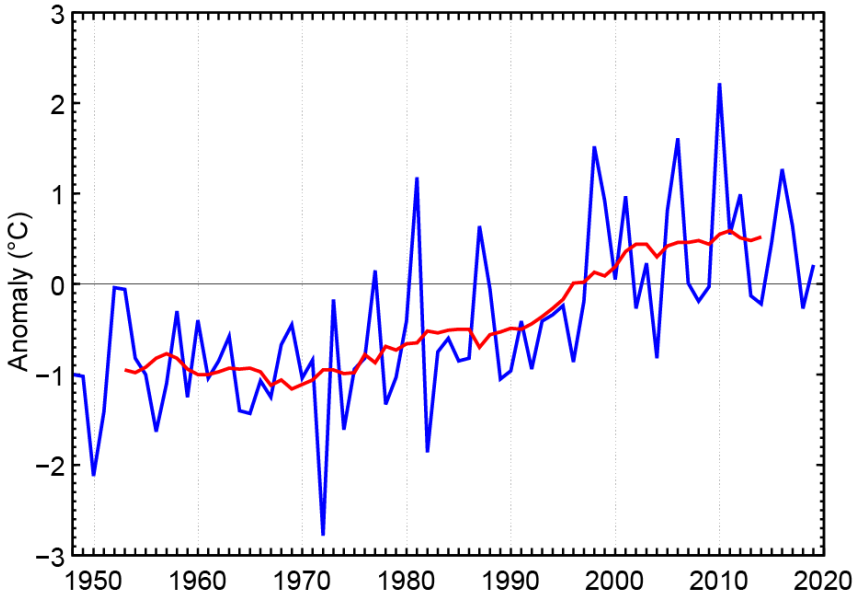

Fig. 7.1. Annual average temperature anomalies (°C; 1981–2010 base period) in Canada for 1948–2019. Red line is the 12-year running mean. (Source: Environment and Climate Change Canada.)

Winter 2018/19 was 0.1°C below average and the 44th coolest on record since nationwide records began in 1948. The national winter average temperature has increased by 3.3°C over the past 72 years. Winter anomalies more than +3.5°C above average were recorded in northwestern Canada, with the Northwest Territories having its 10th warmest winter on record. The remainder of the provinces experienced winter temperature anomalies more than –0.5°C below average.

During spring, below-average temperatures were recorded from southeastern British Columbia eastward to the Atlantic provinces. Above-average temperatures were observed over northern Canada, with northwestern parts of Canada notably above average by more than 3.5°C. The national average temperature for spring 2019 was 0.3°C above the 1981–2010 average and the 13th highest in the 72-year record. The national average spring temperature has increased by 1.7°C over the past 72 years. Four provinces/territories experienced an average spring temperature that ranked among the 10 highest since 1948: Yukon (second highest), Northwest Territories (third highest), Nunavut (fourth highest), and British Columbia (10th highest).

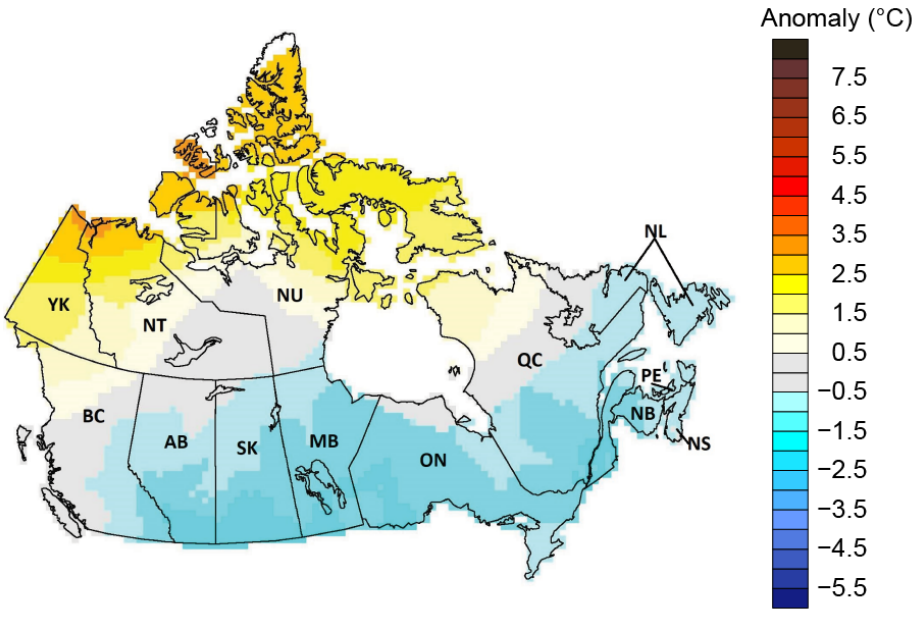

Fig. 7.2. Annual average temperature anomalies (°C; 1981–2010 base period) in Canada for 2019. YK=Yukon; NT=Northwest Territories; NU=Nunavut; QC=Quebec; NL=Newfoundland and Labrador; PE=Prince Edward Island; NS=Nova Scotia; NB=New Brunswick; ON=Ontario; MB=Manitoba; SK=Saskatchewan; AB=Alberta; and BC=British Columbia. (Source: Environment and Climate Change Canada.)

The national average temperature for summer 2019 was 0.1°C above average and the 25th highest since 1948. Parts of Yukon and northeastern Canada experienced summer anomalies above +1°C, with Nunavut and Quebec having their sixth- and 10th-warmest summers on

record, respectively. In contrast, below-average summer temperatures were experienced in the Northwest Territories, Alberta, Saskatchewan, and Labrador, with the Northwest Territories and Alberta having their 8th- and 10th-coolest summer on record, respectively. The national average summer temperature has increased by 1.4°C over the past 72 years.

The national average temperature for autumn 2019 was 0.9°C above average and the 13th highest since 1948. Above-average temperatures were experienced across northern Canada, with three provinces/territories having autumn average temperatures among their 10 highest: Northwest Territories (third highest), Nunavut (third highest), and Yukon (fifth highest). Conversely, autumn anomalies of –1°C or lower were experienced along the southern border from southeastern British Columbia to Atlantic Canada. The national autumn temperature has increased by 1.7°C over the past 72 years.

(II) PRECIPITATION

Over the past decade, precipitation-monitoring technology has evolved, and Environment and Climate Change Canada (ECCC) and its partners implemented a transition from manual observations to the use of automatic precipitation gauges. Extensive data integration is required to link the current precipitation observations to the long-term historical manual observations. The update and reporting of historical adjusted precipitation trends and variations will be on temporary hiatus pending the extensive data reconciliation, and resumed thereafter. ECCC remains committed to providing credible climate data to inform adaptation decision making, while ensuring the necessary data reconciliation occurs as monitoring technology evolves.

(III) NOTABLE EVENTS AND IMPACTS

The year 2019 will be remembered as the year of the big flood in eastern Canada. The country experienced a catastrophic spring flood along the Ottawa and St. Lawrence Rivers, with record-breaking discharge. This was even larger than the 2017 event, which was considered at the time to be the flood of the century. A number of factors contributed to the flood. The region experienced seven straight months of below-normal temperatures from October 2018 through April 2019. These temperatures ensured that the ground froze deeply and thawed late, preventing the infiltration of rain and snowmelt runoff. In addition, snowfall accumulation was 50% greater than normal in upstream catchments of the Ottawa River and, with little melting by mid-spring, the deep and icy snowpack remained for longer than normal. Multiple rounds of heavy spring rains fell over a five-week period between mid-April and mid-May, adding 150 mm of additional rainwater to the already heavily saturated region. All of these ingredients coincided, causing this catastrophic event that claimed at least two lives and flooded about 6000 dwellings and other infrastructure.

A similar situation also occurred in the spring of 2019 in the Fredericton-Saint John Region of New Brunswick. During April, precipitation in the region was nearly double the monthly average with six more wet days than normal and twice the number of heavy rain days (days with >10 mm) recorded. Up to 130 mm of rain fell along the Saint John River region within 10 days in late April. Mild temperatures and significant rains combined to rapidly melt the snowpack in New Brunswick. The Saint John River at the Maine–New Brunswick border had its largest peak streamflow in 67 years. Farther downstream, the peak river level in Fredericton was over 8.3 m, the second-highest level on record (behind 1973). As a result, more than 5500 dwellings were flooded or at risk, and over 4000 hectares of land were flooded.

Canada was hit directly by Category 2 Hurricane Dorian during the active 2019 Atlantic hurricane season. By the time Dorian entered Canadian waters near Nova Scotia, the hurricane had weakened from its peak wind speed of 300 km h^{-1} to about 160 km h^{-1}. Dorian made landfall in Halifax on 7 September as a post-tropical cyclone and brought sustained winds of 155 km h^{-1}, torrential rains, storm surges, and over 20-m waves for more than a 24-hour period. High winds toppled trees and power lines, and storm surges caused widespread flooding. More than 500 000

homes and businesses were without electricity at the peak of the storm, and over 100 mm of rain fell across the Atlantic region during the storm.

In contrast to the record-breaking wildfire seasons experienced in British Columbia in the last two years, statistics from the Canadian Interagency Forest Fire Centre revealed a relatively quiet fire season in 2019. The area consumed by wildfires in British Columbia was about 0.02% of the area burned in each of the past two summers. A notable exception to the quiet wildfire season was in Alberta. The number of fires there was on par with 2018, but the area that fire consumed was nearly 14 times greater. In May, the "spring dip," when trees and grasses have low moisture content, was underway, and hot, very dry, strong gusty winds came early. Around mid-May, the Chuckegg Creek fire erupted near the town of High Level in far northwestern Alberta. It burned over 350 000 hectares and lasted over 100 days, making it one of the longest wildfires on record. Over 10 000 Albertans were displaced from their homes as a result of this fire. Overall, wildfires in Alberta burned 883 000 hectares in 2019, making it the second-greatest area burned in 60 years and four times greater than the 25-year average.

2) United States—K. Gleason, C. Fenimore, R. R. Heim Jr., and A. Smith

During 2019, above-normal temperatures were observed across much of the Southeast and parts of the Mid-Atlantic, while below-normal temperatures were present across the northern and central Plains and part of the Great Lakes (Fig. 7.3a). Overall, the 2019 annual average temperature for the contiguous United States (CONUS) was 11.5°C, which is 0.1°C below the 1981–2010 average (Fig. 7.4). The annual CONUS temperature trend over the 125-year period of record is increasing at an average rate of 0.08°C decade^{-1}, 0.26°C decade^{-1} since 1970. Above-normal precipitation was observed across much of the nation, with a large portion of the central United States and parts of the West receiving above- to much-above-normal precipitation. Below-normal annual precipitation was observed across parts of the Northwest and the South (Fig. 7.3b). Average precipitation totaled 883 mm, which is 112% of the 1981–2010 average and the second-largest value in the 125-year record, behind 1973. The annual precipitation total is increasing at an average rate of 5 mm decade^{-1} since 1970. Alaska had its warmest year (+2.8°C departure; 0.2°C warmer than previous warmest year of 2016) since statewide records began in 1925. Precipitation across Alaska was near normal at 104% of average.

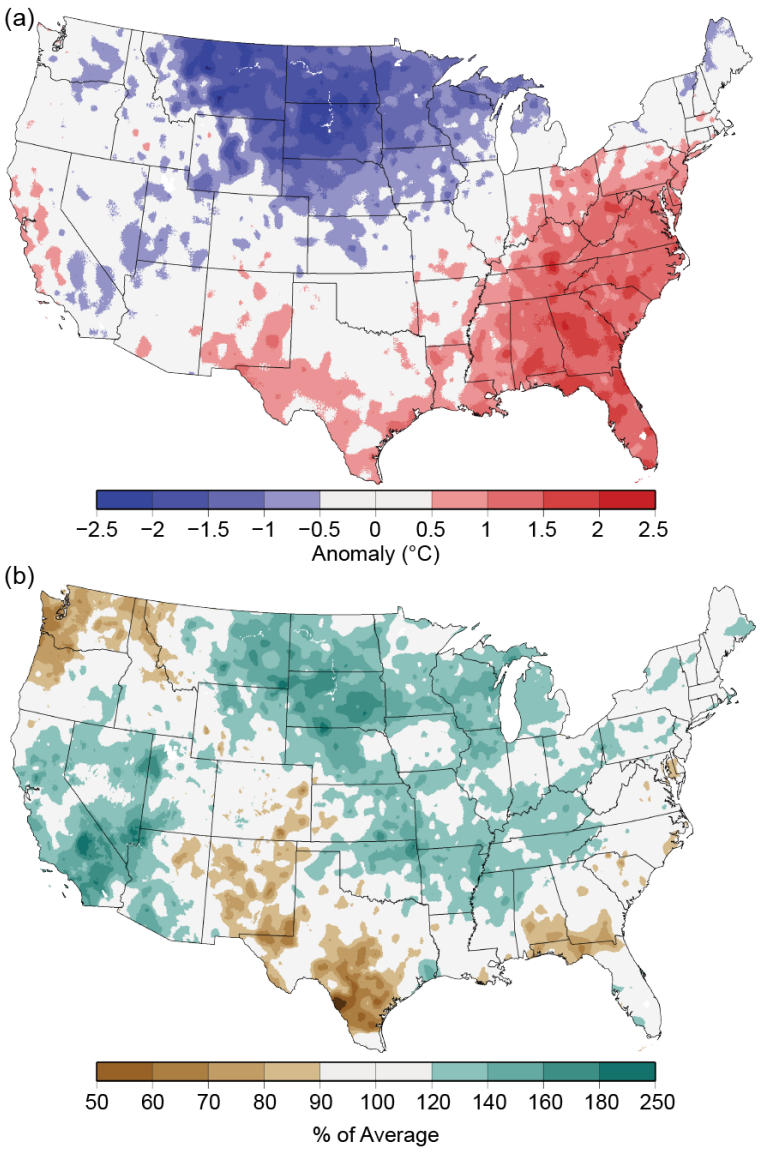

Fig. 7.3. Annual (a) average temperature anomalies (°C) and (b) total precipitation (% of average) in the CONUS for 2019 (1981–2010 base period). (Source: NOAA/NCEI.)

(I) TEMPERATURE

Across the CONUS, 2019 was the coolest year since 2014 and the first year since then in which some states ranked in the lowest third of their historical record for annual temperatures. Nevertheless, 2019 ranked in the warmest third of the 125-year historical distribution for the CONUS as a whole. South Dakota recorded its 12th coldest year on record, one of six states across the northern Plains that ended the year in the coldest third of their historical distribution. In contrast, it was a warm year from the Gulf Coast to the mid-Atlantic region. Georgia and North Carolina each ranked warmest on record, with Florida, South Carolina, and Virginia ranking second warmest.

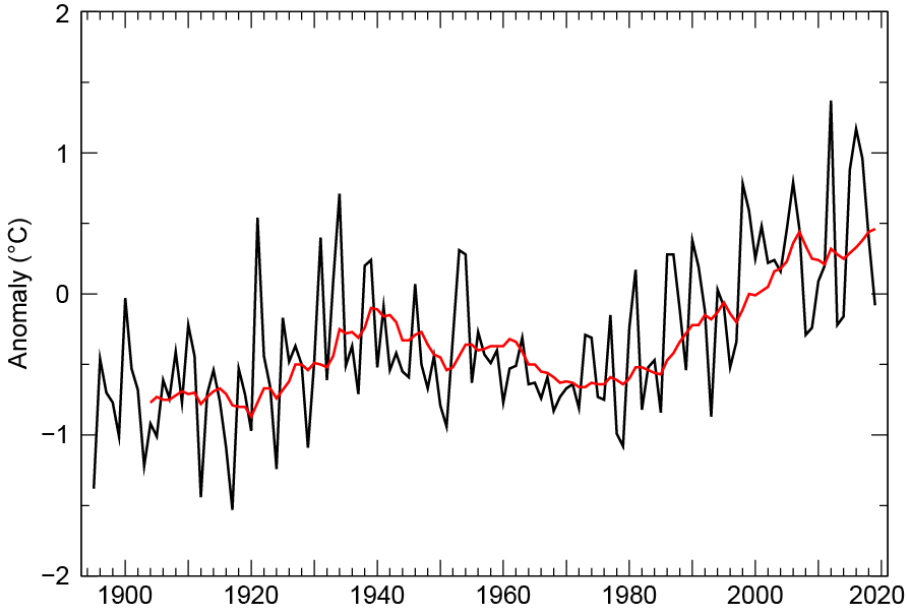

Fig. 7.4. Annual mean temperature anomalies (°C; 1981–2010 base period) for the CONUS for 1895–2019. Red line is the lagged 10-year running mean. (Source: NOAA/NCEI; for precipitation time series, see www.ncdc.noaa.gov/cag/national/time-series.)

The winter 2018/19 CONUS temperature was 0.1°C below the base period average, but still ranking in the warmest third of its record. Above-average warmth was confined to portions of the Southeast, while average- to below-average temperatures were evident from the Great Lakes and central Plains to the West Coast. The CONUS spring temperature was 0.6°C below average, ranking in the middle third of the record. Above-average temperatures were observed across the Pacific Northwest and the Southeast. Florida had its warmest spring season on record with Georgia, South Carolina, and North Carolina all having their second-warmest spring season on record. Below-average spring temperatures were present from the West Coast to the Great Lakes and into parts of New England. Summer CONUS temperatures were 0.3°C above average, ranking in the warmest third of the 125-year record. Florida and Delaware ranked fifth warmest while much of the central United States had near-average temperatures. The autumn CONUS temperature was 0.1°C below average, ranking in the middle third of the record. Below-average temperatures were present across the northern tier, while above-average temperatures were observed from California to the Southeast and into the mid-Atlantic states. Florida ranked sixth warmest for the season.

(II) PRECIPITATION

At the start of 2019, nearly 22% of the CONUS was in drought, according to the U.S. Drought Monitor, mostly concentrated across the West and Southwest. Abundant precipitation during the first few months of the year, especially over the western drought areas, helped improve conditions, bringing the drought to its minimum extent of approximately 2% in April. Winter precipitation across the CONUS was a record 134% of average. Much of the Ohio and Tennessee Valleys, as well as the central Plains and Great Lakes received above-average precipitation during this period. Both Wisconsin and Tennessee had a record wet winter. Below-average precipitation was confined to parts of the Northwest, central Rockies, and Texas.

Spring 2019 precipitation was 122% of average and ranked fifth wettest on record. Above-average precipitation occurred from parts of the West to the Great Lakes. Kansas observed its wettest spring season on record. Precipitation was below average from the state of Washington to northern Minnesota as well as across much of the Southeast. Record flooding along the

Missouri, Mississippi, Platte, and Arkansas Rivers during the spring and summer months was the result of rapid snowmelt in the spring as well as heavy and frequent precipitation throughout the first six months of 2019.

Summer precipitation was 104% of average across the CONUS, with the wettest conditions occurring across much of the Plains, as well as the Mississippi and Ohio Valleys. Conditions were dry across much of the western United States and portions of the Midwest. By August, the weather pattern turned dry and hot across parts of the country, increasing the drought footprint to 9% of the CONUS, and continued to expand across the Southwest into October.

The autumn CONUS precipitation total was 101% of average and ranked in the wettest third of the historical record. North Dakota, Minnesota, and Wisconsin were record wet for this period, with dry conditions observed across the West, the central Rockies and Plains, as well as parts of Texas and Florida. Five states had their wettest annual period on record, namely North Dakota, South Dakota, Minnesota, Wisconsin, and Michigan (Fig. 7.3b). For the year, the CONUS ranked second wettest behind 1973. Dry conditions were not as extensive or as frequent as the wet conditions, except during the late summer to early autumn. By the end of the year, drought was mainly confined to the Pacific Northwest, the Southwest, and parts of the southern Plains, accounting for 11% of the country.

(III) NOTABLE EVENTS AND IMPACTS

There were 14 weather and climate events during 2019 with losses exceeding $1 billion (U.S. dollars) each across the United States and yielding 44 fatalities (www.ncdc.noaa.gov/billions): three inland flooding events, eight severe storm events, two tropical cyclone events (Dorian and Imelda), and one wildfire event (Fig. 7.5). The year's loss total of $45.0 billion (U.S. dollars) was above average, as the 40-year (1980–2019) annual cost average, adjusted for inflation, is $43.9 billion (U.S. dollars). The combined cost of $20.0 billion (U.S. dollars) associated with the Missouri, Arkansas, and Mississippi River flooding was nearly half of the U.S. cost total during 2019. The total cost of U.S. billion-dollar disasters over the last five years (2015–19) exceeds $525

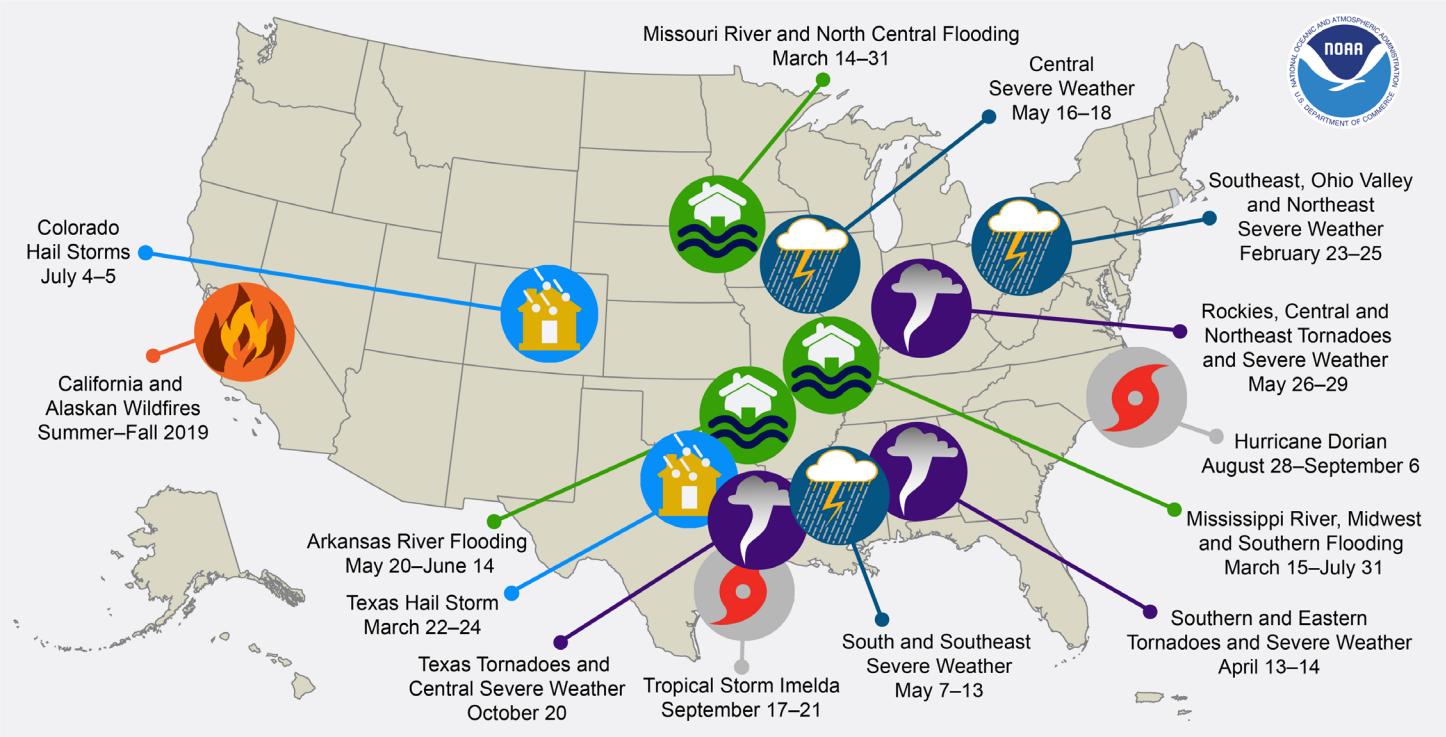

Fig. 7.5. Map depicting date, approximate location, and type of the 14 weather and climate disasters in the United States in 2019 with losses for each exceeding $1 billion (U.S. dollars). (Source: NOAA/NCEI.)

billion (U.S. dollars), with a five-year annual cost average of $106.3 billion (CPI-adjusted U.S. dollars), both of which are records. The damage costs from 2010 to 2019 for the United States were also historically large—exceeding $800 billion (U.S. dollars) from 119 separate billion-dollar events (Smith 2020).

During 2019, there were 1520 tornado reports, including preliminary numbers for September–December. This was well above the 1991–2010 U.S. annual average of 1251 tornadoes. Once preliminary numbers are finalized, it is likely that 2019 will rank among the top five years for tornado counts since 1950.

Nearly 50 000 wildfires were recorded across the CONUS in 2019. Since 2000, only 2013 had fewer wildfires than what was observed during 2019. The 2019 fires consumed approximately 1.9 million hectares, which was the sixth-smallest area in the last 20 years.

SIDEBAR 7.1: **Record wetness and the impact on U.S. Midwest/Plains agriculture growing season 2019**—D. TODEY

The U.S. flooding issues of 2019 were well-reported nationally, capturing a great deal of attention because of their widespread impacts on the Missouri and Mississippi River systems. There were direct flooding impacts to agriculture (including livestock, soil damage, and loss of grain in flooded bins) due to the flooding associated with the March Bomb Cyclone (Bosart et al. 2020) and season-long flooding along many rivers throughout the Corn Belt and Northern Plains. However, the wider-spread agricultural impacts were due more to overall soil wetness than direct flooding (Todey et al. 2020).

Because autumn 2018 and spring 2019 were very wet across the Midwest and Plains, extremely wet soils were present in the region early in the year. This resulted in delayed planting, because excessively wet soils limit field access to plant crops as soils can be damaged by compaction from large equipment traversing fields. Excessively wet fields can also limit crop development and increase disease risk. Due to the preseason precipitation and a wet, cool spring, planting moved at a record slow pace for corn, soybeans, small grains, and other crops. Typically, corn is nearly half emerged by mid-May. Figure SB7.1 depicts how far behind corn emergence was in mid-May 2019.

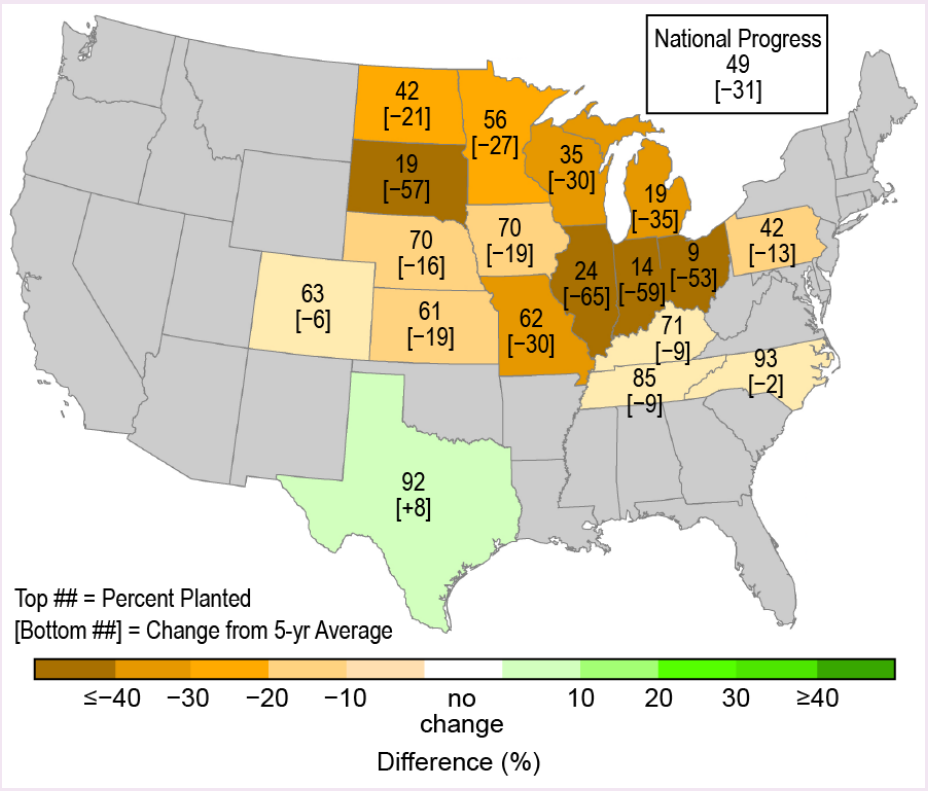

Fig. SB7.1. State corn emergence numbers as of 19 May 2019 and a comparison to the 5-year average. Corn is usually nearly half emerged by mid-May. (Image courtesy Brad Rippey [USDA-OCE].)

Many hectares went unplanted because of the excess wetness. Federal crop insurance plans cover, among other losses, "prevented planting," where conditions are too wet to plant during the crop planting time frame. The Upper Midwest set a record number of prevented planting hectares with nearly eight million hectares unplanted. Large areas of corn

were planted well into June, much later than is usually recommended. A sampling of crop records are:

- Least amount of corn planted by 2 June (67% planted).
- Least amount of corn emerged by 2 June (46% emerged), which broke established records between 70% and 80%.
- Least amount of soybeans emerged by 2 June (19% emerged).

The most affected areas included (Fig. SB7.2, highest indemnity): northwest Ohio, northern Illinois, the Missouri River valley, and the eastern Dakotas/western Minnesota. Some counties in these areas planted less than half of their agricultural hectares.

Because of the widespread late planting, crops had a shorter season to complete development. For crops such as soybeans, a shortened season is a minor issue. Corn, however, requires a certain amount of heat (measured by Growing Degree Days) to complete phenological development. The late start and moderate temperatures, which would be good for crop development in an on-time planting year, slowed crop progress through the season. Wet years do not limit grain production (yield) as much as drought years. The issues during wet seasons tend to be limited development time, excessively wet crops at harvest, and poor grain quality. In addition, wetness leads to additional disease issues.

Despite the delays, most row crops (i.e., corn/soybeans) did reach maturity but had not dried down in the field as much as producers would like. This resulted in a large amount of time and management to dry the grain after harvesting it, which in turn slowed the harvest progress. The additional drying costs (propane/electricity) further reduced profit during a time of very limited profit margins on most crops. Above-average precipitation occurred during harvest, further slowing crop harvest.

Relatively early snow in the Dakotas limited harvest, leaving some sunflowers and nearly half the corn in North Dakota still in the field at the end of the year, according to the USDA National Agricultural Statistics Service. The crops with the largest yield losses were corn (3% below trend) and soybeans (4% below trend). Winter wheat, grown more extensively in the Plains, was able to utilize the additional moisture and cooler spring conditions in 2019, leading to larger yields (7% above trend).

The additional grain-handling issues also produced associated impacts. The heavy drying requirement, along with an early cold event, caused shortages of propane needed for drying. Handling wet grain can lead to packed grain, which is dangerous to dislodge from within grain bins. Several deaths were reported because of people accidentally becoming entrapped in grain bins. The additional stress of a difficult growing season, along with low grain prices, led to many Midwestern states setting up state efforts to deal with rural/farm stress and mental health issues.

Additional stress occurred in the spring of 2019 when several blizzards covered the Plains during calving periods. Most cattle on rangeland are not housed inside. Consequently, blizzards during calving are very dangerous. Beef cattle losses during the spring in Nebraska and South Dakota were significant. Reports on losses are still being developed at the time of this writing.

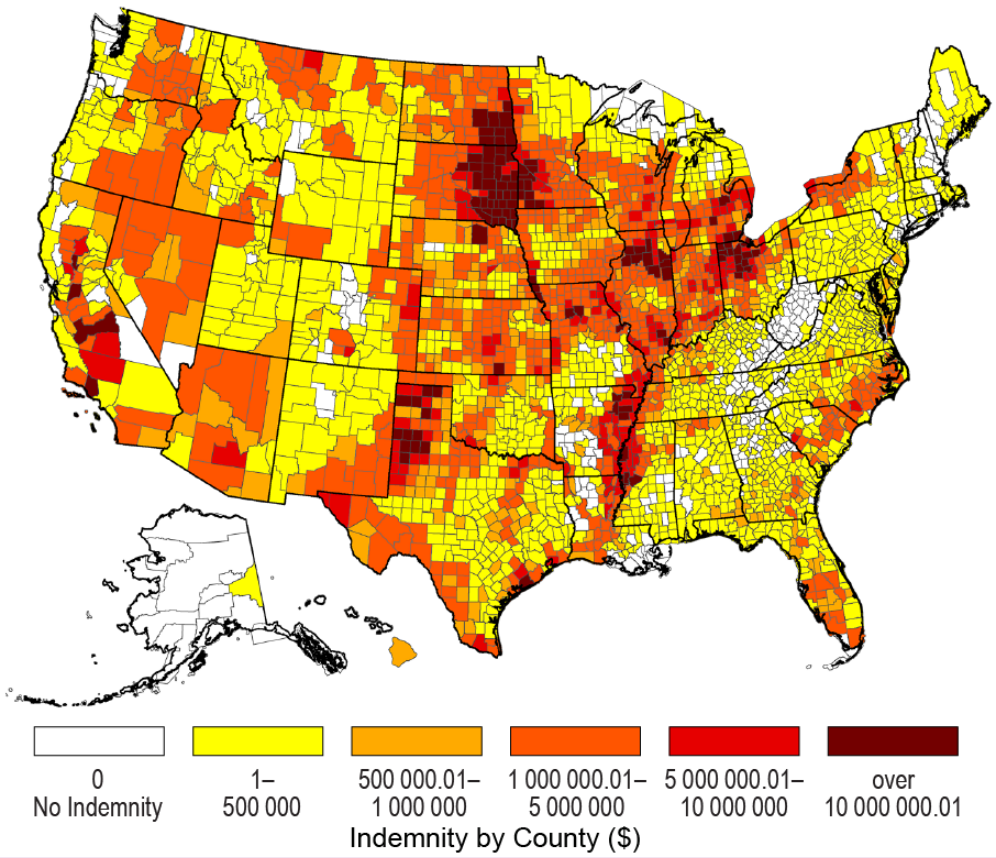

Fig. SB7.2. USDA Risk Management Agency Crop county-level indemnities (insurance payments for unplanted crops) paid. The darker the color, the higher the indemnity—mostly crop insurance payments for spring prevented planting across the Midwest and Plains.

3) Mexico—R. Pascual Ramírez

The 2019 precipitation total for Mexico was near average at 96.8% of normal, making it the 19th-driest year since records began in 1941. Regionally, the entire coastal zone of the Gulf of Mexico, the southeast, the Yucatan Peninsula, as well as several regions of the Pacific, had the greatest rainfall deficits for the year. Above-average precipitation fell in the northwest and parts of the central and northern regions of the country. Temperatures were higher than average during all months of the year, tying with 2016 as the second-warmest year on record.

(I) TEMPERATURE

The 2019 national mean temperature of 22.4°C was 1.5°C above the 1981–2010 average and tied with 2016 as the second-warmest year since records began in 1953 (Fig. 7.6). The year 2017 is the warmest year on record. The year 2019 also marked the 15th consecutive year with temperatures above average. All months of the year were warmer than average, with August being exceptionally warm. The national August 2019 average temperature was 27.0°C, or 3.3°C above average—the warmest August on record and the warmest month for any month since 1953.

The 2019 mean temperature was above average across much of the country, with a few exceptions across the northwest and the Baja California Peninsula, as well as southern parts bordering the Pacific (Fig. 7.7a). Twelve states across central to southern Mexico had their warmest year on record. Meanwhile, no state had a top-10 cold year on record.

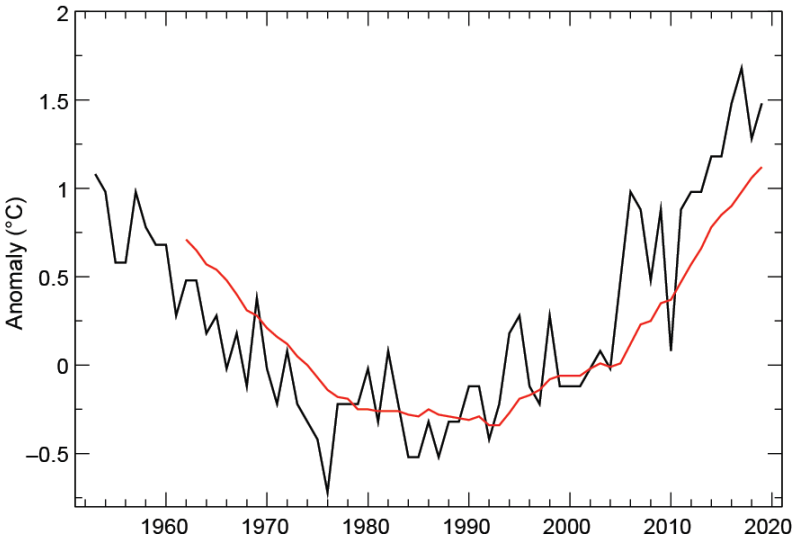

Fig. 7.6. Annual mean temperature anomalies (°C, black line; 1981–2010 period) for Mexico for 1953–2019. Red line depicts the lagged 10-year running mean. (Source: National Meteorological Service of Mexico.)

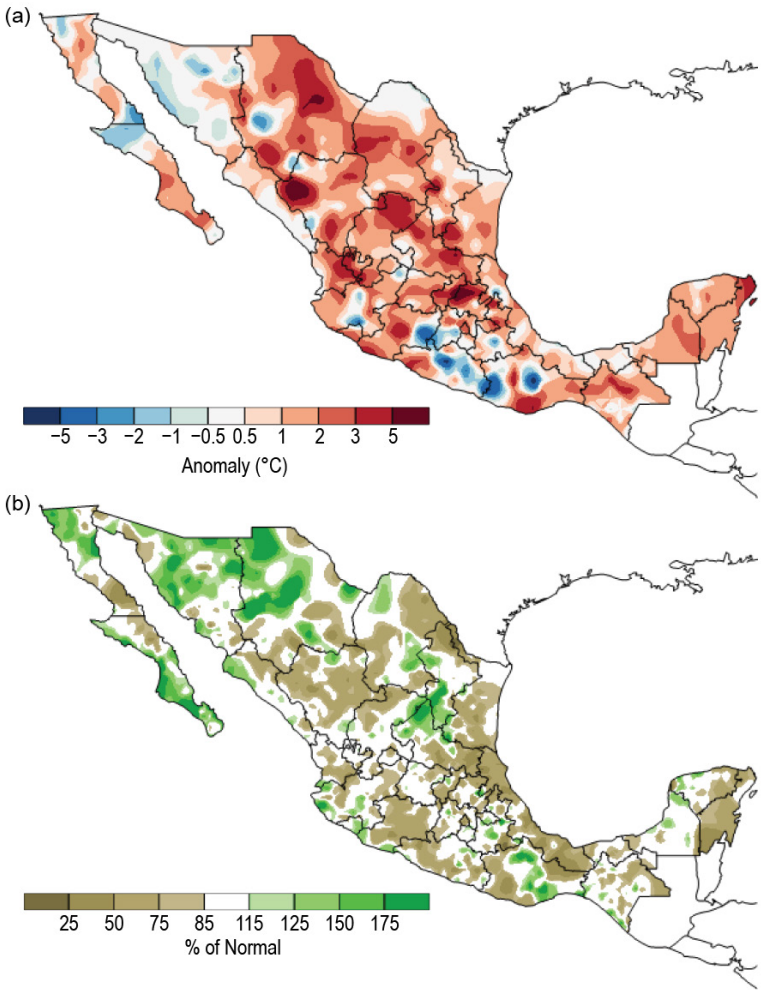

Fig. 7.7. 2019 annual (a) mean temperature anomalies (°C) and (b) precipitation anomalies (% of normal; 1981–2010 base period) over Mexico. (Source: National Meteorological Service of Mexico.)

(II) PRECIPITATION

Rainfall distribution varied regionally (Fig. 7.7b), with above-normal precipitation across the northwest, especially parts of Chihuahua and Sonora. Other regions with above-average rainfall include the northeast, specifically southern Nuevo León and northern San Luis Potosí, along with small regions in the central Pacific and a small area in central Oaxaca. The rest of the country had below-average precipitation, with the three eastern states of San Luis Potosí, Veracruz, and Hidalgo having their driest, second-driest, and third-driest year on record, respectively.

The first three months of the year produced two dry months and a wet one, resulting in the 28th-driest January–March period. However, dry conditions persisted across much of the rest of the year. The three-month period of April–June is the transition from the dry season to the rainy season; it ranked ninth-driest such period on record. The July–September period was the eighth-driest such period on record. Beneficial rains returned during the last three months of the year, giving way to the fourth-wettest October–December period on record. The dry conditions across eastern Mexico were mostly attributed to the lack of tropical cyclones affecting the region.

Climatologically, September is the nation's rainiest month of the year, contributing about 18.4% of the annual rainfall. September was indeed the nation's rainiest month of 2019, and it contributed 20.1% of the annual rainfall. Much of September's rainfall was associated with three tropical cyclones: Hurricane Lorena and Tropical Storm Narda, both on the Pacific side, and Tropical Storm Fernand along the Gulf of Mexico. Tropical Storm Fernand was the only storm to affect the country's Gulf of Mexico coast, with copious rain in early September. The storm's rainfall benefited only northeastern Mexico, farther north from drought-stricken areas in the east. On the Pacific side, Hurricane Lorena made landfall along the nation's coasts three times, but its greatest rainfall occurred across the central-western part of Mexico.

Climatologically, March is the driest month of the year, contributing only 1.8% to the annual rainfall. However, in 2019, April was the driest month of the year, contributing only 0.9% of the total annual rainfall.

(III) NOTABLE EVENTS AND IMPACTS

Typically winds and rains from tropical cyclones (TCs) begin to significantly affect Mexico when they come within 100 km of the coast. Five TCs affected Mexico during 2019. Four storms approached within 100 km of, or made landfall on, the nation's Pacific coast, while one TC made landfall from the Gulf of Mexico, as noted above. Five storms affecting Mexico is near the long-term average, but it is low when compared to the very active recent years. Considering only the decade of 2010–19, 2019 tied with 2016 for the second-fewest (to 2015, with three) number of active TCs.

For a third consecutive year, drought conditions deteriorated in southern Mexico due to the absence of TCs near this region. Hidalgo, San Luis Potosi, Veracruz, and Tabasco, some of Mexico's rainiest states, each reported a September among their eight driest, with Hidalgo having its third-driest September on record. Drought impacts for the region included water shortages in southern Veracruz and Tabasco, lack of pasture forage and water supplies, and reduced runoff in streams (made worse by higher temperatures). In Chiapas, Sumidero Canyon was closed in February to recreational navigation due to the very low water levels in the Grijalva River.

c. Central America and the Caribbean—A. Sánchez-Lugo, Ed.

During 2019, much of Central America and the Caribbean had near- to above-normal temperatures and near- to below-normal precipitation. Several tropical systems impacted the region; however, only two named storms formed in the Caribbean Sea.

Unless otherwise noted, all anomalies are with respect to the 1981–2010 base period.

1) Central America—J. A. Amador, H. G. Hidalgo, E. J. Alfaro, B. Calderón, and N. Mora

For this region, nine stations from five countries were analyzed (see Fig. 7.8 for data and station list). The station distribution covers precipitation (Magaña et al. 1999), wind (Amador 2008), and temperature (Hidalgo et al. 2019) on the Caribbean and Pacific slopes of Central America. Precipitation and temperature records for the stations analyzed and regional wind were provided either by Central America National Weather Services (NWS), National Oceanic and Atmospheric Administration (NOAA), or the University of Costa Rica. Anomalies are reported using a 1981–2010 base period and were calculated using Central America-NWS data. The methodologies used for all variables can be found in Amador et al. (2011).

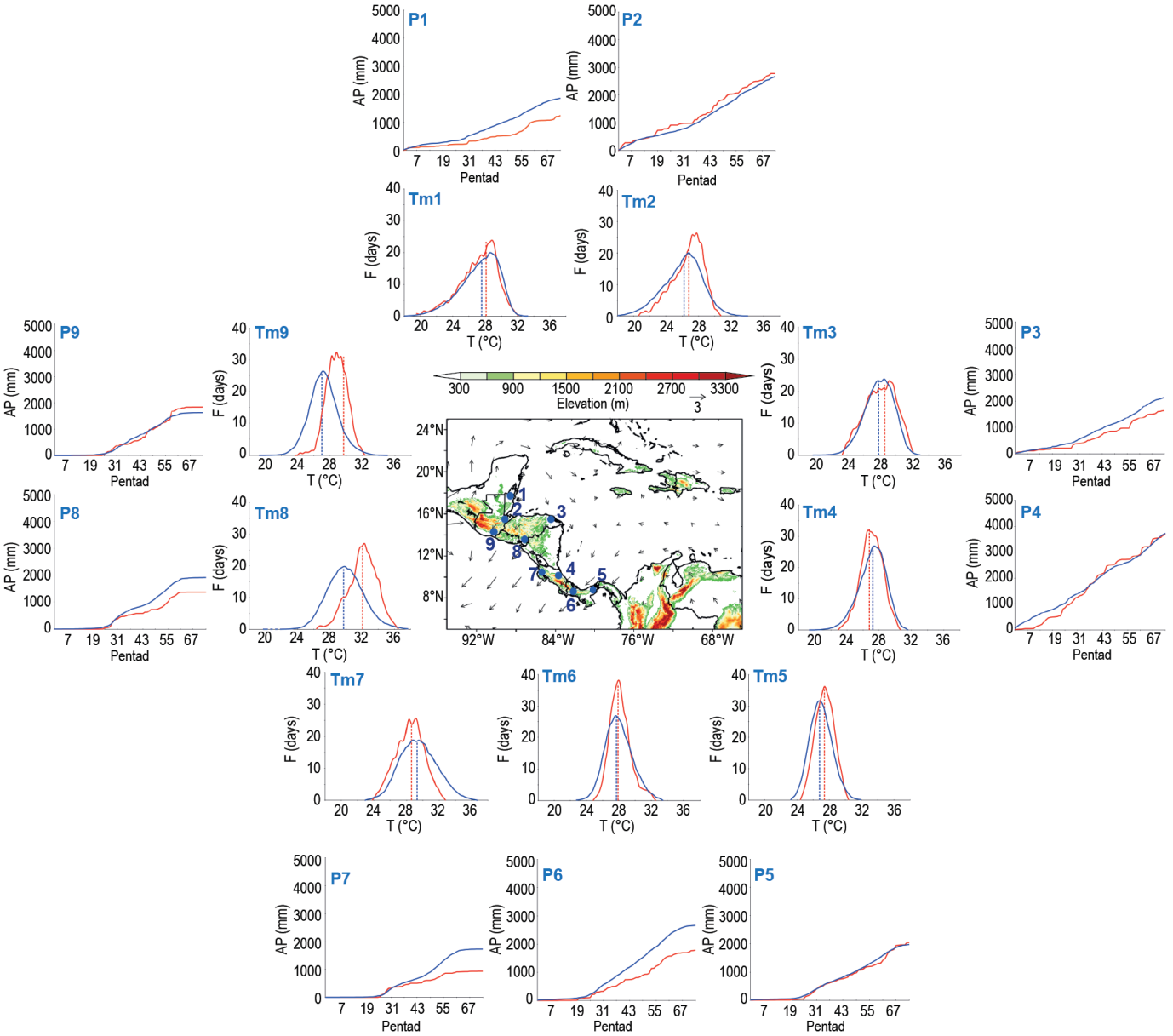

Fig. 7.8. Mean surface temperature (Tm; °C) frequency (F; pentads), and accumulated pentad precipitation (P; mm) time series are shown for nine stations (blue dots) in Central America: (1) Philip Goldson International Airport, Belize; (2) Puerto Barrios, Guatemala; (3) Puerto Lempira, Honduras; (4) Puerto Limón, Costa Rica; (5) Tocumen International Airport, Panamá; (6) David, Panamá; (7) Liberia, Costa Rica; (8) Choluteca, Honduras; and (9) Puerto San José, Guatemala. The solid red line shows 2019 values; the solid blue line represents the 1981–2010 average values. Vertical dashed lines show the mean temperature for 2019 (red) and the 1981–2010 period (blue). Vectors indicate Jul wind anomalies (m s^{-1}) at 925 hPa (1981–2010 base period). Shading depicts regional elevation (m). (Sources: NOAA/NCEI and Central America-NWS.)

(I) TEMPERATURE

The mean temperature (Tm) frequency pentad distribution for the climatology and for all stations analyzed in 2019 is shown in Fig. 7.8. During 2019, most stations had a discernible shift in their distribution toward warmer-than-normal conditions. Puerto Limón (Tm4 in Fig. 7.8) and Liberia (Tm5), both in Costa Rica, were the only two stations that observed slightly below-normal temperatures in 2019. The 2019 temperature means of Choluteca (Tm8) and Puerto San José (Tm9) were significantly different compared to their climatology when using the two-sample t-tests, with 2019 having a mean 2°–4°C higher than the 1981–2010 base period. All other stations showed no significant differences in their means with respect to the base period. When comparing the 2019 Tm pentad distributions to the 1981–2010 base period, most stations failed two-sample Kolmogorov-Smirnov tests (KS2; Wilks 2011) at the 95% confidence level, suggesting that 2019 was distributed significantly different from climatology. It should be noted for some stations that there is a great difference in the tail densities and shapes of the probability density functions between the climatology and the 2019 curves, suggesting the degree to which 2019 was an atypical year.

(II) PRECIPITATION

The accumulated pentad precipitation (P) time series for the nine stations in Central America are presented in Fig. 7.8. Precipitation showed different probability distributions throughout the year for all stations according to KS2, with most stations having near- to below-normal precipitation by the end of 2019. Only Puerto Barrios (P2) and Puerto San José (P9), both in Guatemala, had slightly above-normal annual precipitation. However, no station had annual rainfall deficits or excess beyond the 95% confidence interval of the normal distributions constructed from the base period annual precipitation totals. Even though 2019 will not be considered an extreme year at that significance level, the precipitation deficits in some of the stations were nevertheless considerably large. Of note, Philip Goldson International Airport (P1), David (P6), Liberia (P7), and Choluteca (P8) received 54%–71% of normal precipitation for the year. Low-level circulation anomalies in the westernmost Caribbean Sea and Pacific regions displayed slightly above-average values during July (vectors in Fig. 7.8) in the trade wind system. This condition is usually associated with above-normal precipitation along the Caribbean slopes and with below-normal precipitation on the Pacific slopes during summer, where it is especially related to the mid-summer drought condition impacting hydropower generation, tourism, and agriculture, among other sectors (Amador 1998, 2008; Magaña et al. 1999; Hidalgo et al. 2019).

(III) NOTABLE EVENTS AND IMPACTS

Tropical cyclone activity during 2019 was below normal in the Caribbean basin and the eastern tropical Pacific (ETP). In the Caribbean basin, there were only two named tropical storm systems: Dorian (27–28 August; see Sidebar 4.1 for details) and Karen (22–24 September; see *Notable events and impacts* in section 7c2). On 23 October, Tropical Depression Seventeen developed near Belize, intensifying over the Gulf of Mexico to become Tropical Storm Olga. In the ETP, no tropical storms made landfall in the isthmus; however, during 21–27 May, a significant low-pressure system was generated offshore the Pacific Coast of Costa Rica and Nicaragua. Heavy rainfall associated with the low-pressure system was recorded in the North Pacific region of Costa Rica. During 2019, a total of 21 fatalities were reported and at least 41 people were injured by lightning (Table A7.1). Additional information on regional impacts from hydrometeorological events during 2019 can be found in Table A7.2.

2) Caribbean—T. S. Stephenson, M. A. Taylor, A. R. Trotman, J. M. Spence, K. A. Stephenson, A. C. Joseph, C. J. Van Meerbeeck, J. D. Campbell, and L. A. Clarke

Temperatures are drawn from the Global Historical Climatological Network-Monthly version 4 (GHCN-M-v4), with a climatological baseline of 1981–2010.

(I) TEMPERATURE

In 2019, the Caribbean experienced above-average annual mean surface temperatures with the largest positive anomalies over the north and, in contrast, below-normal temperatures over the U.S. Virgin Islands, Guadeloupe, and Monserrat (Fig. 7.9a). The average temperature anomaly over the domain was approximately +0.81°C higher than baseline and represents the greatest departure from this mean since records began in 1891 (Fig. 7.10). The warmth persisted throughout the year, although a few locations in the southern Caribbean experienced cooler-than-normal conditions during the first six months. Notably, 2019 was the warmest year on record since the start of the record in 1977 for Sangster, Jamaica (32.5°C), and Grand Cayman (31.1°C).

Monthly Caribbean sea surface temperatures (SSTs) exhibited increasingly warm anomalies as the year progressed. By December, most areas recorded SSTs 0.5°–1.0°C above average.

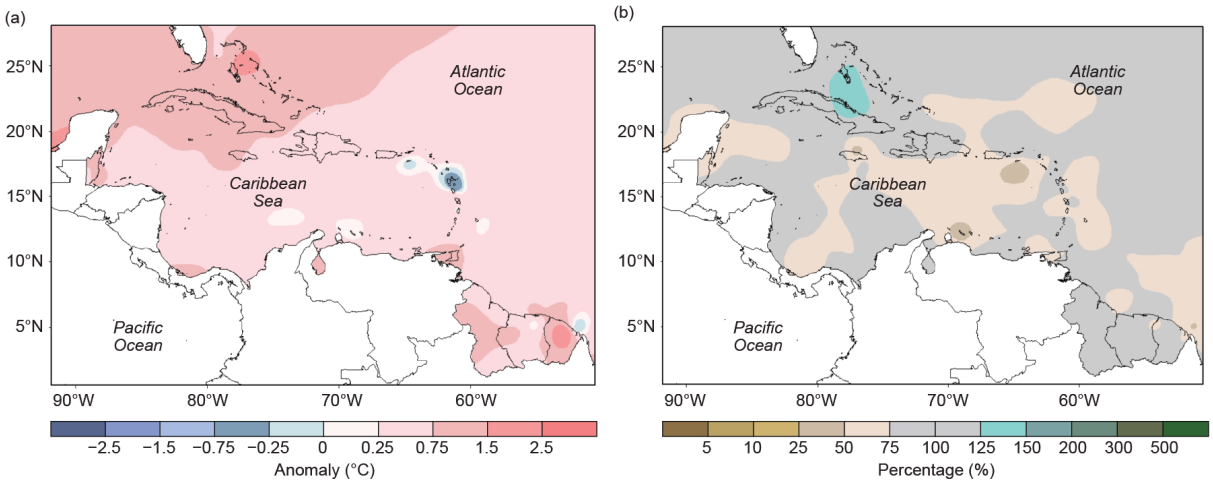

Fig. 7.9. Annual (a) mean temperature anomalies (°C) and (b) total precipitation anomalies (% of normal) relative to the 1981–2010 base period. (Source: Caribbean Climate Outlook Forum and the Caribbean Institute for Meteorology and Hydrology.)

(II) PRECIPITATION

Normal to below-normal rainfall anomalies were observed over the region in 2019 (Fig. 7.9b), continuing from relatively dry conditions in late 2018, related to a weak El Niño event that began in January and ended in July (see section 4b for details). During January–March 2019, normal to below-normal rainfall was observed across the region. During these climatologically dry months, the northern islands exhibited slightly dry to very wet anomalies, while eastern islands were slightly dry to exceptionally dry (Fig. 7.9b). This pattern of a wetter northern and drier eastern Caribbean is a signature pattern of El Niño events (e.g., Spence et al. 2004). March 2019 was the driest

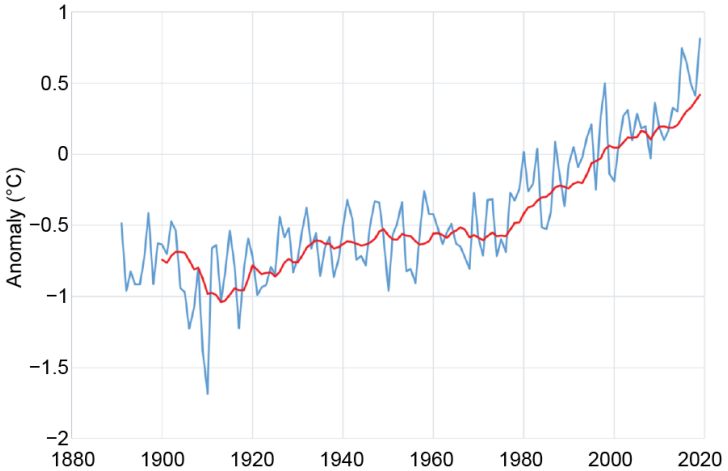

Fig. 7.10. Annual average 2-m temperature anomalies (blue line, °C) for the Caribbean (9°–27°N; 58°–90°W) for 1891–2019 relative to the 1981–2010 average. The red line is the 10-year running mean. (Source: NOAA/NCEI from the KNMI Climate Explorer.)

March since 1951 at the Henry E. Rohlsen Airport, Saint Croix (0.5 mm), contributing to its fourth-driest year on record (618.7 mm).

For April–June, which is climatologically the start of the rainy season, rainfall ranged from normal to below normal across the eastern islands, with the exception of Antigua and Guadeloupe, which were normal to slightly wet. The northern and larger Caribbean countries (e.g., Jamaica, Hispaniola, and Puerto Rico) showed oppositely signed anomalies. Countries in the far north, e.g., The Bahamas and Cuba, showed normal to moderately wet anomalies. The extent of drier-than-normal conditions expanded in the third quarter, coinciding with the climatological mid-summer dryness experienced by northern Caribbean countries. The overall dry Caribbean basin was interspersed with normal to above-normal anomalies over much of the northern and northeastern Caribbean. For October–December, normal to below-normal anomalies were recorded over many of the islands. Of 113 Caribbean rainfall stations, seven stations recorded their driest year on record, 47 recorded totals in the 10th percentile, and two in the 90th percentile. Stations recording their driest year are noted in Table 7.1.

Table 7.1. Record low annual rainfall totals for 2019.

Country	Station	Rainfall Total (mm)	Starting year of record
Barbados	Caribbean Institute for Meteorology and Hydrology	804.5	1969
Barbados	Grantley Adams International Airport	736.5	1942
Belize	Punta Gorda Airport	1245.6	1971
Belize	Spanish Lookout	900.0	1984
Curaçao	Hato International Airport	248.9	1972
Dominican Republic	Monte Cristo	311.1	1973
Trinidad	Piarco	1413.4	1971

(III) NOTABLE EVENTS AND IMPACTS

Short- and long-term drought conditions were observed across several Caribbean islands during the year. Additionally, June–December was generally characterized by dry and warm conditions that resulted in heat waves in most locations. From August to October, ocean warming levels necessitated Level 1 (bleaching expected) and Level 2 (widespread bleaching and some mortality expected) coral bleaching heat stress alerts for the region (Caribbean Coral Reef Watch October 2019).

The slow-moving Category 5 Hurricane Dorian hit the Bahamas on 1 September with winds of 160 kt (82 m s^{-1}) and storm surges of approximately 6.1–7.6 m. This was the strongest hurricane on record to impact the Bahamas. Destructive winds, extensive flooding, and storm surges led to 67 deaths, with over 300 missing as of December 2019. Homes, essential services, telecommunications, boats, cars, and government infrastructures were destroyed. Total damage was estimated over $3.4 billion (U.S. dollars). Please refer to Sidebar 4.1 for more details about this storm.

Tropical Storm Karen formed on 22 September and was briefly downgraded to a tropical depression as it traversed the region. Karen caused flooding and storm surges in parts of the southeastern and northeastern Caribbean, impacting Trinidad and Tobago, Dominica, Puerto Rico, and other islands (NOAA 2019). In Trinidad and Tobago, flooding caused damage to roadways and other critical infrastructure, power outages, landslides, fallen trees, and overflowing rivers. The storm impacted Puerto Rico the day after the island experienced a 6.0 earthquake on the Richter scale. The combined effects resulted in destruction of infrastructure, landslides, flooding, and the closure of government offices and schools.

Flooding occurred in northern Dominica in relation to a tropical wave impacting the island on 4 October. A series of troughs over Jamaica and the central Caribbean in late 2019 caused thunderstorms, flooding, and landslides across most of island. Lightning strikes led to the postponement of several sporting activities. At least six players were struck at two football matches.

d. South America—A. Sánchez-Lugo, Ed.

Much of South America had above-average temperatures during 2019, resulting in the second-warmest year on record at 0.69°C above the 1981–2010 normal, behind only 2015. The last five years were South America's warmest years in the continent's 110-year record. Precipitation varied spatially, with the most notable anomalous wet conditions across Peru and parts of Venezuela. The most notable precipitation deficits were observed across southern South America. Unless otherwise noted, the reference period is 1981–2010.

1) Northern South America—J. J. Nieto, F. Costa, E. A. Díaz, D. Marín, R. Hernández, and G. Carvajal

This region includes Colombia, Ecuador, French Guiana, Guyana, Suriname, and Venezuela.

(I) TEMPERATURE

The year 2019 was characterized by warmer-than-average conditions across much of northern South America, with mean temperatures 0.50°–0.75°C above the 1981–2010 normal (Fig. 7.11). The warmer-than-average conditions in the region coincided with above-normal sea surface temperatures (SSTs) that were present in the tropical Pacific Ocean, especially during the first half of the year (see Fig. 4.2).

Northern Colombia, Suriname, French Guiana, Guyana, and Venezuela all had annual maximum temperatures that were 1.0°–1.5°C above normal, while southern Colombia and most of Ecuador had near-normal annual maximum temperatures. Most of northern South America also experienced above-normal annual minimum temperatures, ranging from 0.5°C to 1.5°C above normal. Minimum temperature anomalies were more than +1.5°C in the Andes of Colombia, Ecuador, and Venezuela.

Above-average mean temperatures prevailed in Colombia during the first quarter of the year (January–March), while the rest of the region had near-normal temperatures. During March–September, temperatures were 0.75°C above normal on average across the region. During the last quarter of the year (October–December), temperature anomalies were as much as +1.0°C above normal

(II) PRECIPITATION

Much of northern South America had near- to below-normal precipitation during 2019 (Fig. 7.12), while parts of central and northern Venezuela, as well as Guyana, had above-normal precipitation (20%–30% above normal). The largest precipitation deficits occurred during February–April when monthly precipitation totals were 75%–80% below normal in French Guiana, Guyana, and Venezuela, and isolated parts of the Colombian and Ecuadorian Andes. During the rest of the year, above-normal rainfall prevailed in eastern Colombia, Guyana, French Guiana, Suriname, and Venezuela.

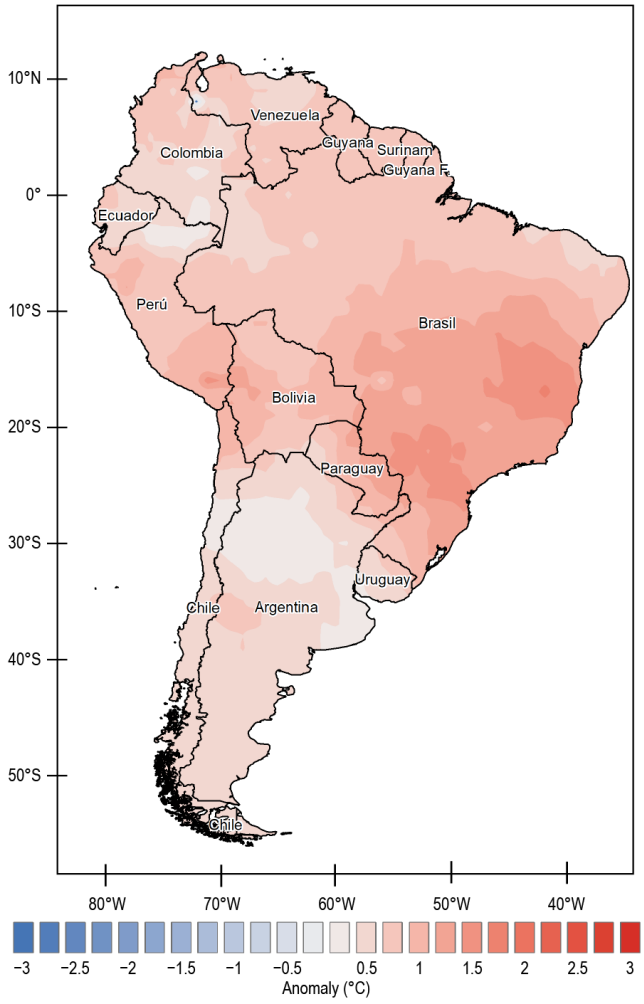

Fig. 7.11. 2019 Annual mean temperature anomalies (°C; 1981–2010 base period). (Source: Data from NMHSs of Argentina, Bolivia, Brazil, Chile, Colombia, Ecuador, Paraguay, Peru, Suriname, and Venezuela; processed by CIIFEN.)

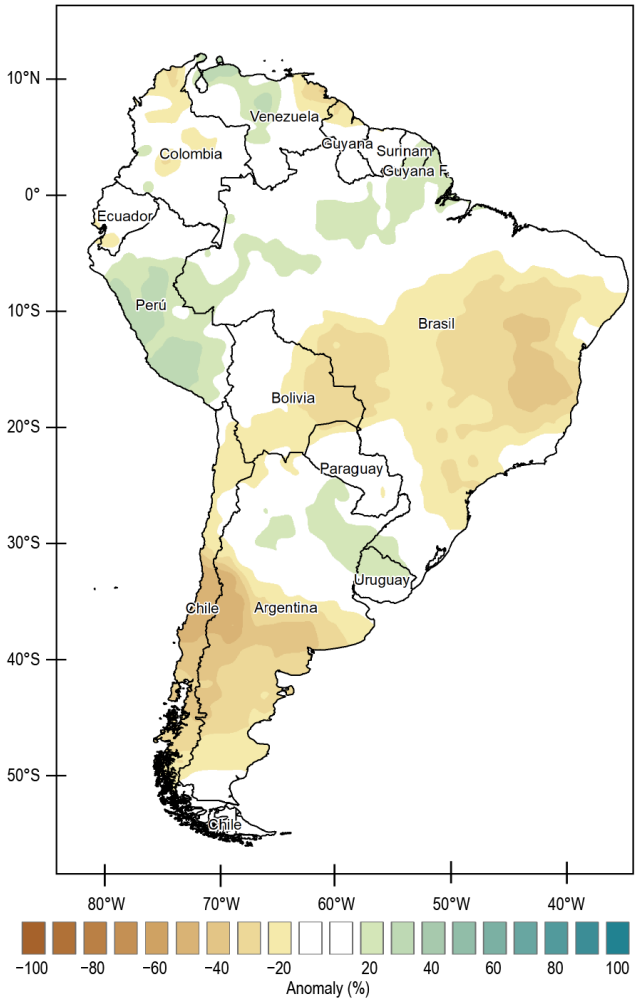

Fig. 7.12. 2019 Annual precipitation anomalies (%; 1981–2010 base period). (Source: Data from NMHSs of Argentina, Bolivia, Brazil, Chile, Colombia, Ecuador, Paraguay, Peru, Suriname, and Venezuela; processed by CIIFEN.)

(III) NOTABLE EVENTS AND IMPACTS

Very dry conditions affected parts of northern South America early in the year, with several locations experiencing drought. The marked water deficit across much of Venezuela favored the occurrence of a large number of forest fires, especially during February–March. Drought affected 108 of Colombia's 1103 municipalities during January–March, resulting in water shortages. In the department of Cordoba in Colombia, drought caused the loss of 60% of its plantain crops. In Guyana, drought in the region of Rupununi and Barima-Waini caused a sugar cane yield loss of 35%, water scarcity for human consumption and irrigation, and forest fires.

Even though much of Colombia was affected by drought, several significant rainfall events occurred in western Colombia during the year, affecting thousands of people and damaging hundreds of houses. Colombia's municipality of Rosas (department of Cauca) had a very wet April, receiving 450 mm of rain, double its monthly average rainfall, in just 20 days. On 21 April, a landslide was triggered in the region, causing 14 fatalities. In May, Colombia's municipality of Pereira, Risaralda, had a total of 485 mm of rain, which is nearly twice its normal May monthly precipitation.

Heavy precipitation and floods also affected Ecuador during the year. Of note, flooding in the Province of Los Ríos affected 733 families and damaged more than 4000 ha of crops. In the Province of Santo Domingo, a landslide in mid-January and a second one in mid-February blocked the main road that connects the Coast and Highland regions, causing economic losses and food supply chain problems. A landslide was triggered in late April after 80 mm of rain fell in one hour in Riobamba, resulting in 20 collapsed homes and blocked roads.

Hurricanes had a significant impact in the region during the season. Hurricane Dorian (27–28 August, for this region) affected Venezuela's northeast and north coastal regions and its Caribbean territory, including Islas Las Aves and Nuevo Esparta, with heavy rainfall, lightning, wind gusts, and large swells (see Sidebar 4.1 for more details). Hurricane Karen (15–22 September) formed from a tropical wave, affecting Venezuela with intense rainfall, lightning, wind gusts, and strong swells.

In Guyana, flooding during the last week of September in Mahaica-Berbice, Demerara-Mahaica, and Essequibo Islands severely affected several small farms and more than 300 homes across seven villages.

October rainfall totals in the municipality of Jericó, in the northwestern department of Antioquia, Colombia, were 400–470 mm, followed by an additional 270–280 mm in November. The heavy rainfall in the region caused total and partial losses in the agricultural and infrastructure sectors, as well as problems in food security and public health.

In Venezuela, a short-lived but high-intensity rainfall event caused the Kunana River (also known as the Negro River) to overflow in October, causing mudslides in the Sierra de Perijá of Zulia state. These affected six Indigenous communities.

2) Central South America—J. A. Marengo, J. C. Espinoza, L. M. Alves, J. Ronchail, W. Lavado-Casimiro, A. M. Ramos, J. Molina-Carpio, K. Correa, J. Baez, and R. Salinas

This region includes Brazil, Perú, Paraguay, and Bolivia.

(I) TEMPERATURE

Central South America had higher-than-normal annual mean temperatures during 2019 (Fig. 7.11). The most notable warmth was observed across much of southeastern Brazil, where temperature anomalies were at least +1.0°C.

During 2019, the most notable positive temperature anomalies occurred in January, February, June, and September–December. Mean temperatures in January were 1.5°–2.5°C above normal in southeastern Bolivia and Paraguay, while the northern coast of Peru and tropical Brazil had temperatures 2.0°–5.0°C above normal. Unusually warm temperatures affected the southern region of central South America at the end of January, with several locations observing daily

maximum temperatures that were their warmest on record for January. Some locations surpassed the previous record by 5.0°–8.0°C. During 25–28 January, the northern coast of Peru experienced its most intense heat wave of the last 30 years. Paraguay observed its hottest days on record on 23–24 January, when maximum temperatures soared to 39.4°–43.0°C. Another significant heat wave affected Bolivia, southeastern Brazil, and Paraguay in mid-September. The region-wide heat produced several record-breaking maximum temperatures.

Several cold fronts affected parts of central South America during May, July, August, and October. During 7–11 May and 7–8 July, minimum temperatures dropped more than 10°C in southeastern Brazil. The lowest temperatures of 2019 were recorded across most of Bolivia during 3–7 August. Below-freezing temperatures were also recorded in Peru's departments of Pasco, Huánuco, Apurimac, and Huancavelica.

(II) PRECIPITATION

Annual precipitation was spatially variable across the region, with much of Peru and parts of northern Brazil experiencing wetter-than-normal conditions, while much of the southern half of Brazil and Bolivia were drier than normal. Paraguay had near-normal conditions for the year (Fig. 7.12).

During the 2019 austral summer, there were six episodes of the South Atlantic Convergence Zone (SACZ; Rosa et al. 2020), contributing to exceptionally wet conditions in the second half of January through February across Bolivia and Peru east of the Andes (see *Notable events and impacts* section). Northern Paraguay had extremely wet conditions in March, receiving over 300% more precipitation than normal. Furthermore, the Atlantic Intertropical Convergence Zone (ITCZ) was active in March, producing intense rainfall in northeast Brazil. After seven years of drought, the semiarid region of northeast Brazil recorded near-normal rainfall during November 2018–April 2019, but hydrological deficits persisted across most of the region. During November–December 2019, drought varied from severe to extreme in the northeast Brazilian semiarid region, particularly for the states of Piaui and Bahia, and in southern Brazil (see Fig. SB7.4). Below-normal precipitation was observed from July to October across most of Peru, Paraguay, and the Bolivian lowlands. The number of forest fires in those countries and the southern Brazilian Amazonia significantly surpassed the figures for the same period in the past four years (see Sidebar 7.2).

(III) NOTABLE EVENTS AND IMPACTS

Heavy rainfall events were observed in January along the dry southern coast of Peru, resulting in some locations breaking precipitation records of more than 30 years. Heavy rainfall during February led to 42 landslides across Peru and, by the end of summer, 77 people were reported dead, 165 wounded, and 3285 affected. More than 2600 homes were destroyed by floods and landslides.

In the Bolivian Andes, an intense rainfall event triggered flash floods when 55 mm fell in Cochabamba on 20 February. This was Cochabamba's fourth-highest daily precipitation on record and produced 2019's biggest flood on the Rocha River.

In Paraguay, daily precipitation exceeding 100 mm day^{-1} was observed in March, with 142 mm day^{-1} in Puerto Casado. On 10–11 May, extreme rainfall and floods were reported in the city of Pilar with 297 mm in two days, affecting about 10 000 families.

In Brazil, several episodes of intense rainfall occurred during summer and autumn, producing flash floods and landslides that affected homes and blocked roads. São Paulo's February 2019 precipitation was 137% of normal and was the wettest February in 15 years. On 6 February, 162 mm of rain fell in Rio de Janeiro in just 24 hours, which is more than half the normal monthly precipitation of 273 mm for February. On 8–9 April, another intense rainfall event affected Rio de Janeiro when a total of 189 mm of rain fell in 24 hours, almost double the monthly normal of 101 mm, producing landslides in the area. Similarly, on 10 April, rainfall was nearly twice the month's climatology in São Paulo. During 17–19 May, a total of 308 mm of rain was reported in

Santos, which is a little over twice May's normal precipitation total of 148 mm. On 12 June, 117 mm of rain fell in just six hours in Recife (monthly climatology of 389.6 mm). More than a month's worth of rain fell in a three-hour period in Salvador, capital of the Bahia State, on 26 November, with a total of 169 mm of rain (climatology of 106.5 mm). The heavy rains produced flooding and landslides across the city, leaving streets flooded and around 100 homes damaged.

3) Southern South America—L. Aldeco, J. L. Stella, N. Misevicius, D. Campos Díaz, and J. Vicencio Veloso

This region includes Argentina, Chile, and Uruguay.

(I) TEMPERATURE

The 2019 mean temperatures across most of southern South America (SSA) were slightly above normal (Fig. 7.11). Above-normal temperatures were limited to central and northern parts of Argentina and central Chile. Annual mean temperature anomalies ranged between −0.5°C and +1.2°C across the region. The 2019 national mean temperature anomaly for Argentina (+0.32°C) and Chile (+0.24°C) were each 12th highest of their respective national records dating back to 1961, while Uruguay had a near-average temperature, making it the 27th-warmest year on record, which also extends back to 1961 (Fig. 7.13).

Summer (December–February) 2018/19 was characterized by normal to below-normal temperatures across much of the region with pronounced sub-seasonal variability. Several episodes of extreme warm temperatures occurred during the season, with the most significant episode occurring in February. Southern Argentina and Chile set new daily maximum temperature records. On 4 February, the maximum temperature in Río Grande, Tierra del Fuego, rose to 30.8°C, marking the first time on record a temperature above 30°C was recorded so far south in South America.

Below-normal temperatures dominated the beginning of austral autumn (March–May). March was particularly cold over Argentina and Uruguay, with mean temperature anomalies ranging between −3°C and −1°C across a large area. Meanwhile, April and May had normal to above-normal temperatures across SSA.

Winter (June–August) was slightly warmer than normal across the region. However, the above-normal seasonal anomalies were driven by the well-above-normal temperatures in June. Uruguay and Argentina national temperature anomalies during June were +2.8°C and +1.5°C, respectively. June 2019 was Argentina's fifth-warmest June since 1961. Daily maximum temperatures were extremely high over Uruguay and northeastern Argentina. Artigas, Uruguay,

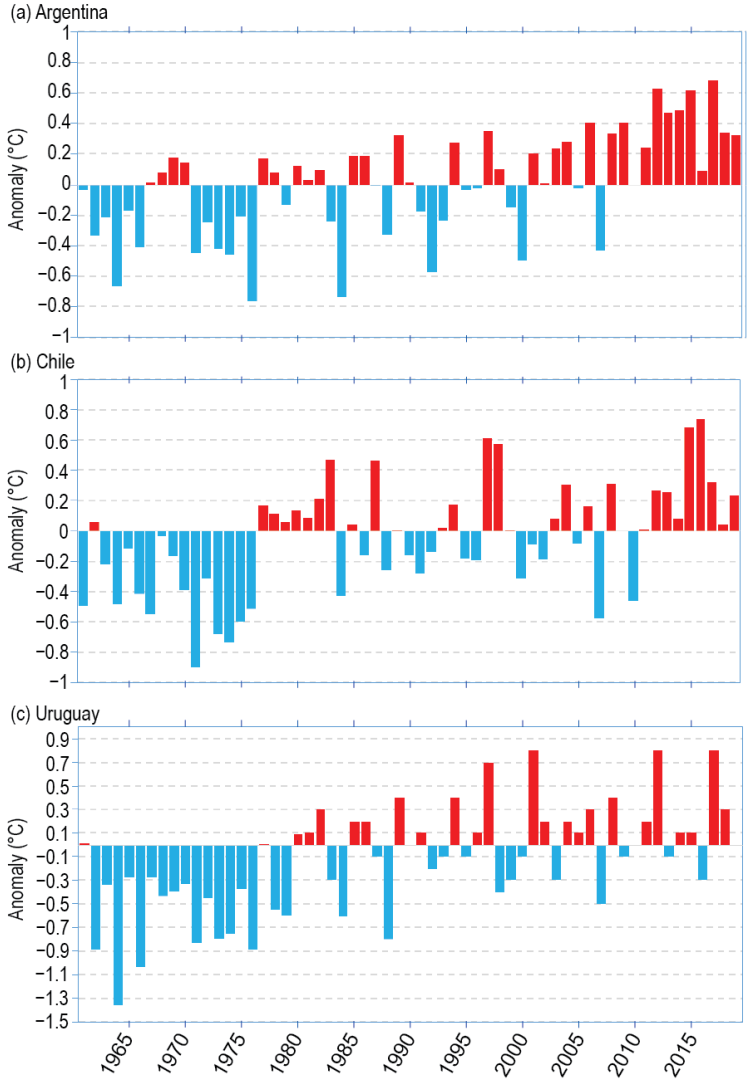

Fig. 7.13. Annual temperature anomaly (°C; 1981–2010 base period) time series from 1961–2019 for (a) Argentina, (b) Chile, and (c) Uruguay.

recorded a maximum temperature of 29.6°C on 13 June—the second-highest June daily temperature since 1981 for this location. A daily record was set in Posadas, Misiones, with a maximum temperature of 31.2°C on 29 June. Meanwhile, extreme cold conditions affected eastern Argentina and Uruguay during 1–9 July. August was particularly cold over Uruguay, which had an August national mean temperature anomaly of 1.2°C below normal.

Intraseasonal variability dominated during spring (September–November). Several cold eruptions, mixed with short warmer-than-normal periods, prevailed during September and October. Several daily records were broken in Argentina during this period. Orán, in the province of Salta, recorded its highest maximum temperature on record (44.5°C on 28 October). The cities of Pehuajó and Junín (Buenos Aires province) recorded their lowest minimum temperatures on record for September (–5.8°C and –5.4°C, respectively). November temperatures were well above average across the region, particularly over Uruguay and the central and northern parts of Chile and Argentina.

(II) PRECIPITATION

Much of central and southern SSA had below-average annual rainfall during 2019. Chile and central Argentina had the largest rainfall deficits, with 20%–60% of normal precipitation (Fig. 7.12). In south-central Chile, rainfall deficits in 2019 added to a prolonged drought that began there in 2010. The cities of Valparaiso and Curicó (Chile) and Bahía Blanca (Argentina) had their driest year on record since 1961. For Santiago, Chile, 2019 was the third-driest year since records began in 1866. Meanwhile, northeastern SSA experienced a wetter-than-normal year, with the most significant anomalies ranging between 120% and 140% of normal across Uruguay and scattered areas in Argentina.

Despite the weak El Niño present in the tropical Pacific Ocean at the beginning of the year, sub-seasonal forcings were quite active and modulated precipitation patterns. While January 2019 had heavy rainfall and flooding over northeastern SSA, February turned particularly dry in the same region.

During austral autumn, the lack of precipitation continued to affect the central parts of Chile and Argentina, reinforcing drought. In addition, Uruguay had drier-than-normal conditions. Meanwhile, northern SSA had above-normal rainfall.

Winter and spring were characterized by below-normal precipitation across much of SSA, while Uruguay and adjacent areas in Argentina had above-average precipitation.

(III) NOTABLE EVENTS AND IMPACTS

Figure 7.14 depicts extreme climate and weather events that affected the region, several of which are described in further detail below.

The year 2019 began with extraordinary precipitation over northeastern Argentina and Uruguay, producing major damage, flooding, and forcing evacuations. During 6–17 January, several storms with daily rainfall totals of up to 250 mm severely affected this region. Monthly precipitation amounts of more than 500 mm led to new January precipitation records: Artigas (670.3 mm) and Paysandú (541.3 mm) in Uruguay; Monte Caseros (644.0 mm), Paso de los Libres (622.0 mm), and Resistencia (554.8 mm) in Argentina.

In the Atacama Desert in northern Chile, intense rainfall and storms during the first half of February caused flooding, affecting thousands of people and cutting off roads, especially for coastal locations between Arica and Antofagasta. At the same time, southern Chile and Argentina were affected by intense heat waves. Twelve locations in Chile and five in Argentina set new all-time high daily maximum temperature records, including 38.5°C in Valdivia, 38.2°C in Perito Moreno, 35.8°C in Río Gallegos, 35.4°C in Bariloche, and 35.1°C in Puerto Montt. The extreme high temperatures over Patagonia triggered severe bush fires near the city of Cochrane. This was one of the largest and most destructive bushfire events in Chile's history, lasting three months and burning about 15 000 ha of native forest (Fig. 7.14).

At the end of May, central and southern Chile experienced an unprecedented occurrence of at least seven tornadoes recorded between 30 and 31 May. These produced major damage to infrastructure, buildings, homes, and vehicles. The unusual phenomenon injured hundreds of people, caused one fatality, and produced massive power outages. Two tornadoes reached F2 category in Los Angeles on 30 May, and one reached F1 in Concepción on 31 May (Fig. 7.14).

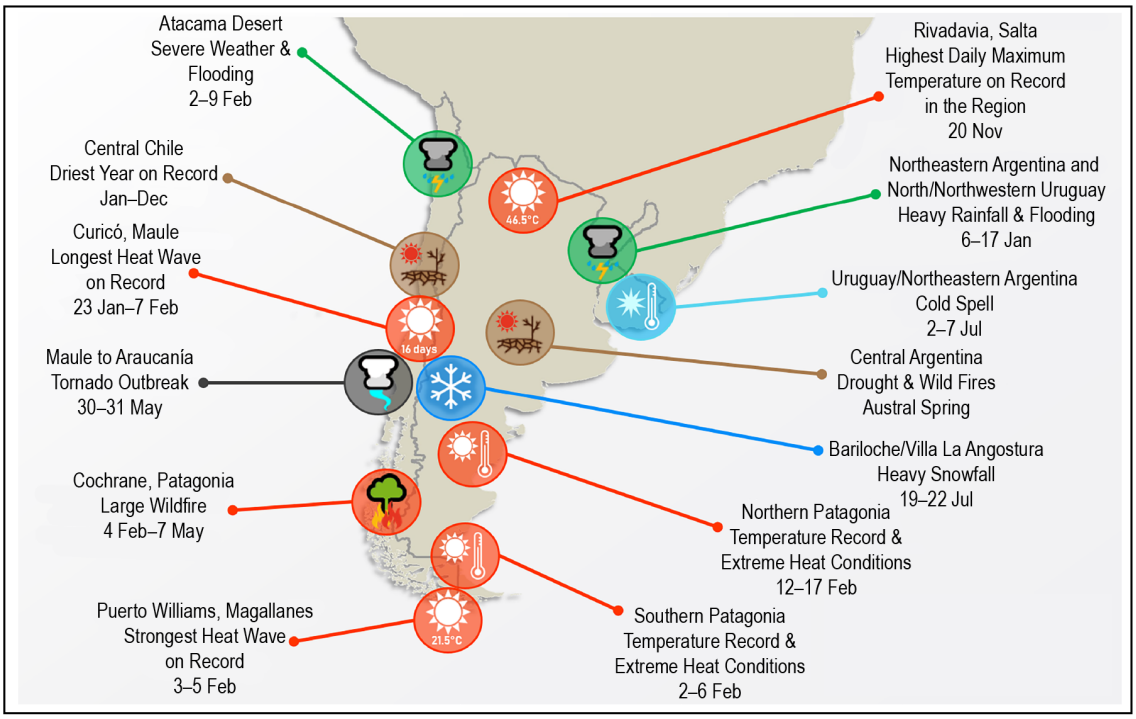

Fig. 7.14. Map depicting date, approximate location, and type of extreme weather events across SSA.

SIDEBAR 7.2: **Fires in southern Amazonia in the dry season of 2019**—J. MARENGO, L. ALVES, J. MOLINA, E. BROEDEL, AND A. P. CUNHA

Forest wildfires are common in the Amazon. Fire activity in the Amazon varies considerably from month to month and year to year, and it peaks during Brazil's dry season from July to October. Fires are primarily driven by drier seasonal conditions and occur in association with human management—farmers or ranchers clearing existing farmland, or illegal land-grabbers destroying trees. As witnessed in 2019, wildfires scorched vast areas of the southern Amazon region and northern Paraguay. According to the Monitoring of the Andean Amazon Project (MAAP 2019), fires burned in the Amazonian forest in Bolivia, Brazil, and Peru during the year.

The number of fires detected in the Brazilian Amazon region was 89 178 in 2019, compared to 68 345 fires in 2018. The number of fires in 2019 significantly surpassed the figures of the past four years. The number of fires peaked in August, with 30 868 fires widespread across the southern and eastern Amazon. The fire-monitoring program of the National Institute for Space Research also identified a larger-than-normal number of fires in 2019 in other Brazilian ecosystems such as Pantanal (a wetland in the upper reaches of the Paraguay River basin) and Cerrado (a large tropical savanna across central Brazil). In addition, the Brazilian Amazon experienced deforestation of 976 200 hectares in 2019 compared to 753 600 hectares in 2018.

Other Amazonian countries were affected by wildfires to some degree. Brazil and Bolivia struggled to curb massive forest fires in 2019. Fires affected 6.4 million hectares in Bolivia in 2019, significantly above the 3.5 million hectares yearly average, and the second largest surface burned in a year (FAN 2019). The most affected Bolivian region was Santa Cruz (65% of the burned surface), followed by Beni (29%), and northern La Paz (5%). In Santa Cruz, forests represented 31% of the burned surface, particularly the Chiquitanian dry forest (1.46 million hectares). These losses resulted in the death of millions of trees and wild animals, and in some cases, caused local extinctions. National protected areas were also affected (1.25 million hectares). Five firefighters and several hundred cattle died, and hundreds of homes were burned. In Paraguay, blazes destroyed tens of thousands of hectares of protected wetlands and other areas.

Beginning in mid-August, the country lost roughly 40 000 ha of forest from the perennial floodplains in the north of its sparsely populated western Chaco region (SEN 2019).

In 2019, the large number of monthly burned areas was related to a weak El Niño event, associated with below-average precipitation during the austral summer in some locations in southern Amazonia. (It was identified, but the illegal burning worsened that situation.) This, in turn, caused droughts and significant water reduction in the forest due to higher temperatures and lower atmospheric humidity. The illegal burning of land and crops complicated the situation by augmenting the risk of forest fires.

Figure SB7.3 shows a time series of rainfall from January 2015 to December in 2019 in southern Amazonia. The drought during the 2015/16 El Niño is clear in the figure, with 50–100 mm month^{-1} below normal from November 2015 to February 2016 (with the exception of January 2019 that was 20 mm month^{-1} above normal). From December 2018 to January 2019, rainfall was about 50 mm month^{-1} below normal, while rainfall during the rest of the year was near normal, with small negative rainfall anomalies in August and September. The below-normal rainfall during December 2018–January 2019—the peak of the rainy season—probably contributed to drier-than-normal soil conditions at the end of the rainy season. Figure SB7.4 shows monthly maps of drought intensity for Brazil in 2019. The maps from January to March depict mostly weak-to-moderate drought in southern Brazilian Amazonia, consistent with below-normal rainfall that persisted through August. Figure SB7.3 shows that rainfall deficits during the dry season were small.

Therefore, rainfall reductions during the summertime peak of the rainy season may be in part responsible for the fires during the winter season, while during the dry season (fire season), drought across the southern Amazonia was mostly weak.

According to the International Federation of Red Cross and Red Crescent, no human injuries or fatalities were reported due to the 2019's forest fires. However, these fires affected biodiversity, fauna, flora, and generated negative impacts on the Amazon biome. Wildfires have the potential to be extremely destructive, burning large areas of forests and regions recently deforested and producing smoke that affects ecosystems and people even outside the Amazon region. On 19 August, smoke from wildfires burning about 3000 km away in the Amazon shrouded the megacity of São Paulo in darkness. This was caused by a cold front from the southeast running into warm winds bringing fire smoke particles from southern Amazonia and Paraguay over the city of São Paulo.

Drought-induced fires may be partially offsetting reductions in Amazonian deforestation fires since ~2000. Preserving rainforests and restoring former forested land, together with wildfire management, are economical ways to meet climate change mitigation targets (Aragão et al. 2018).

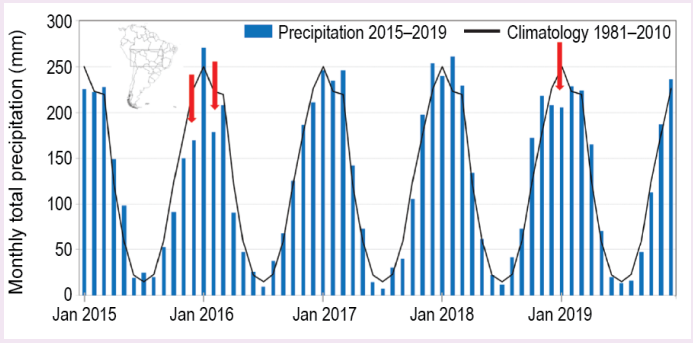

Fig. SB7.3. Mean monthly rainfall and rainfall anomalies (mm) in southern Amazonia (see map with location of the region under analysis in upper left corner). Red arrows show the drought of 2015–16 and the less-rainy-than-normal peak of the rainy season from Dec 2018 to Jan 2019. (Source: CHIRPS dataset [Funk et al 2014].)

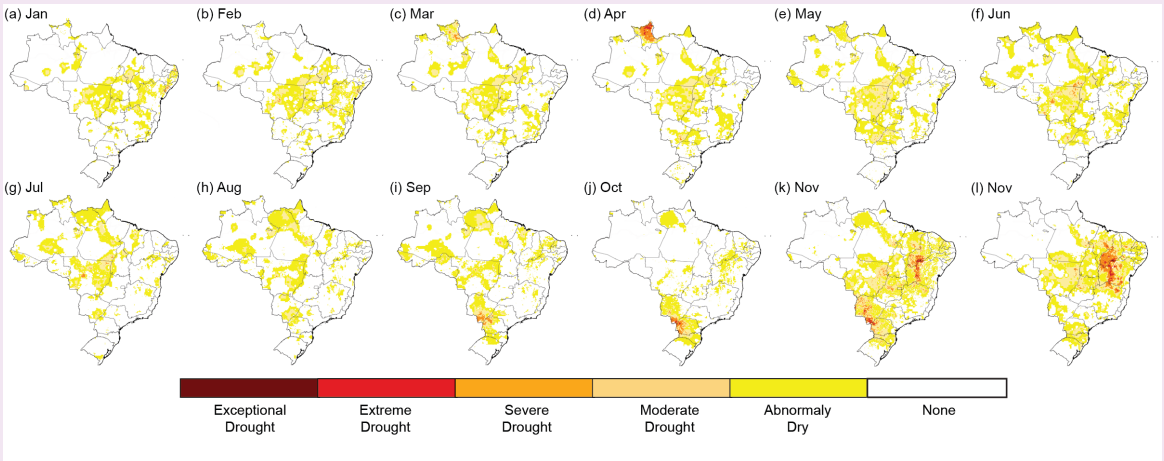

Fig. SB7.4. Monthly maps of drought characterization for Brazil in 2019, based on the Standard Precipitation Index-6 month (SPI-06, provided by CPTEC INL) and the Vegetation Health Index (VHI, provided by NOAA). The methodology for drought characterization is explained in Cunha et al. (2019).

e. Africa—A. Mekonnen, Ed.

This report was compiled using observational records from the meteorological and hydrological services of Morocco, Algeria, Tunisia, Egypt, Nigeria, South Africa, and the southern Indian Ocean island countries of Seychelles, Mayotte (France), La Réunion (France), Mauritius, and Rodrigues (Mauritius). Global Precipitation Climatology Project (GPCP) rainfall data and reanalysis data from the National Centers for Environmental Prediction/National Center for Atmospheric Research (NCEP/NCAR) were also used. Fatalities and flooding hazards are as reported in news outlets or by official agencies. The climatological base period used is 1981–2010.

In 2019, most of Africa (south of 10°N and east of 20°E) experienced above-normal surface air temperatures. Northern Nigeria, southern Niger, and southwestern Chad experienced below-normal air temperatures (Fig. 7.15). Annual rainfall was generally above normal over the Sahel and savannas north of the equator, equatorial Africa, and the region between the equator and 15°S. Excessive rainfall in 2019 was observed over the eastern half of Tanzania, Mozambique, and onshore over the Indian Ocean north of Madagascar. Southern Africa south of 15°S experienced mostly below-normal rainfall in 2019 (Fig. 7.16). Below-normal rainfall was observed over southeastern Nigeria, southwestern Cameroon, Equatorial Guinea, and northwestern Gabon.

Extreme weather events were reported in several African countries. In August, September, and October, North Africa reported storm events and flooding that resulted in deaths and property damage. West Africa received 24-hour rainfall totals ranging from about 69 mm to 110 mm, which caused widespread flooding and the Niger River to overflow. Many people died and hundreds of others were displaced. Severe damage to property and croplands was also reported. Extreme rainfall was reported from the Greater Horn of Africa countries in October. Mombasa (Kenya)

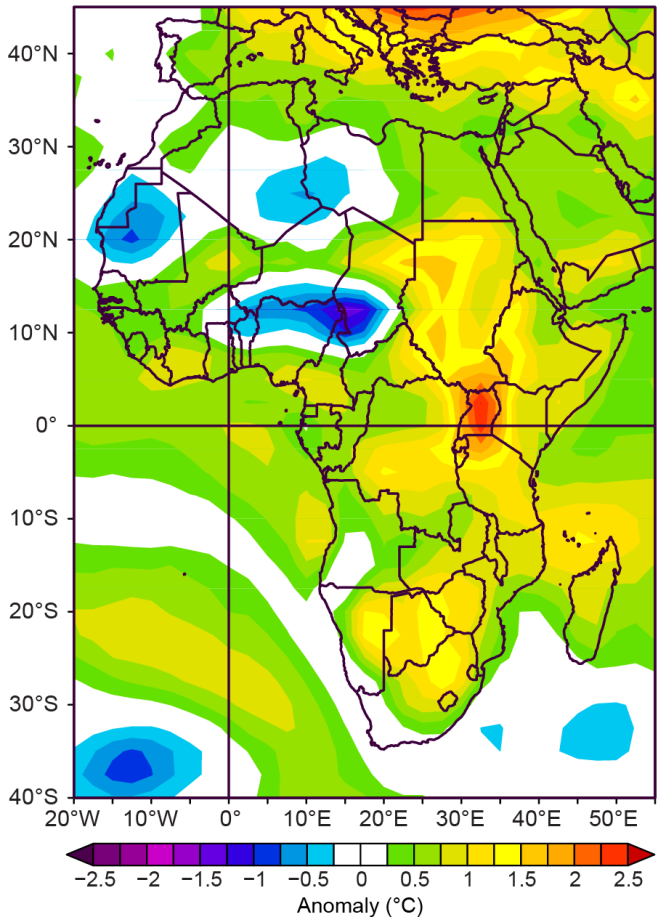

Fig. 7.15. Mean annual air temperature anomaly (°C; 1981–2010 base period) for 2019 over Africa. (Source: NOAA/NCEP.)

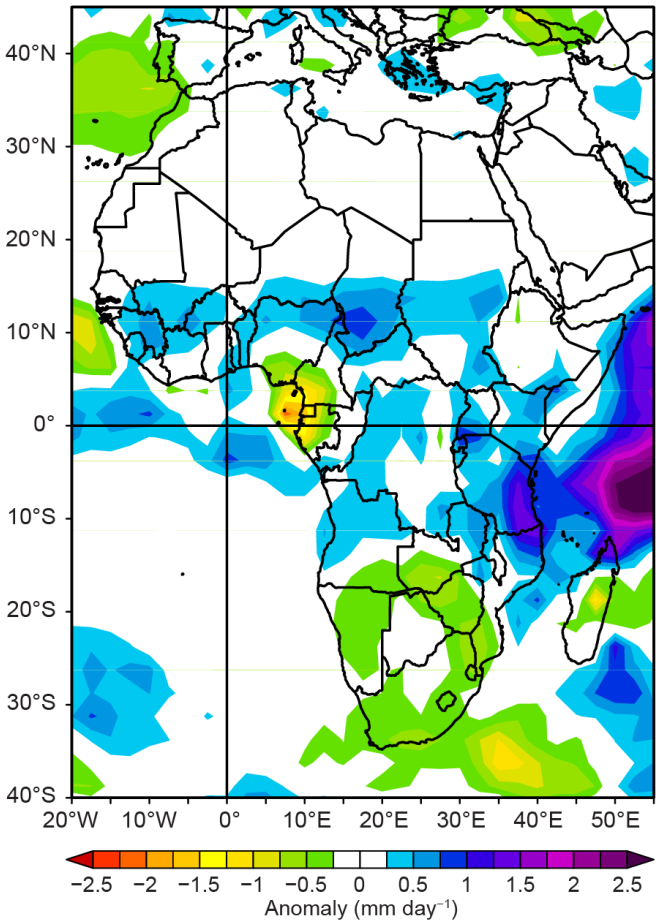

Fig. 7.16. Mean annual rainfall anomaly (mm day^{-1}; 1981–2010 base period) for 2019 over Africa. (Source: NOAA/NCEP.)

reported more than five times its normal October rainfall, as did Kinshasa and Pt. Noire in the Republic of Congo. Windstorms in The Gambia affected many communities and caused numerous deaths. Heat waves, with daytime temperatures exceeding 40°C, were also reported in North African countries, and Morocco and Algeria reported forest fires.

This year, due to unforeseen circumstances, the Southern Africa section contains analyses for South Africa only. We hope to return to a fuller analysis of the region next year, to once again include the countries of Angola, Botswana, Zimbabwe, Namibia, Malawi, Zambia, Lesotho, Swaziland, and Mozambique. We do include a sidebar that describes the impacts of Cyclones Idai and Kenneth to southeastern Africa and the southwest Indian Ocean islands.

1) North Africa—K. Kabidi, A. Sayouri, M. ElKharrim, and A. E. Mostafa

Countries considered in this section are Morocco, Algeria, Tunisia, Libya, and Egypt.

In 2019, the annual temperature over Morocco was about 0.3°C above normal, while annual precipitation was about 136% of normal (54% less than in 2018). The annually averaged temperatures in southern and central Algeria were near normal, while northern Algeria and Tunisia were above normal. Several climate stations in Egypt observed above-normal temperatures during the summer. Severe storms, heat waves, and forest fires were reported in Morocco and Algeria.

(I) TEMPERATURE

Winter (December 2018–February 2019) mean temperatures over Morocco, Algeria, Tunisia, and Libya were below normal, while above-normal temperatures were observed over Egypt (Fig. 7.17a). In January and February, temperatures approximately 2.8°C below normal were reported in the mountain regions while temperatures 0.5°–2°C below normal were reported across Morocco's coastal and interior regions. Stations from southern Algeria and Libya reported temperatures up to 3°C below normal in February.

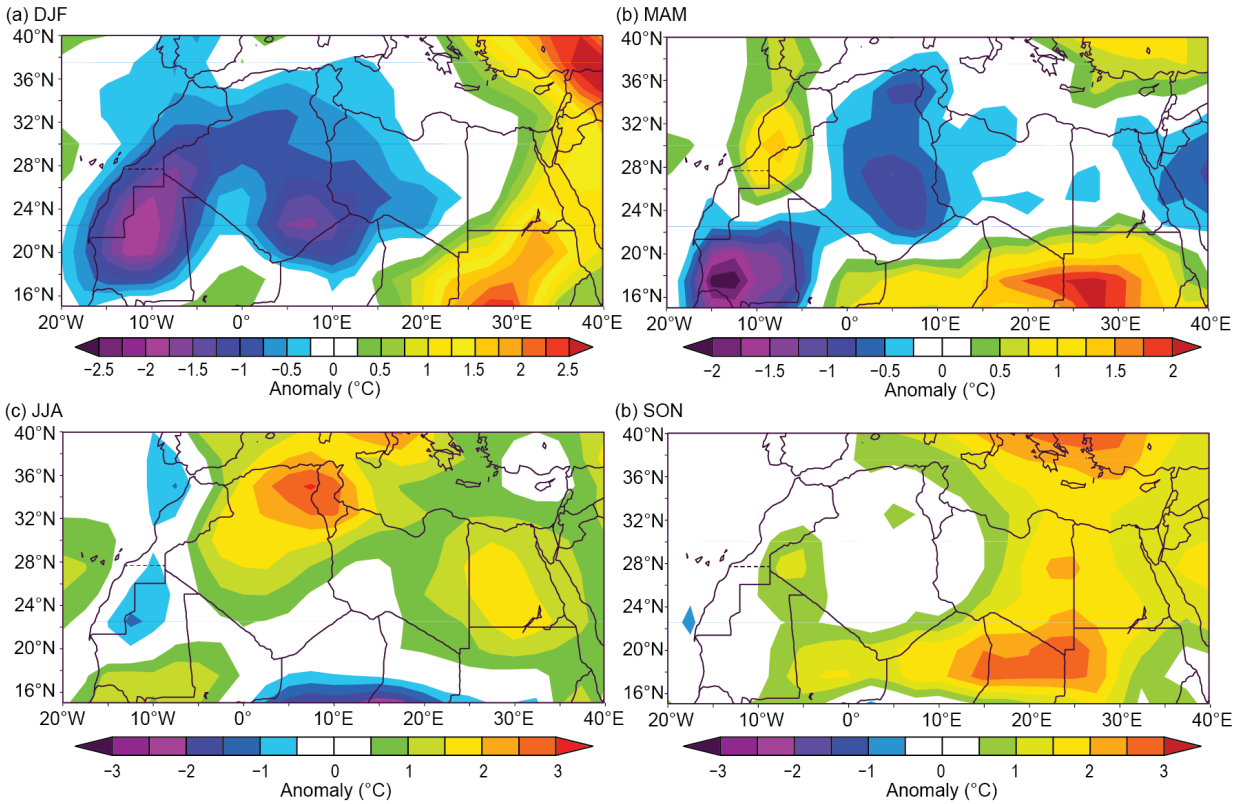

Fig. 7.17. North Africa seasonally averaged mean temperature anomalies (°C; 1981–2010 base period) for (a) DJF 2018/19, (b) MAM 2019, (c) JJA 2019, and (d) SON 2019. (Source: NOAA/NCEP.)

Spring (March–May) temperatures over most of Morocco were 1°C above normal, while temperatures over most of Algeria, Tunisia, and western Libya remained below average (Fig. 7.17b), and those across Egypt were mainly near normal. Southern Morocco and adjoining southwestern Algeria experienced temperatures more than 3.5°C above average in May (not shown). In contrast, May temperatures of about 2.5°C below normal were observed in northeastern Algeria-Tunisia (not shown).

Summer (June–August) temperatures over the region were above normal—more than 2.5°C above normal over the Algeria–Tunisia border. Most of Egypt experienced summer temperatures 1.5°C above average (Fig. 7.17c). Some stations in Tunisia, Algeria, and Libya reported summer temperatures 4°C above normal. Record high temperatures of 47°C were recorded in Egypt in June. More record temperatures, ranging from 43.5°–50°C, were reported at several stations in Algeria during July.

Autumn (September–November) temperatures were near to above normal, with generally warmer-than-normal conditions across eastern portions of the region (Fig. 7.17d). Most of Libya and Egypt saw temperatures between 1°C and 2°C above normal.

(III) PRECIPITATION

Winter precipitation over Morocco, western Algeria, and northern Tunisia was below normal. Pockets of southeast Tunisia bordering Libya received above-average rainfall, as did northern Egypt near Alexandria (Fig. 7.18a). Heavy rains were reported at Alexandria and several stations in northern Egypt.

Below-normal rainfall occurred in spring over northern and coastal parts of Morocco and northwestern Algeria, while a small area in northern Egypt recorded slightly above-average precipitation (Fig. 7.18b). Several April storms that produced copious rainfall helped alleviate the dryness in Morocco. Different parts of Morocco received above-average rainfall for the month, ranging from 114% to 225% of normal in the south, 139% to 174% in the north, and 139% to 198% in central Morocco.

Summer rainfall over North Africa was near normal (Fig. 7.18c), although station reports indicated strong monthly variability. Autumn brought near-normal rainfall to most of the region

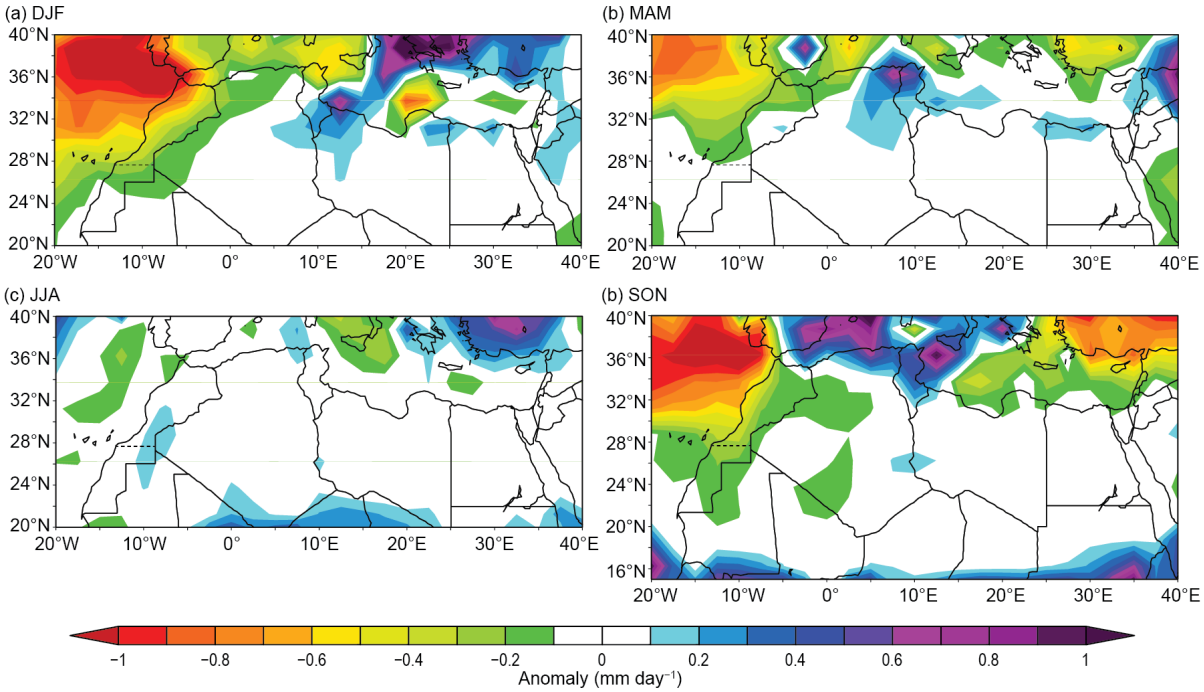

Fig. 7.18. North Africa seasonally averaged rainfall anomalies (mm day^{-1}; 1981–2010 base period) for (a) DJF 2018/19, (b) MAM 2019, (c) JJA 2019, and (d) SON 2019. (Source: NOAA/NCEP.)

(Fig. 7.18d), except for Morocco's Atlantic coast, which saw a dry start to its wet season with deficient November rains, relative to climatology.

(III) NOTABLE EVENTS AND IMPACTS

A succession of heat waves (temperatures ≥ 40°C) occurred in Morocco, Algeria, and Tunisia during May and July. As a result of the heat, along with dry conditions, more than 200 fires caused significant damage in northern Morocco, while more than 20 000 hectares were burned in eastern Algeria.

In August, southern Morocco experienced several storms that resulted in floods. Deaths and property damage associated with this extreme weather were reported. During September and October, severe storms that brought heavy rain were reported in Algeria (for example, 147 mm of rain fell on 1 September in the town of Skikda, which is close to five times its September average and about 20% of its annual total).

2) West Africa—S. Hagos, Z. Feng, I. A. Ijampy, F. Sima, and S. D. Francis

For this report, West Africa is defined as the region between 17.5°W (the eastern Atlantic coast) and approximately 15°E (along the western border of Chad) and from 5°N (near the Guinean coast) to 20°N. It is typically divided into two climatically distinct sub-regions: the Sahel region (north of about 12°N) and the coast of Guinea region to the south. The Sahel is semi-arid, while the coast of Guinea region has a wet tropical climate. West Africa's rainy period (the West African monsoon [WAM] season) is associated with the latitudinal movement of a section of the deep convective zone, and the season extends from June through September. Variations of the north–south movement of the deep convective zone are controlled by the El Niño–Southern Oscillation (ENSO), cross-equatorial sea surface temperature (SST) contrasts over the equatorial Atlantic, as well as SSTs over the Mediterranean Sea (Rodriguez-Fonseca et al. 2015). The boreal spring and summer of 2019 had near-neutral ENSO conditions with a Niño 3.4 index of around 0.5 (see section 4b for details). In general, the SSTs over the tropical Atlantic Ocean and the Mediterranean Sea were close to the climatological average, except for the region off the coast of Senegal, which was cooler by up to –1.0°C throughout the summer season.

(I) TEMPERATURE

In 2019, annual temperatures in the region west of the prime meridian and south of about 15°N in West Africa were generally above average, while the border areas between Niger, Nigeria, and Chad were below average (Fig. 7.15).

Overall, the 2019 hot season (March–May) was generally warmer than normal in northern Nigeria, except in Ilorin, where it was cooler. Daily maximum temperatures of 44°C were recorded in the Nigerian cities of Maiduguri, Sokoto, and Yola between 4 and 6 April, about 3°C above average. Notably, Maiduguri reported daily maximum temperatures of 40°–44°C for 26 days in April.

The summer temperature over much of West Africa was slightly above average, with much-warmer-than-average conditions over northern Senegal, southern Mauritania, and the Niger Delta region (not shown). Figure 7.19 shows the average temperature anomaly in June, which was particularly high over central Cameroon, southern Mali, southern Mauritania, and Guinea. These regions experienced temperatures at least 2°C above average for the month. Meteorological stations across Nigeria reported monthly mean maximum temperatures ranging from 31.7°C in Jos in the Middle Belt to 41.0°C in Sokoto and Maiduguri in the north. In southern Nigeria, Eket and Oshogobo recorded mean maximum temperatures of 30.2°C and 36.7°C, respectively.

(II) PRECIPITATION

Precipitation over the Sahel region was significantly higher than normal during the WAM season (Fig. 7.20), while southern (Guinean) and western coastal regions were drier. This pattern is a typical mode of precipitation variability over West Africa. In 2019, it was likely related to persistent below-average SSTs off the coast of West Africa. Several single-day rainfall values of 100 mm and above were observed in northern Nigeria during the season.

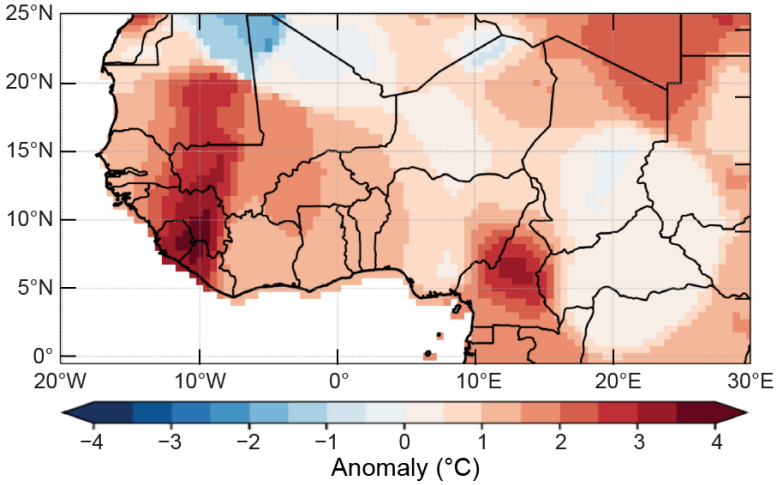

Fig. 7.19. Mean temperature anomalies (°C; 1981–2010 base period) for West Africa in Jun 2019. (Source: NOAA/NCEP.)

(III) NOTABLE EVENTS AND IMPACTS

In 2019, extreme events started early before the summer season. On 13 May, several areas in Ghana experienced heavy rain. The national capital, Accra, recorded 75 mm and Tema observed 52 mm of rainfall over two days, about half and one-third of their average monthly totals for May, respectively. At least 14 people died in flash flooding triggered by sudden torrential rain in Mali's capital city of Bamako on 16 May. According to the Red Cross, the floods also destroyed two houses and 10 cars while several people were forced to move to temporary shelters. According to the International Organization for Migration (IOM), in June heavy rains in Mali's Mopti region caused floods, exacerbating the dire conditions of internally displaced persons. Local news outlets in Sierra Leone reported that four people died after flash floods in the capital, Freetown, on 2 August. In the same week, rainstorms and flooding occurred over northeastern Nigeria. The News Agency of Nigeria (NAN) reported that seven people died while dozens of houses were damaged in Yola. In the southeastern part of the country, heavy rain on 4 August caused flooding in Oguta, displacing about 6000 people and damaging 200 homes. In late August and early September, northeastern Nigeria was once again affected by floods. The United Nations Office for the Coordination of Humanitarian Affairs (UNOCHA) reported that at least 10 people died, with thousands displaced in Borno, Adamawa, and Yobe states. In Ngala, over 600 homes were destroyed. The total number of affected persons was estimated to be 3500. In Niger, the UNOCHA reported that floods caused by heavy rains dating to June killed 57 people and affected 211 000 because the Niger River reached flood stage. Overflow from dams in neighboring Burkina Faso and Mali contributed to the surging waters.

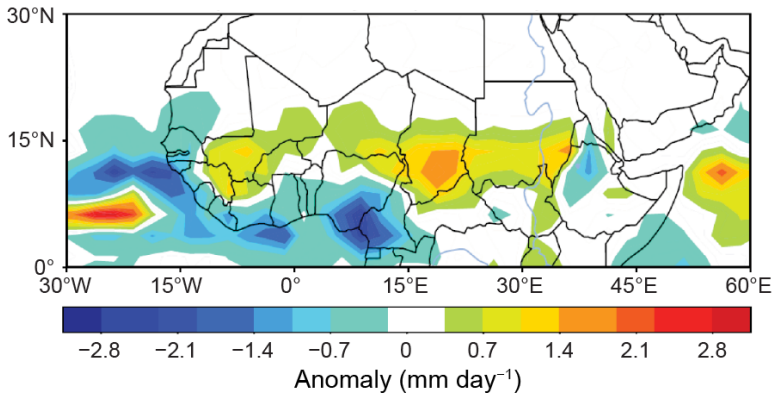

Fig. 7.20. Departure of Jun–Sep 2019 rainfall (mm day^{-1}; 1981–2010 base period) for West Africa. (Source: Global Precipitation Climatology Project [GPCP].)

In The Gambia, on 19 June, a windstorm hit five districts in the Upper River Region—Jimara, Tumanna, Wuli East, Wuli West, and Sandu—and three districts of the Central River Region—Upper Fulado East, Upper Fulado West, and Niani. This storm affected 67 communities according to the International Federation of Red Cross and Red Crescent Societies. The Gambia Red Cross Society and National Disaster Management Agency reported that over 15 000 people were

affected, including 1425 people who were displaced. Per their report, there were four fatalities due to building collapse and flying debris. In addition, 101 people were injured, and more than 900 houses were damaged or destroyed. According to the National Meteorological Department of The Gambia and authorities in the affected regions, this was the first time in recorded history that Gambia had experienced such a windstorm disaster with this scale of destruction. On 31 August, heavy downpours caused flooding in many households in Ebo-Town.

Similarly, in Mauritania, the country's news agency reported that at least five people died in floods there, and dozens of homes were damaged or destroyed in the Guidimaka Region following heavy rains that began around 25 August. Fatalities were reported in Sélibaby City, the regional capital with a population of around 26 000. Roads, bridges, and other infrastructure were also damaged.

3) East Africa—B. D. Enyew and A. Mekonnen

The East African region includes Kenya, South Sudan, Sudan, Uganda, Tanzania, Ethiopia, Eritrea, and Djibouti (an area within 10°S–15°N, 20°–50°E, also referred to as the Horn of Africa). The region has complex terrain, with elevations ranging from about 100 m below sea level at Ethiopia's Afar triangle to more than 4000 m above sea level at the Semien Mountains and Mount Kilimanjaro in Tanzania-Kenya.

The complex terrain and the geographic placement of East Africa give rise to different climatic zones—from very dry and arid to wet and humid. The rainfall climatology is also complex. Lower latitude regions such as Kenya, Uganda, southern Ethiopia, and parts of Somalia and Tanzania have two peak rainy seasons during March–May and October–December. Central, western, and northern Ethiopia, Sudan, and South Sudan have a single dominant peak rainfall season during June–September (JJAS). In western, northwestern, and northern Ethiopia, climatologically, over 70% of annual rainfall is received during JJAS, locally referred to as "Kiremt." Central and northeastern Ethiopia also receive short rains during mid-February to mid-May, a time locally referred to as "Belg." Therefore, while the temperature analysis is based on four seasons (winter, spring, summer, and autumn), the 2019 rainfall analysis is presented based on January–February (JF), March–May (MAM), June–September (JJAS), and October–December (OND). As in West Africa, rainfall over East Africa is influenced by SST changes over the equatorial Atlantic, equatorial east Pacific, and Indian Oceans (Bahaga et al. 2019). Temporal and spatial variability of the deep convective zone associated with seasonal rainfall over East Africa are also determined by large-scale circulation systems and moisture transport from the southern Atlantic and Indian Oceans.

(I) TEMPERATURE

Generally, annual temperatures for 2019 in East Africa were above normal, with Uganda and bordering areas observing temperatures more than 2°C above normal (Fig. 7.15).

The region experienced above-normal temperatures during winter (December 2018–February 2019), spring (March–May), and autumn (September–November), with some areas more than 3°C above normal (Fig. 7.21). Largely near-normal temperatures dominated the region during summer (June–August), except pockets of central Sudan, where temperatures were below normal, and southwest Ethiopia and Uganda, where temperatures were about 1°C above normal.

(II) PRECIPITATION

Figures 7.22a–d show the 2019 rainfall anomaly for the four rainfall seasons defined above. East Africa north of 5°N is normally a dry season during JF. During JF, below-normal rainfall dominates the Lake Victoria region (eastern Uganda–western Kenya–northwestern Tanzania). During MAM, below-normal rainfall was observed over the region around Lake Victoria, including most of Kenya, Uganda, and northern Tanzania. Southeastern coastal Tanzania experienced above-average rainfall (Fig. 7.22b). During JJAS, central Sudan and northern South Sudan experienced

above-normal rainfall, while the western-most parts of Ethiopia experienced below-average rainfall (Fig. 7.22c). The Kiremt (JJAS) rainfall over most of Ethiopia was near normal. For equatorial countries such as Kenya, JJAS is normally dry.

Rainfall was above normal from the southern half of Ethiopia southward to Tanzania during OND (Fig. 7.22d). Rainfall of more than 3 mm day^{-1} above normal was observed around the Lake Victoria region and eastern Tanzania. The Famine Early Warning System Network (FEWS-NET; https://fews.net/east-africa/) reported that the OND rainfall total was among the highest in the region since 1981. The FEWS-NET report indicated excessive rains were associated with the positive Indian Ocean dipole (IOD), which was the strongest since 1997 (see section 4h for more details).

(III) NOTABLE EVENTS AND IMPACTS

The following notable events are based on information from FEWS-NET during OND 2019.

Widespread flooding over South Sudan caused extensive damage to crops and livestock, affected several hundred people, and displaced nearly half a million citizens. Similar damage was reported from Somalia. In southern Ethiopia, Kenya, and Uganda, loss of human lives, crop damage, and extensive flooding affected communities.

Widespread locust invasion was reported from Eritrea southward through eastern Ethiopia, Kenya, and Sudan to Somalia. The following conditions were favorable for locust invasions during the season: heavy rainfall, moist soil conditions, abundant vegetation, and dominant northerly/northeasterly persistent winds. The locust infestation led to extensive crop and vegetation damage over the region.

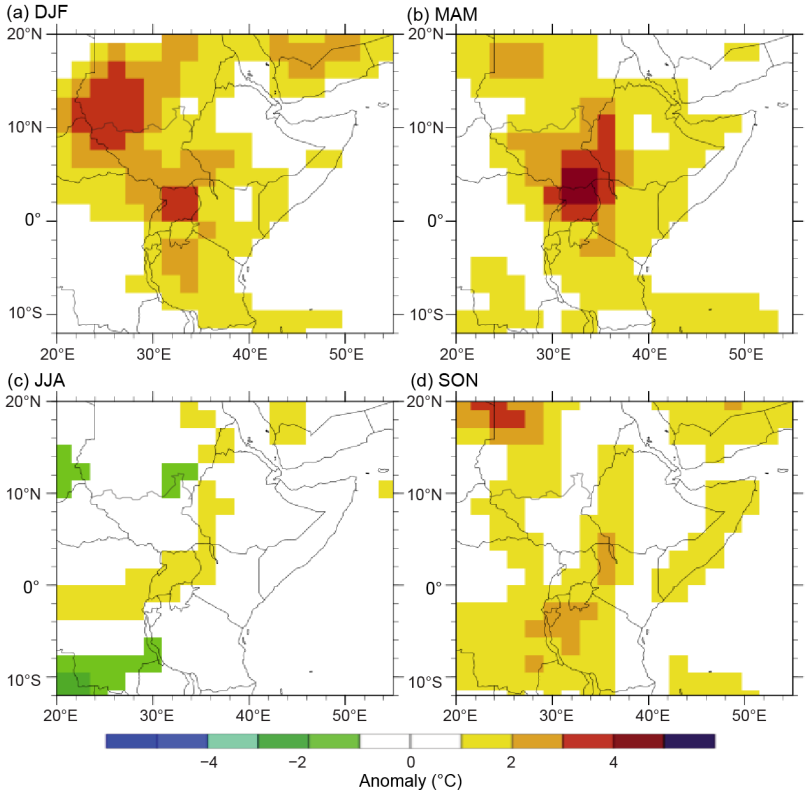

Fig. 7.21. Temperature anomaly (°C; 1981–2010 base period) for (a) Dec 2018–Feb 2019, (b) Mar–May 2019, (c) Jun–Jul 2019, and (d) Sep–Nov 2019 over East Africa. (Source: NCEP/NCAR reanalysis.)

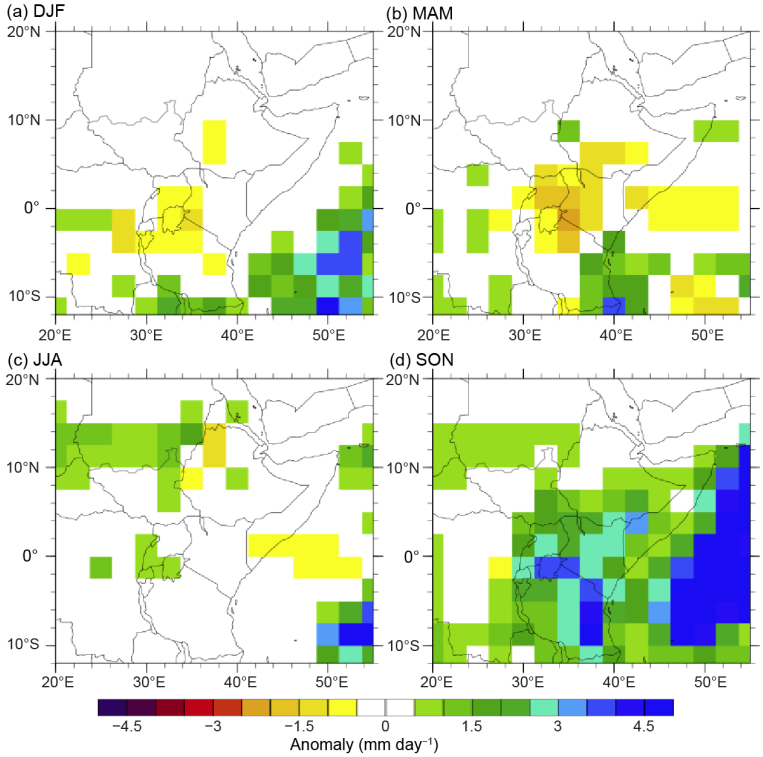

Fig. 7.22. East Africa rainfall anomaly (mm day–1; 1981–2010 base period) in 2019 for (a) Jan–Feb, (b) Mar–May, (c) Jun–Sep, and (d) Oct–Dec over East Africa. (Source Global Precipitation Climatology Project [GPCP].)

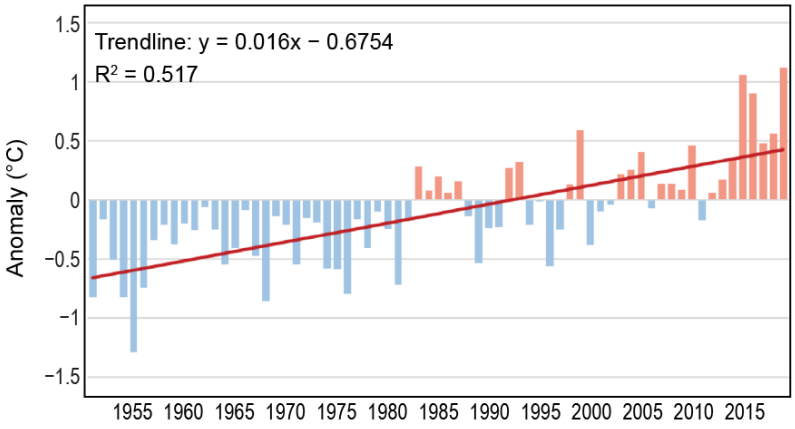

Fig. 7.23. Average surface temperature deviation (°C; 1981–2010 base period) over South Africa based on 26 climate stations: 1951–2019. The linear trend is indicated. (Source: South African Weather Service.)

2) South Africa—A. C. Kruger and C. McBride

(I) TEMPERATURE

South Africa experienced a very hot year. The 2019 annual mean temperature anomalies, based on data from 26 climate stations, was about 1.1°C above the reference period (1981–2010), an approximate tie with 2015 for the warmest year on record since 1951 (Fig. 7.23). The nation's warming trend of 0.16°C decade^{-1} is statistically significant at 5%.

(II) PRECIPITATION

The dry conditions in western South Africa were the most significant feature of the rainfall during 2019 (Fig. 7.24). A substantial area received less than 50% of normal rainfall, while the southwestern part and eastern half of the country received rainfall amounts close to normal. Figure 7.25 presents the 12-month standardized precipitation index (SPI), a widely used index to characterize meteorological drought, for 2019. Somewhat dry to moderately dry conditions dominated the northern and northeastern parts of the country. No significant area of South Africa received substantially more than the normal amount of rainfall.

(III) NOTABLE EVENTS AND IMPACTS

Dry conditions persisted over larger parts of western South Africa, in some parts having continued for approximately seven years. The effects of these prolonged dry conditions are mainly agricultural, resulting in no significant production on many farms, with the subsequent layoffs of farm workers.

In January, these dry conditions persisted

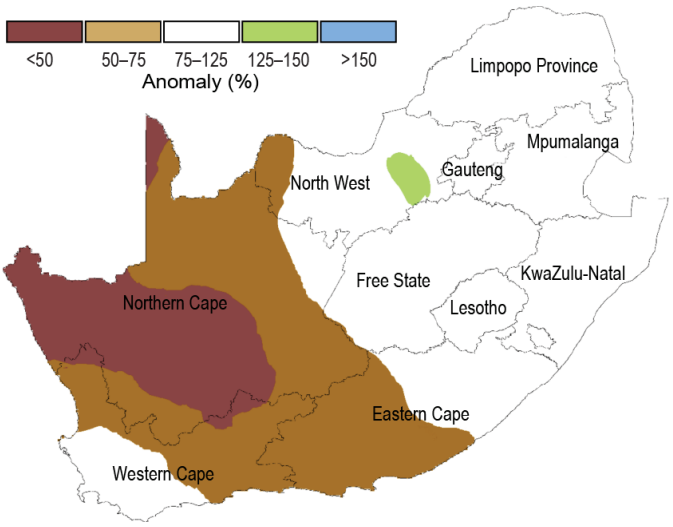

Fig. 7.24. Rainfall anomalies (expressed as percentage of 1981–2010 base period) for South Africa for 2019. (Source: South African Weather Service.)

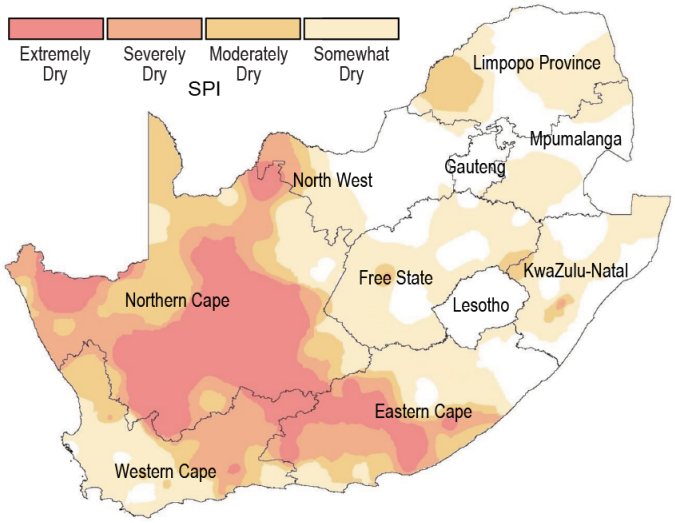

Fig. 7.25. Twelve-month SPI map for South Africa for 2019. (Source: South African Weather Service.)

in most parts of the western interior, with warmer-than-usual conditions in the central parts. Good rains were received in the Limpopo province with several weather stations breaking daily and monthly rainfall records. By March, the eastern parts received good rains that persisted into April. However, heavy rain in the KwaZulu-Natal province on 22 and 23 April caused severe flooding that resulted in extensive damage to infrastructure and about 70 deaths. An additional 50 people were injured and 1469 people were displaced. The estimated damage was R1.1 billion (South African Rand; ~$66 million U.S. dollars), with damage in eThekwini (Durban) alone estimated to be more than R685 million (~$41.2 million U.S. dollars).

By austral winter a clear pattern emerged from the previous year's rainfall, which was below normal in most parts of the west and above normal in most of the eastern half of the country. Temperatures followed similar patterns, with very high temperatures recorded in the west, especially in May. June brought strong cold fronts reaching the southwestern Cape with accompanying flooding and displacement of people in the Cape Town metropolitan area. These incidents continued into July. High maximum temperatures were reported in the east during June and July, with places in extreme eastern South Africa more than 3°C above normal.

During the spring months, dry conditions persisted over the western interior. November saw a number of tornadoes in the eastern parts, with at least four occurring in the KwaZulu-Natal province. On 12 November, a tornado destroyed several houses in Mpolweni village near New Hanover in KwaZulu-Natal. Two people died and 20 sustained injuries. The village's power substation was also structurally damaged. On 26 November, 13 houses and several schools were damaged after a tornado hit Ulundi in KwaZulu-Natal, one day after a tornado hit Utrecht, which is roughly 120 km northwest of Ulundi.

In December several large flood events were reported in the east. The worst of these occurred on 9 December when several parts of northern Gauteng province were underwater following five days of persistent rain. Rivers overflowed, causing devastating floods that damaged roads and local buildings. Hundreds of people were left homeless and infrastructure was severely damaged. Several cars were swept away during intense flooding in Centurion, Pretoria. Several roads were closed, causing traffic delays in most parts of the city. At least 700 shacks were destroyed in the Eerste Fabriek informal settlement in Mamelodi, displacing thousands of people.

5) Western Indian Ocean island countries—G. Jumaux, K. R. Dhurmea, B. Andrade, A. Abida, and L. Labbé

Western Indian Ocean island countries consist of Madagascar, Seychelles, Comoros, Mayotte (France), Réunion (France), Mauritius, and Rodrigues (Mauritius).

Positive SST anomalies over the region during the summer (January–April) and a very strong positive IOD during the last quarter (October–December) contributed to making 2019 the warmest year on record in the region, while rainfall was more varied (Fig. 7.26).

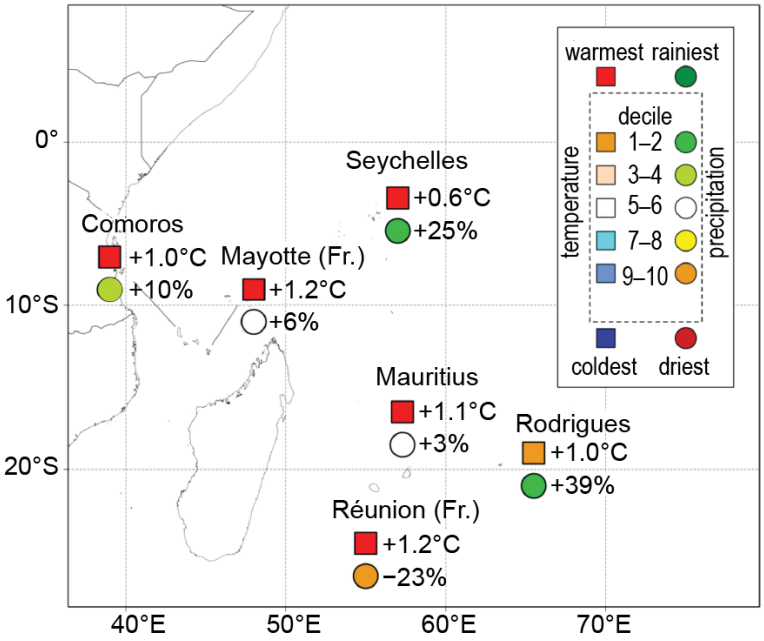

Fig. 7.26. Mean annual temperature anomalies (°C; 1981–2010 base period), annual rainfall anomalies (% of average), and their respective deciles for the Western Indian Ocean islands countries in 2019. (Sources: Météo France; and Meteorological Services of Mauritius, Seychelles and Comoros.)

(1) TEMPERATURE

Based on data from three stations, the annual mean temperature anomaly for Réunion Island was +1.2°C, the highest since 1968 when recordkeeping began and 0.3°C higher than the former highest in 2017. Monthly records for mean temperature were broken for six months of the year, in January, March, April, and October through December (Fig. 7.27). The highest all-time maximum temperature for Réunion Island—37.0°C at Pointe des Trois-Bassins—was recorded on 25 January.

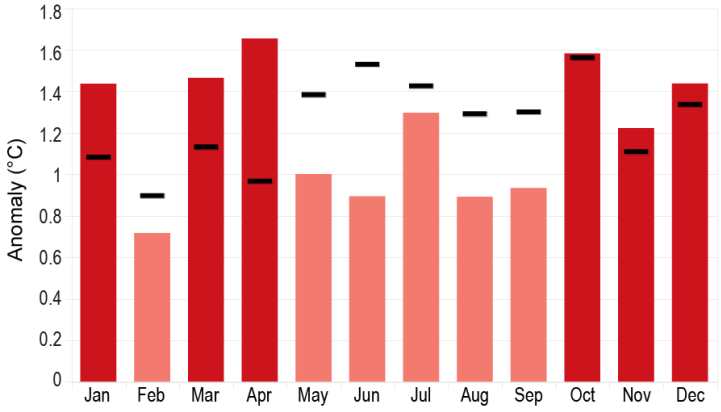

Fig. 7.27. Monthly mean temperature anomalies (°C; 1981–2010 base period) in 2019 in Réunion Island (average of three stations). Black dashes are the previous highest anomalies. (Source: Météo-France.)

In Mauritius, the average temperature over the island was the highest on record since 1960 (1.1°C higher than the 1981–2010 normal; Fig. 7.28). The mean maximum temperature was 1.0°C above normal while the minimum was 1.2°C above average, indicating greater nighttime warming compared to daytime. Over the central part of the island, the mean temperature was more than 1.5°C above normal. March and December 2019 were the warmest for their respective months since records began in 1971, while April, August, and November were among their five warmest for the same period. In December, both nighttime and daytime temperatures were at least 2°C above normal for more than 10 consecutive days. Warm conditions also prevailed at Rodrigues with a mean temperature anomaly of +1.0°C compared to normal. This made 2019 the fourth-warmest year on record since records began in 1960.

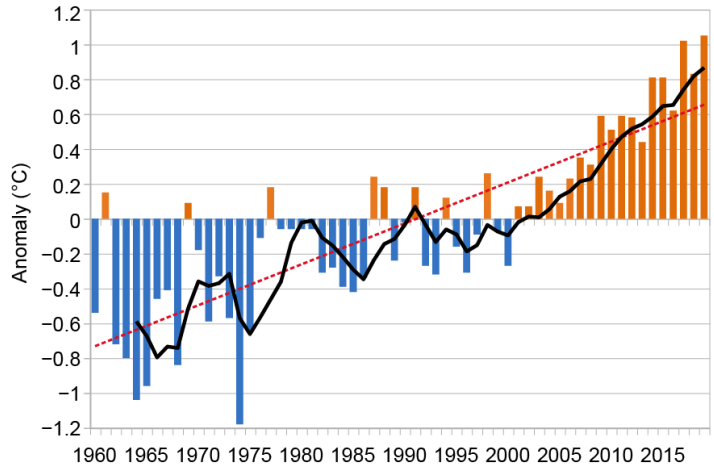

Fig. 7.28. Annual mean temperature anomalies (°C; 1981–2010 base period) in Mauritius, 1960–2019. Black line is the 5-year running mean. The linear trend for the period of record is shown as a dashed line. (Source: Mauritius Meteorological Service.)

For Mayotte, the annual mean temperature was 1.2°C above normal, the highest since records began in 1961 and 0.3°C warmer than the previous record set in 2017. Monthly mean temperature records were broken for nine consecutive months, from April through December. In Comoros, the annual mean temperature was 27.6°C, which is 1.0°C above normal. It was also the warmest year since records began in 1981, ahead of 2017.

At Seychelles International Airport, the annual mean temperature anomaly for 2019 was 0.6°C above normal, which was the highest since records began in 1972, surpassing 2009. All months were above normal, especially December, which was the warmest on record. April, June, and July were second warmest.

(II) PRECIPITATION

The annual rainfall total over Réunion Island was 77% of average, making 2019 the sixth-driest year since 1972. With high cyclonic activity in the southwestern Indian Ocean basin (15 tropical storms or cyclones) during the 2018/19 season, one might have expected above-normal rainfall. However, the trajectories of these tropical depression systems largely spared Réunion Island, resulting in the driest rainy season (December–April) recorded on the island, at 52% of average.

However, the dry season (May–November) was slightly above average, and the last quarter of the year was the fifth wettest, related to the strong positive IOD.

In Mauritius, the mean annual rainfall total was close to normal with 2054 mm, compared to the long-term average of 1999 mm. This made 2019 fall near the middle of the record, which dates to 1904. The intra-annual variability in rainfall was rather marked (Fig. 7.29), with deficient rainfall during the peak of rainy season (January–March) while April, June, and December had notably excessive rainfall. The mean annual rainfall at Rodrigues (based on the station at Pointe Canon) was 1541 mm, compared to the 1981–2010 mean of 1105 mm. This made 2019's total rainfall amount the sixth highest since records began in 1954.

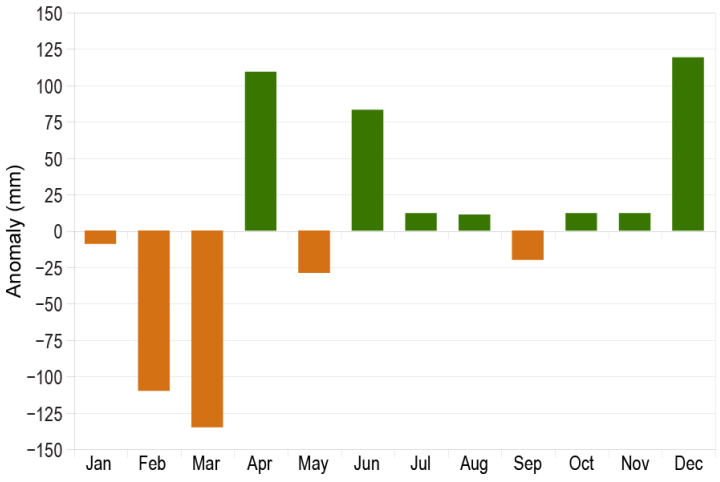

Fig. 7.29. Monthly rainfall anomalies (mm; 1981–2010 base period) over Mauritius in 2019. (Source: Mauritius Meteorological Service.)

For Mayotte, the total annual rainfall amount (an average of two stations) was 1579 mm, which is 106% of average. The total rainfall during the rainy season (November–April 2018/19) and the dry season (May–October) was 91% and 77% of average, respectively. The July–September quarter was 23% of average and the driest of the 59-year record, causing concern about drought. However, rainfall related to the strong positive IOD during November and December ameliorated the accumulated deficits. On the Comoros archipelago, the islands to the northwest, particularly Grande Comore, were comparatively wetter, making 2019 among the wettest recorded.

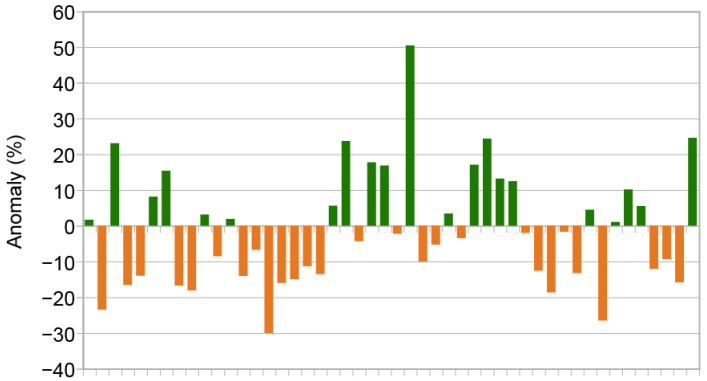

Fig. 7.30. Annual rainfall anomalies (%; 1981–2010 base period) at Seychelles International Airport for the period 1972–2019.

In Seychelles, annual rainfall (2948 mm) was 125% of average, making 2019 the second-wettest year on record (since 1972), behind 1997 (Fig. 7.30). This is also related to the positive IOD. January, May, and June were among their five rainiest months on record.

(III) NOTABLE EVENTS AND IMPACTS

In Mayotte, two cyclones passed close to the island in 2019, which is very unusual. Tropical Cyclone Kenneth passed 180 km north on 24 April, mainly causing damage to food crops with wind gusts close to 30 m s^{-1}. Tropical Cyclone Belna passed 100 km east on 8 December, causing almost no damage on the island because of its very compact size, despite a maximum recorded rainfall of 131 mm in 24 hours (see section 4f6).

Kenneth also affected the Comoros and, more particularly, the Grande Comore Island. During the night of 24–25 April, its eye passed within 50 km of the coast of Grande Comore. The storm caused severe flooding, killed six people, and injured 200. Almost 5000 houses were severely affected or destroyed. Livestock and agricultural production were heavily impacted, jeopardizing food security and local livelihoods. A total of 185 000 people were impacted. The last mature cyclone to have affected Grande Comore was likely in December 1959 (see section 4f6 and Sidebar 7.3 for more details on Kenneth).

Sidebar 7.3: **Record-breaking tropical cyclone landfalls in southeastern Africa—**
W. M. THIAW, J. ZUCULE, E. BEKELE, M. ROBJHON, P.-H. KAMSU-TAMO, A. D. MAGEE, AND C. J. SHRECK

Late in the southern Africa rainfall season of 2018/19, two tropical cyclones (TC)—each record-breaking storms in their own right—made landfall over Mozambique, marking the first time since the advent of reliable satellite imagery over the western Indian Ocean in 1979 that two intense (Category 2 and Category 4) TCs made landfall over the country in a single season. Tropical Cyclone Idai (4–16 March) was the longest-lived tropical system on record in the Mozambique Channel, while Kenneth (23–26 April) became the strongest storm on record to make landfall in Mozambique.

According to the Regional Specialized Meteorological Centre (RSMC) La Réunion Forecast Center tropical storm track, Idai was a long-lived disturbance with an unprecedented path with multiple landfalls that affected all central Mozambique provinces spanning more than 700 km north–south (Fig. SB7.5). Idai formed as a tropical depression (TD) off the east coast of Mozambique on 4 March, then intensified and moved slowly to the northwest and became a tropical storm (TS) just prior to making its first landfall near the town of Namacurra in the Zambézia Province that same day. Upon landfall, the storm immediately weakened to a TD and continued northward, then veering northwest near 16°S. As Idai crossed the border of Mozambique and Malawi on 7 March, it turned southeastward, exiting offshore into the Mozambique Channel at Pebane in the Nampula Province on 9 March. Between 4 and 8 March, the TD dumped extremely heavy rainfall amounts in several areas. In the Zambézia Province, the town of Mocuba observed a 3-day rainfall total of 375 mm on 5–7 March, while Milange recorded a 2-day rainfall total of 290 mm on 6–7 March. To the northwest, in the Tete Province, the town of Ulongué received a total of 448 mm during 7–8 March, while the northwestern district of Tsangano received 438 mm during 6–8 March. The heavy rains caused massive flooding in the region, killing more than 60 people and destroying 6000 houses.

The storm moved back over the warm waters of the Mozambique Channel (sea surface temperature [SST] anomalies > 1°C) and intensified rapidly as it re-approached the country. The Joint Typhoon Warning Center (JTWC) formally named Tropical Storm Idai on 10 March. On 11 March, Idai moved southwestward over the Mozambique Channel. The JTWC upgraded the storm to major TC status (see section 4f6 for details), but it weakened to a TS just before making a second landfall on 15 March near Beira—the fourth-largest city in Mozambique—in Sofala Province with extremely heavy rains, maximum sustained winds of 160–180 km h^{-1}, minimum central pressure of about 980 hPa, and a storm surge of 4.4 m. The storm was so powerful that it destroyed the weather stations in Beira and surrounding areas. A weather station in Espungabera, a town located about 400 km southwest of Beira, recorded a two-day rainfall total of 584 mm on 15–16 March, 69% of its monthly total. About 200 km northwest of Beira, the station at Chimoio Airport observed 310 mm during the same period. Once inland, Idai continued to weaken into a TD in its westward movement into central Mozambique, entering Zimbabwe on 15 March and finally dissipating on 16 March.

According to the Mozambique National Institute of Disaster Management, the storm affected 1.2 million people in Sofala Province, over 200 000 in Manica Province, over 6000 in Zambézia Province, and about 55 000 people in Tete Province. In Beira, hundreds of people were trapped in their homes due to the high water level from the storm surge, contributing to over 500 deaths. Strong winds and flooding across large areas of central

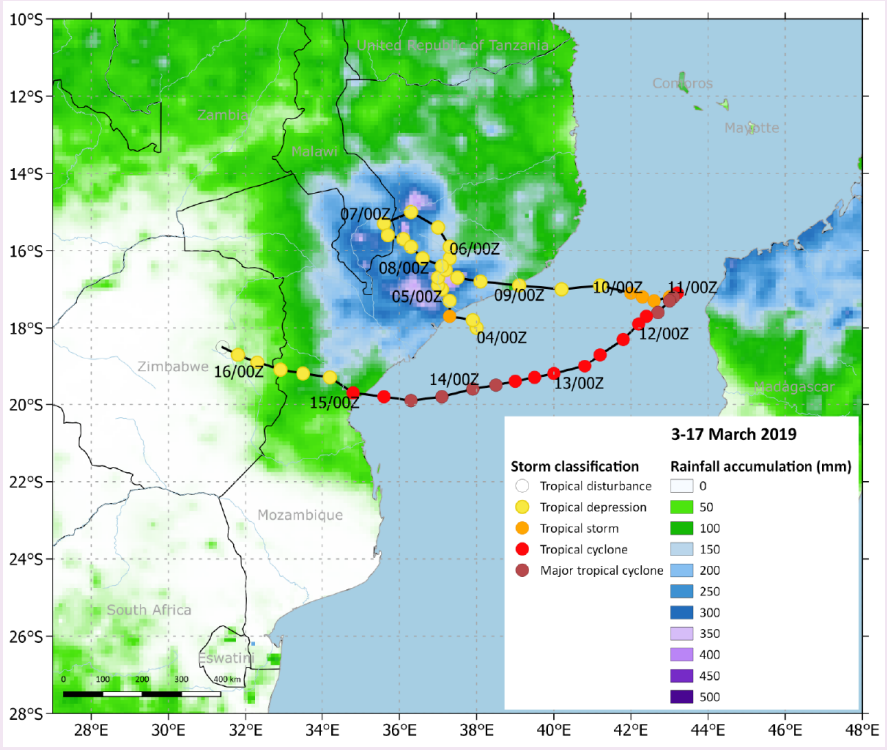

Fig. SB7.5. GIS-reconstructed RSMC La Réunion track of TC Idai overlaid with cumulative satellite rainfall estimate (mm; RFE 2.0) during 3–17 Mar 2019. (Source: NOAA/NCEP.)

and western Mozambique destroyed more than 100 000 homes and wiped out 700 000 ha of crops that were nearing harvest, placing pressure on food reserves. A major cholera outbreak ensued, with over 4000 confirmed cases in total. Malawi was also significantly affected by flooding, killing 60 people and affecting a further 900 000 nationwide. In Zimbabwe, Idai dumped massive amounts of rain, resulting in widespread flash flooding, claiming the lives of at least 630 people and displacing 15 000. A major humanitarian relief effort was triggered to assist affected people and communities. Idai resulted in total damages of at least $2.2 billion (U.S. dollars), the costliest TC on record for the South Indian Ocean basin, as well as the deadliest.

As Mozambique was recovering and assessing the damages and rebuilding costs from Idai, TC Kenneth made landfall on 25 April over the Macomia coastal district less than 100 km north of Pemba, the largest city in the Cabo Delgado Province in northern Mozambique. According to the RSMC La Réunion Forecast Center TS track, Kenneth formed as a tropical disturbance northeast of Madagascar and organized over the warm waters of the Indian Ocean into a TD by 23 April (Fig. SB7.6). Unlike Idai, the TD rapidly intensified the same day, with a fast westward motion. The JTWC upgraded Kenneth to TC status on 24 April as the storm approached the Comoros Islands. Kenneth was the strongest storm on record to affect the Islands. It passed ~60 km north of Grande Comore Island and resulted in significant impacts there, including multiple fatalities, the permanent or partial destruction of 10 000 homes, loss of 64% of food crops, and the displacement of up to 15 000 people. Kenneth then amplified swiftly to gain major TC status on 25 April as it approached the northern Mozambique coastline, making landfall the same day near Pemba, as noted above. With a maximum wind speed of 220 km h^{-1} and minimum central pressure of 988 hPa (equivalent of a Category 4 hurricane), Kenneth became the most intense storm to make landfall in Mozambique's recorded history.

Soon after landfall, on 26 April, Kenneth weakened into a TD while continuing to dump heavy rains over the region, moving southward and then drifting northward before finally dissipating south of Pemba on 29 April. The NOAA Climate Prediction Center African Rainfall Estimation Algorithm Version 2 (RFE 2.0) estimated a 7-day rainfall total of about 485 mm near Pemba, bringing cumulative seasonal rainfall estimates there to about 975 mm, approximately 140% of its 2001–18 average. Kenneth caused widespread flooding in northern Mozambique, with estimated damages of $100 million (U.S. dollars) and over 40 fatalities. Over 250 000 people in Cabo Delgado Province and almost 40 000 people in Nampula Province were affected. The storm also caused damage in southeastern Tanzania.

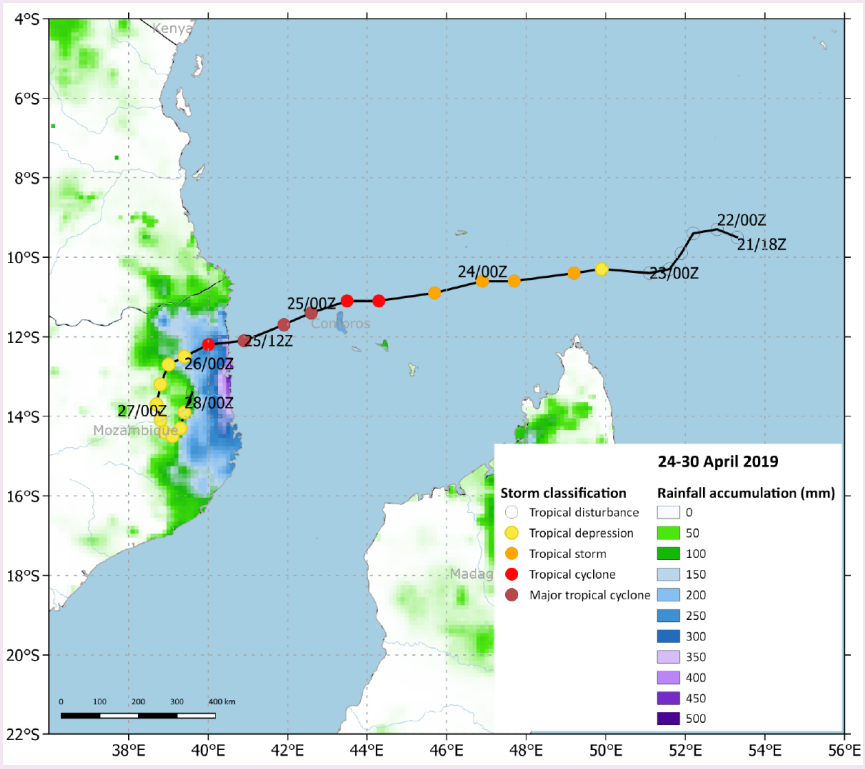

Fig. SB7.6. GIS-reconstructed RSMC La Réunion track of TC Kenneth overlaid with cumulative satellite rainfall estimate (mm; RFE 2.0) during 24–30 Apr 2019. (Source: NOAA/NCEP.)

f. Europe and the Middle East

—P. Bissolli (Ed.), B. Rösner, M. Demircan, J. Kennedy, V. Khan, K. Kokosadze, N. Kutaladze, M. Lakatos, J. Mamen, L. Megrelidze, M. A. Pastor Saavedra, E. Rodriguez Camino, E. Rodriguez Guisado, S. Sensoy, S. Spillane, K. Trachte, and G. van der Schrier

Countries in this section are part of the World Meteorological Organization (WMO) RA VI region. Throughout this section, 1981–2010 is the base period used for both temperature and precipitation, unless otherwise specified. European countries conform to different standards applied by their individual national weather services. The precision of anomalies reported may vary by country. All seasons mentioned in this section refer to the Northern Hemisphere (NH). More detailed information can be found in the *Monthly and Annual Bulletins on the Climate* in RA VI – Europe and the Middle East, provided by WMO RA VI Regional Climate Centre Node on Climate Monitoring (RCC Node-CM; www.dwd.de/rcc-cm). Anomaly information was taken from Figs. 7.32–7.36 and aggregations of CLIMAT station data when national reports are not available.

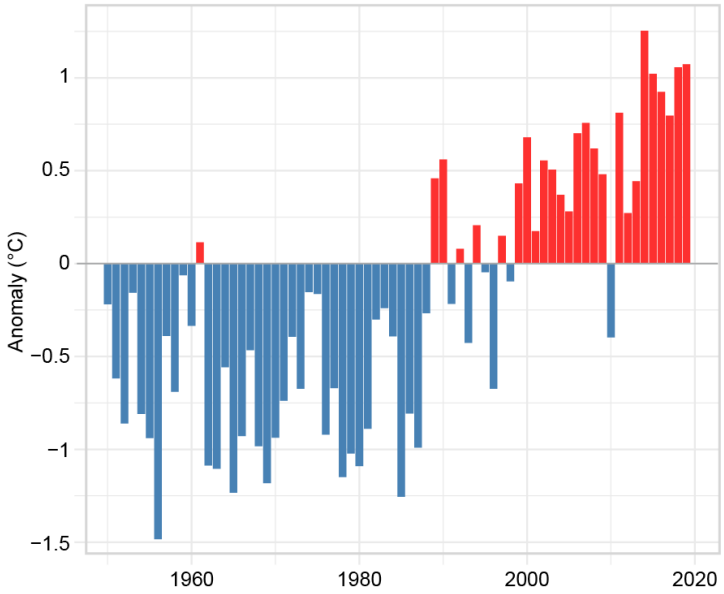

Fig. 7.31. Annual average land surface air temperature anomalies for 1950–2019 for Europe (35°–75°N, 10°W–30°E) relative to the 1981–2010 base period. (Source: GHCN version 4.0.1 dataset [Menne et al. 2018].)

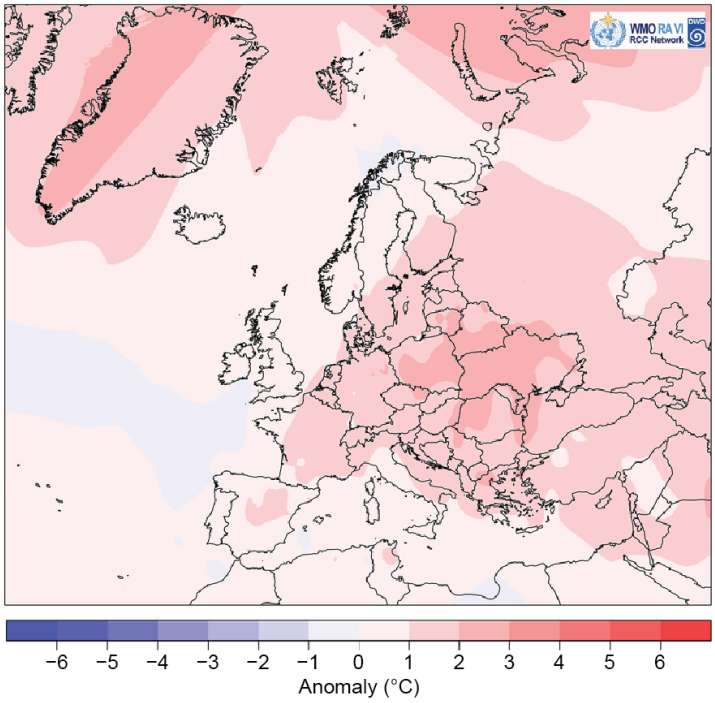

Fig. 7.32. Annual mean air temperature anomalies (°C; 1981–2010 base period) in 2019. (Source: interpolated climate station data, Deutscher Wetterdienst [DWD].)

The North Atlantic Oscillation (NAO) index used throughout the chapter is based on Jones et al. (1997). A positive NAO index value refers to an above-normal mean sea level pressure difference between the Azores high and the Icelandic low and, hence, a stronger-than-normal flow of mild and humid maritime air to the colder continent in winter. The relationship between the NAO and European temperature and precipitation, especially in winter, has long been known (e.g., Uvo 2003). A positive NAO index value is mostly associated with a warmer- and wetter-than-normal winter in northern and central Europe and a colder- and drier-than-normal winter in southern Europe; a negative NAO index value is generally associated with opposite effects.

Table A7.3 lists the beginning years of each country's national temperature and precipitation records for reference, if not otherwise mentioned in the text.

1) Overview

Based on the Global Historical Climate Network (GHCN) v4.0.1 dataset (Menne et al. 2018), Europe (35°–75°N, 10°W–30°E) experienced its second-warmest year since at least 1950 with an anomaly of +1.1°C, very close to 2018 (Fig. 7.31). Other datasets, e.g., Copernicus (https://climate.copernicus.eu/surface-air-temperature-maps), show

slightly different results, dependent on the data basis and the definition of the area of Europe. Nevertheless, 2019 generally ranked among the four warmest years on record of Europe mean temperature, together with 2014, 2015, and 2018.

Overall, the year was exceptionally warm and almost all of Europe reported temperatures higher than normal (Fig. 7.32). With the exception of most of the Iberian Peninsula and Italy, Ireland, the United Kingdom, Iceland, Norway, and the northern parts of Sweden and Finland, Europe showed anomalies well above +1.0°C. For many countries the year proved to be the warmest (Estonia +1.6°C [tied with 2015], Serbia +1.7°C, Belarus +1.5°C, Poland +1.8°C, Latvia +1.4°C, Lithuania +1.5°C, Ukraine +1.6°C, Romania +1.6°C).

The average annual precipitation total in 2019 was 7 mm above normal for Europe and considerably higher than in 2018, which was 32 mm below normal (Fig. 7.33). Annual totals were above 125% of normal in some northern areas (Fig. 7.34) such as small parts of the United Kingdom and Norway and much of northern European Russia, and in the south around the Mediterranean due to locally heavy rain. Dry areas with less than 80% of normal precipitation were observed in other places in the north (Iceland, Svalbard, Baltic States) but also in southern Iberia. The middle latitudes, too, were generally mostly drier than normal due to a longer drought period in the summer half year (April–September), where limited areas observed precipitation less than 80% of normal.

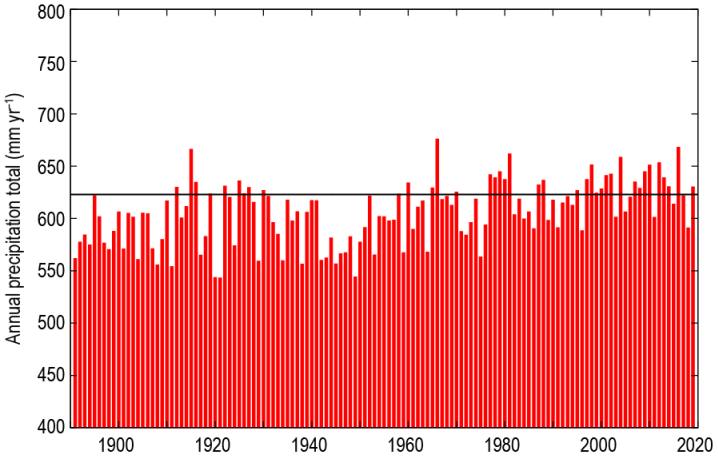

Fig. 7.33. Annual average precipitation totals (bars) for the period 1891–2019 for Europe (36°–72°N, 23°W–60°E) with the 1981–2010 base period (horizontal solid black line: 1981–2010 average is 623 mm). (Source: GPCC, created by DWD.)

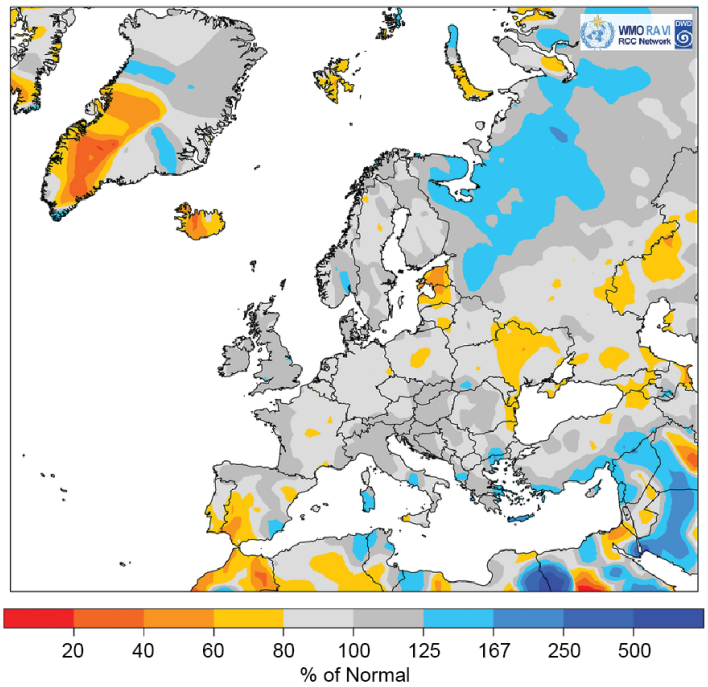

Fig. 7.34. European precipitation totals (% of 1981–2010 average) for 2019. (Source: GPCC, created by DWD.)

Meteorological winter 2018/19 (December 2018–February 2019) was mild in much of Europe (Fig. 7.35a) with an associated NAO index of +1.2 (whole winter average). Winter 2018/19 was Ireland's warmest on record since 1900. February was exceptionally warm (anomalies of +2.0° to +4.0°C in eastern Europe, and even higher in places) due to a strong positive NAO and a blocking high-pressure system over Russia. Many parts of western Europe received only 60%–80% of normal precipitation that winter (Fig. 7.36a) and only 20%–60% in parts of the Iberian Peninsula. In southern central Europe, eastern Europe, and parts of the eastern Mediterranean, precipitation was 125%–250% of normal. Snow was frequent in many parts of Europe in January, but less frequent in February. In parts of central, eastern, and southeastern Europe, the snow frequency (number of days with snow cover) was 125%–150% of normal in January, but 50%–75% of normal in February according to data from the Rutgers Global Snow Lab (https://climate.rutgers.edu/snowcover/index.php; see section 2c2).

Above-normal temperatures continued with the start of spring (Fig. 7.35b). In May, temperatures from Italy to the Nordic countries were below normal by –2.0° to –3.0°C in many regions, making it one of the coldest Mays in a long time for many countries. Many parts of France and the Iberian Peninsula were drier than normal in spring with precipitation 60%–80% of normal while in the rest of Europe it was closer to normal or wetter, with 125%–167% of normal in Scandinavia, Italy, and the northern Balkans (Fig. 7.36b).

Summer was warmer than normal in much of Europe (Fig. 7.35c). June proved to be full of records for many countries with widespread anomalies of +2.0° to +4.0°C. Summer was broadly drier than normal, with 60%–100% of normal precipitation across much of Europe (Fig. 7.36c), except for the eastern Mediterranean, the United Kingdom, Ireland, and southern parts of Norway.

Autumn was also warmer than normal (Fig. 7.35d) except for the Nordic countries, Ireland, and the United Kingdom. The Balkan states were particularly warm, with anomalies well above +2.0°C. For eastern Europe, Turkey, and southwestern Iberia, autumn was rather dry while central and western Europe mostly received above-normal precipitation between 100% and 167% of normal (Fig. 7.36d). December 2019 was mild with anomalies increasing from west to east and mostly wetter than normal except in some limited areas, e.g., parts of central Europe, the Baltic States, the eastern Balkan Peninsula, southern European Russia and South Caucasus, and parts of Italy.

Snow cover frequency was above normal in northern Europe in October and November, while it was below normal in central and eastern Europe in November and December 2019.

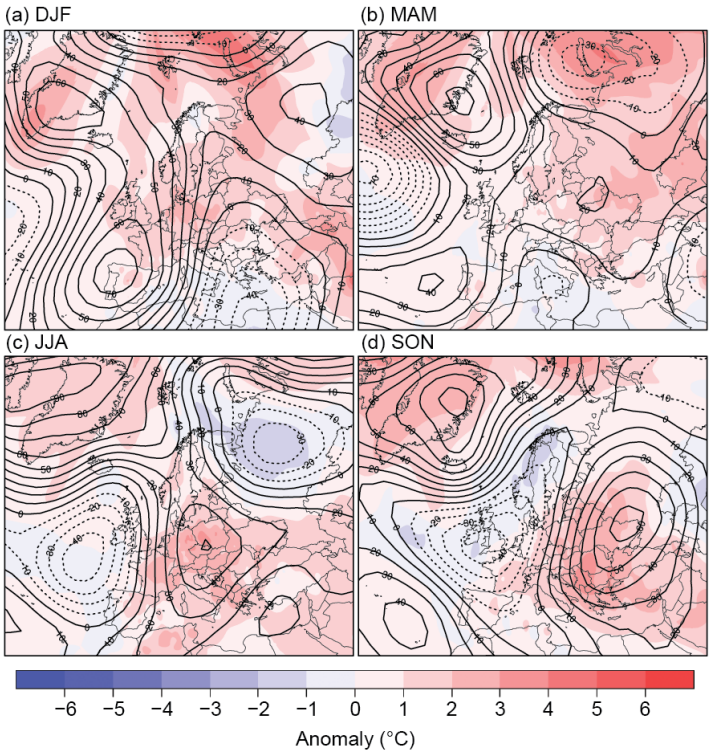

Fig. 7.35. Seasonal anomalies (1981–2010 base period) of 500-hPa geopotential height (contour; m) and surface air temperature (shading; °C) using data from the NCEP/NCAR reanalysis and DWD, respectively, for (a) DJF 2018/19, (b) MAM 2019, (c) JJA 2019, and (d) SON 2019.

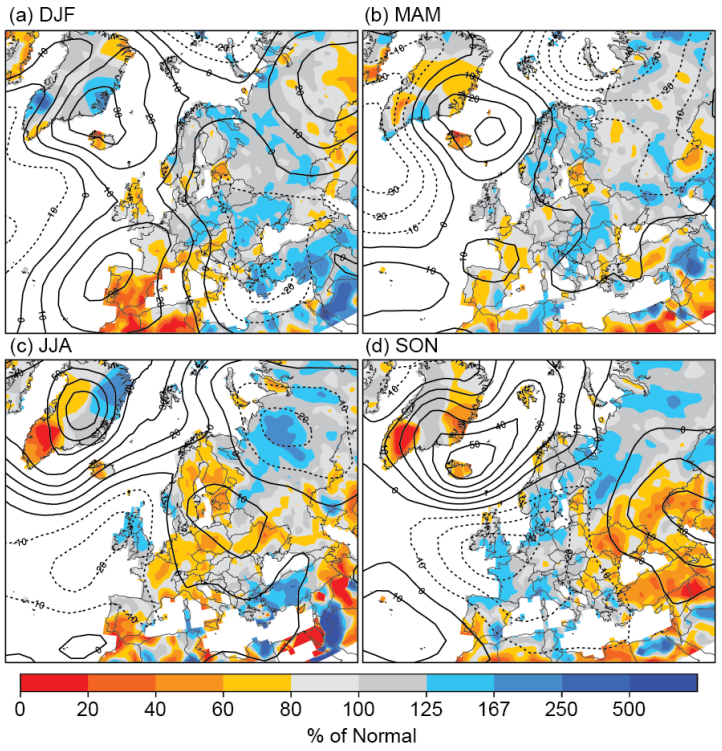

Fig. 7.36. Seasonal anomalies for 2019 (1981–2010 base period) of sea level pressure (hPa) from NCAR/NCEP reanalysis (contours) for (a) DJF 2018/19, (b) MAM 2019, (c) JJA 2019, and (d) SON 2019. Colored shading represents the percentage of seasonal mean precipitation for 2019 compared with the 1981–2010 mean from GPCC (Schneider et al. 2018).

2) Western Europe

This region includes Ireland, the United Kingdom, the Netherlands, Belgium, Luxembourg, and France.

(I) TEMPERATURE

The year was characterized by well-above-normal temperatures for western Europe with anomalies greater than +1.0°C, except for the United Kingdom and Ireland, which were lower but still above normal. For the continental countries, the year ranked third or fourth warmest.

Due mainly to a very warm December 2018 and exceptionally warm February, winter 2018/19 was very mild, with large positive temperature anomalies: United Kingdom +1.4°C above normal, Netherlands +1.8°C, Luxembourg +1.8°C, France +1.3°C, Ireland +1.8°C (highest on record). The United Kingdom reported its second-warmest February on record (+2.4°C above normal), and Luxembourg and Ireland their third warmest (+3.7°C and +2.4°C, respectively). In France, the countrywide average maximum temperature was +4.1°C above normal, making it the second-warmest February (after 1990). Similarly in Ireland, it was the warmest winter on record for many stations, and more than half of Irish stations set new monthly maximum temperature records on 25 and 26 February. Other countries in western Europe reported new records as well in late February (see *Notable events and impacts* for details).

Spring was also mild. Anomalies ranged from +0.3°C in France, to +0.7°C in the Netherlands, to +0.8°C in the United Kingdom. Only May had below-normal temperatures, with anomalies below –1.0°C in the Benelux countries and in eastern and southern France.

Summer was close to normal (+0.4°C) in Ireland and only slightly warmer in the United Kingdom (anomaly of +0.8°C, 12th warmest). Belgium (+1.5°C), Luxembourg (+2.4°C), and France (+1.7°C) each observed their third-warmest summer on record. The Netherlands observed its fourth-warmest summer with an anomaly of +1.4°C at De Bilt. June was very warm for most of Europe. It was the warmest June in the Netherlands, second warmest in Luxembourg (anomaly +3.6°C), and fifth warmest in France (anomaly +1.8°C). Ireland was below normal with an anomaly of –0.3°C. It was the fourth-warmest July on record for France (+2.2°C), and many daily maximum temperature records were broken, especially on 25 July (see Sidebar 7.4 for more details).

While autumn brought below-normal temperatures to Ireland (anomaly –0.4°C) and the United Kingdom (anomaly –0.3°C) and slightly-above-normal temperatures in the Benelux countries (Netherlands +0.2°C, Belgium +0.3°C, Luxembourg +0.7°C above normal), France reported its sixth-warmest autumn since 1900 with an anomaly of +1.0°C. December 2019 was mild with anomalies of +0.8°C in Ireland, around +1°C in the United Kingdom, and +2°C in the Benelux and France.

(II) PRECIPITATION

The year as a whole was wetter than normal in the western parts of western Europe. Precipitation of 100%–125% of normal was reported for Ireland, the United Kingdom, and western France, while much of the Benelux, and central and eastern France had below-normal precipitation (80%–100%).

Winter precipitation was close to normal or below normal. The United Kingdom and Ireland reported 77% and 66% of normal precipitation, respectively. In the Benelux and most of France, precipitation was close to normal, and only portions of western, central, and southern France recorded precipitation less than 60% of normal.

While Ireland and the United Kingdom reported slightly-above-normal totals for the spring season, March was very wet in both countries. The United Kingdom reported its eighth-wettest March since 1910, at 136% of normal. The Benelux countries were slightly drier than normal in spring with around 90% of normal precipitation. Parts of France remained dry with amounts as low as 50%–80% of normal.

Summer was predominantly characterized by low pressure, leading to a rather wet season in Ireland and the United Kingdom. The United Kingdom reported its 10th-wettest summer with 138% of normal precipitation as well as some new seasonal records, including 425.4 mm in South Yorkshire, which is double its seasonal average. In contrast, summer was drier than normal in France and the Benelux, with only 80%–90% of normal precipitation on average and less in localized areas.

Autumn was wetter than normal in the Netherlands and Luxembourg with precipitation around 115% of normal. Belgium reported 95% of normal. France, with 130% of normal, had its fifth-wettest autumn (since 1959), although its countrywide average for September was only 60% of normal. December 2019 was wetter than normal in western Scotland, southern England, and France, with some areas observing more than 125% of normal; the Netherlands received only around 80% of its normal precipitation.

(III) NOTABLE EVENTS AND IMPACTS

A warm spell during 21–27 February brought exceptionally mild weather and record high temperatures to many areas in the United Kingdom. Kew Gardens in London reached 21.2°C on 26 February. This was the first temperature above 20°C recorded in winter in the United Kingdom. Achnagart (Highland) set a new highest daily minimum temperature record for the winter for the United Kingdom with temperatures not dropping below 13.9°C on 23 February. More than half of France's 150 measurement stations broke maximum temperature records for February—for example, Istres (Provence region in southeastern France) with 23.4°C on 28 February (previous record 23.3°C on 27 February 1960) and Cazaux (military airport near the Atlantic coast) with 26.2°C on 27 February (previous record 26.0°C on 23 February 1929). Similarly, a run of new records was set at De Bilt in the Netherlands with 18.3°C on 25 February, rising to 18.9°C the following day, and finally 20.5°C on the 27th, also breaking the monthly and winter record for all Dutch stations. In Uccle, Belgium, 26 February was an extremely early first spring day—defined as daily maximum temperature above 20°C—making it the first winter day meeting this definition of a spring day in Belgium's history.

On 9 August, a tornado classified as EF-2, with wind speeds between 178 km h^{-1} and 217 km h^{-1}, formed from a supercell thunderstorm and brought considerable damage to northeastern France and southwestern Luxembourg. Almost 500 buildings were damaged in the communities of Pétange and Käerjeng, Luxembourg, and 30 buildings were damaged in the province of Meurthe-et-Moselle, northeastern France. Trees were knocked down, roads blocked, cars damaged, and 19 people in Luxembourg were injured.

3) Central Europe

This region includes Germany, Switzerland, Austria, Poland, Czechia, Slovakia, and Hungary.

(I) TEMPERATURE

Temperatures for the year were well above normal by +1.0° to +2.0°C in central Europe, with 2019 among the five warmest years for all countries of the region. Hungary reported its warmest year on record with an anomaly of +1.9°C. Germany (+1.4°C), Slovakia (+1.8°C), and Czechia (+1.6°C) were second warmest, while Austria (+1.4°C) and Switzerland (+1.1°C) had their fourth- and fifth-warmest year, respectively.

Winter was mild in the region with anomalies between +1.0° and +2.0°C. Germany reported its ninth-warmest winter with an anomaly of +1.9°C. February, with an NAO index value of +1.9, was unusually warm with anomalies of +2.0°C and above: Austria +2.0°C, Slovakia +2.9°C, Czechia +2.6°C, Hungary +3.0°C, Germany +3.1°C. An NAO index value of +1.9 indicates a nearly twice standard deviation difference between the normalized sea level pressures of the Azores high and Icelandic low, which is regarded as relatively high. Prior to 2019, the last time a February NAO index value surpassed +1.9 was in 2014.

Spring was slightly warmer than normal for Switzerland and Austria, at +0.1°C and +0.2°C above normal, respectively, +0.5°C in Germany, and +0.7°C for the rest of the countries in the region. While March and April brought widespread temperatures up to +3.0°C above normal, May was far colder than normal due to a northwesterly circulation and below-average solar radiation with anomalies between –2.2°C and –2.6°C, ranking among the 10 coldest Mays for most countries (see Table A7.3 for temperature record lengths of individual countries).

Summer was exceptionally warm. Slovakia and Czechia reported their warmest summer on record with anomalies of +2.4°C and +2.5°C, respectively. Hungary and Austria reported their second-warmest summer (+2.2°C and +2.7°C above normal), and Germany and Switzerland their third warmest (+2.1°C and +2.3°C). All summer months were warmer than normal in the region, but June in particular was the warmest month on record for all but Switzerland, where it was second warmest. Anomalies in June were well above +3.0°C, and close to +5.0°C in places. Many maximum temperature records were broken. In Germany, the previous countrywide record of 40.3°C, measured in summer 2015, was beaten by 14 different stations during the peak of the heat wave on 25 June, and a new countrywide record of 42.6°C was set in Lingen (Emsland region, northwestern Germany). The Austrian meteorological service reported new June records at more than half of its 269 stations.

The year continued with a warmer-than-usual autumn, especially for southeastern parts of the region. Hungary (+2.4°C anomaly), Slovakia (+2.1°C), and Czechia (+1.6°C) reported their warmest autumns; Austria (+1.6°C) its fourth warmest; Switzerland (+1.1°C) its sixth warmest; and Germany, with 1.0°C above normal, its 10th warmest. December 2019 was also a mild month with anomalies ranging from about +1°C in western Germany to +3°C in eastern Poland.

(II) PRECIPITATION

Overall, the year was close to normal or drier. Some places in eastern Germany and Poland received less than 80% of normal precipitation.

The winter season was wetter than normal, except in Hungary, which received 73% of its normal. Germany and Slovakia reported about 110% and Czechia 148% (eighth wettest) of normal precipitation. While January was wetter than normal with widespread precipitation between 125% and 167% of normal, February was dry, especially in Germany, with most of the country receiving between 20% and 60% of normal precipitation, and in Hungary, which received 41% of its normal.

For Germany (98%), Switzerland (102%), and Czechia (103%), spring precipitation was close to normal while for Slovakia (121%) and Hungary (129%), the season was wetter than normal. For Hungary, March was the 10th driest on record with only 28% of normal precipitation. During April, the precipitation deficit shifted to Germany, Czechia (60% of normal and ninth-driest April), and northern parts of Poland where precipitation reached only 20%–40% of normal. At the end of May, there was still snow cover with depths of 270 cm in the Swiss Alps at about 2500 m elevation (Weissfluhjoch), a new seasonal record.

Summer was drier than normal for the whole region. Germany reported 73% of normal precipitation, Slovakia 84%, Czechia 76%, Hungary 91%, and Switzerland 95%. In particular, Austria reported its driest June since the beginning of measurements in 1767 with only 43% of normal precipitation, and parts of southern Poland received just 20%–40% of normal precipitation. In Czechia, precipitation was 67% of normal and the eighth-driest June on record. Germany and Switzerland received 72% and 88% of normal precipitation, respectively, during June, with southern Switzerland (south Ticino) receiving only 30% of its normal.

Autumn precipitation was close to normal in Czechia (99% of normal), Germany, and Hungary (both 104% of normal), while for Slovakia (130%), Switzerland (115%), and Austria (129%), it was a wetter-than-normal season. With a sinking snow line in the Alps in November, higher areas on the south-facing slopes of the Alps received substantial amounts of fresh snow. In certain parts, the fresh snow total set new November records, for example, 220 cm at Segl-Maria station in

Switzerland (Engadin region, 1804 m a.s.l.), with measurements dating back to 1864. December was drier than normal in Germany, western Poland, and western Czechia (60%–100%), but wetter in the Alps and in eastern and southeastern parts of Central Europe, locally exceeding 125% of normal.

(III) NOTABLE EVENTS AND IMPACTS

Between 7 and 14 January, the Alps and other mountainous regions in central Europe experienced extreme snowfall under the influence of northwesterly to northerly flow. Up to 100 mm of precipitation fell in 72 hours in Germany's Ore Mountains and the northern Alps. Correspondingly, the snow depth increased from 24 to 72 cm in Zinnwald-Georgenfeld (eastern Ore Mountains, 877 m a.s.l.) during 8–10 January and from 365 to 465 cm on Germany's highest mountain, Zugspitze (northern Alps, 2964 m a.s.l.), during 11–13 January. On 13 January, central Europe was within the warm air sector of a low-pressure system, which made the snow line temporarily rise to 1200 m. Rainfall up to 109 mm day^{-1} increased the weight of the snow cover dramatically and thus the danger of collapsing buildings or trees. New monthly records of 24-hour precipitation were registered in Saxony (eastern Germany) on 9 January, and new records of snow depth were registered in southern Germany on 11 January. Switzerland recorded up to 160 cm of fresh snow on northern slopes and wind gusts of up to 180 km h^{-1}.

During a warm spell lasting from 21–27 February, exceptionally mild weather brought record high temperatures, with many areas in central Europe exceeding 20°C. Many local monthly and winter records of maximum temperature were reached or broken, even at stations with time series spanning more than 100 years. For Austria and Hungary, countrywide high-temperature records for February were reported.

At the beginning of March, several storms affected western and central Europe. Storm gusts reached above 200 km h^{-1} in exposed places. Due to storm Bennet (Freya in United Kingdom and France), some carnival parades on 4 March had to be canceled in Germany and neighboring countries. Flight and ferry services were disrupted, trees and rooftops were damaged, and some roads and bridges needed to be closed.

Starting with June, an exceptional three-month drought/dry spell affected most of Germany. Soil moisture in large areas was below long-term minimum values, causing economic losses due to crop failure. On several major rivers, low water levels hindered navigation. This was the second major drought period in consecutive years, following an even longer event in 2018.

As a result of a cut-off low, western and central Europe were affected by unusually strong storm events in June. Exceptionally intense hailstorms with hailstones larger than 6.5 cm hit southern Germany on 10–11 June. At least six people were injured, and cars, trees, and houses were damaged in Bavaria. Accompanying heavy precipitation led to flooding of homes. In Berlin and surrounding areas, thunderstorms brought daily rain totals of 60–70 mm on 11 and 12 June, causing road closures. Similarly, northern Poland reported heavy winds and precipitation causing flooding, uprooted trees, and power outages for thousands of households on 10 June. Record large hailstones of 12 cm were reported in western Poland.

Thunderstorms caused wind damage and flash floods in Hungary during 16–23 June. Daily precipitation totals above 100 mm were measured at several stations in northeastern Hungary during this period. On 16 June, 144.4 mm of precipitation was recorded at Rakamaz, nearly twice its normal for the month of June (73.5 mm). On 20 June, a new daily record of 117.8 mm of rain was set at Szőlősardó, beating its previous record high for this date of 101.3 mm set in 1956.

Sidebar 7.4: **Record June and July heat waves across western and central Europe**—

B. RÖSNER, P. BISSOLLI, J. W. KAISER, U. PFEIFROTH, A. SPITZER, AND G. VAN DER SCHRIER

Summer 2019 was warmer than normal by +2.0°C to +4.0°C for western and central Europe. This was especially the case during the record warm June and July, when two outstanding heat waves occurred.

June 2019 was the warmest June on record, globally as well as for Europe. Similar to previous heat episodes, the extreme temperatures were a result of blocking omega patterns caused by a long-lasting, high-pressure system over Europe, especially during the last week of June. This pattern produced an inflow of warm subtropical air leading to anomalies up to +10°C in France and numerous temperature records for many countries as well as many hours of sunshine.

On 26 June, new German monthly records of 38.6°C were set at Coschen and Bad Muskau near the Polish border, surpassing the previous record of 38.5°C set in 1947. Just three days later, this record was broken again with 39.6°C at Bernburg/Saale in eastern Germany. Apart from the new national record, new station records were set at 209 of 458 (45%) DWD (Deutscher Wetterdienst, German Meteorological Service) stations on 26 June. In southern France, 13 stations surpassed France's 2003 records, exceeding a temperature of 44.1°C, and at Gallargues-le-Montueux (Gard) a new national record of 45.9°C was measured. Switzerland, Austria, Italy, Slovenia, and Croatia also reported new June station records, some of which were also all-time records for the stations. Also noteworthy are new temperature records at higher elevations. including new records of 29.8°C set on 26 June at Davos, Switzerland (previous record 29.3°C in 2015; 1637 m a.s.l.) and 25.0°C set on 27 June at Schmittenhohe, Austria (previous record 24.6°C in 1952; 1973 m a.s.l.).

In addition to maximum temperature records, new highest minimum and daily mean temperature records also were broken. On 27 June, a new national record with a daily mean temperature of 27.9°C was set in France. In Vienna, Austria, a new record of 13 tropical nights (minimum temperature ≥ 20.0°C) was observed during June.

Just a few weeks later, from 24 to 26 July, another omega weather pattern (Fig. SB7.7) and associated heat wave, albeit short, brought additional new records. In western Germany, the temperature at many stations exceeded 40°C on three consecutive days for the first time since measurements began in 1881. On 24 July, a new German national record of 40.5°C was set at Geilenkirchen, surpassing the old record measured in July and August 2015 by 0.2°C. Just one day later, on 25 July, 14 stations beat the old record, with Lingen taking the new German record with a temperature of 42.6°C. New national all-time record temperatures were also set at Gilze-Rijen (Netherlands) with 40.7°C, Begijnendijk (Belgium) with 41.8°C, Steinsel (Luxembourg) with 40.8°C, and Cambridge Botanic Garden (England) with 38.7°C. Temperatures above 40.0°C had never before been observed in Belgium and the Netherlands. The heat wave extended all the way to Scandinavia, with maximum temperatures locally surpassing 33.0°C in southern Finland and 34.0°C in Norway. Many other European stations reported temperatures approaching or exceeding 40°C, with many new local records often beating the old ones by 2°C to 3°C. This large exceedance of previous records made this heat wave extraordinary.

Train services were disrupted in Germany, Switzerland, and Austria due to buckling of tracks. Locally, train tracks were painted white in an attempt to prevent further buckling (and thus closures). Power plants in France and Germany had to be

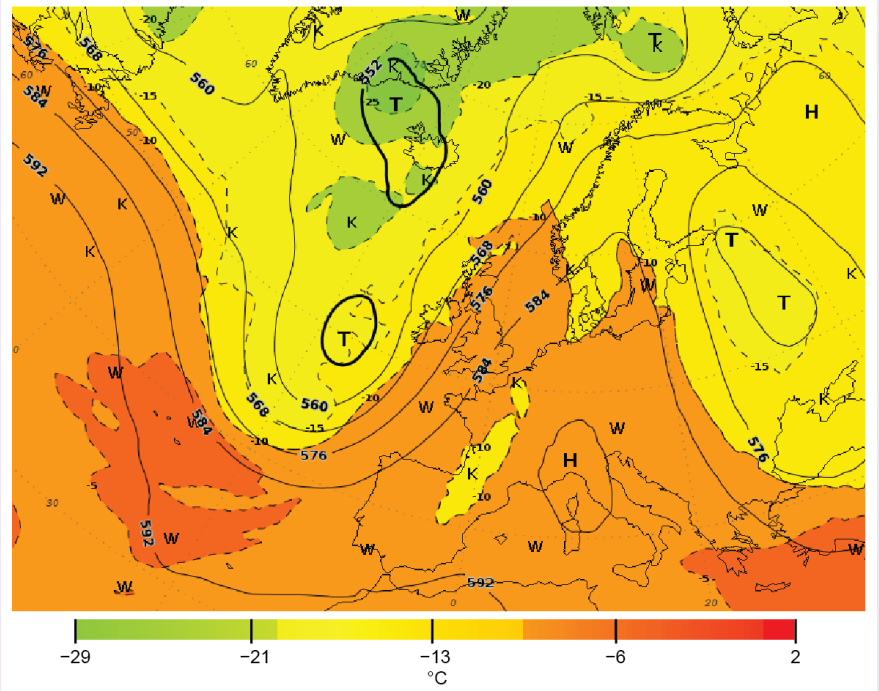

Fig. SB7.7. 500 hPa geopotential (contours) and temperature (color shading) on 25 Jul 2019, 00 UTC. (Source: DWD.)

shut down when river waters became too warm for use in cooling. In northern Spain and France, where the heat wave was accompanied by dry conditions, wildfires broke out.

Daily temperature records highlight European warming

The record high temperatures over extensive areas in Europe are consistent with the warming climate. According to an analysis conducted by the World Weather Attribution Project (Vautard et al. 2019) regarding the effects of climate change on the occurrence of such extreme events, the estimated return period of such an event for France and the Netherlands is about 50 to 150 years in the current climate. The analysis concluded that, without climate change, the return period would be at least 10, and perhaps up to 100, times longer, or more than 1000 years. For the United Kingdom and Germany, the estimate for the return period in the current (changed) climate is around 10 to 30 years, and roughly 10 times (at least three times) longer without climate change. Climate change is simulated either by fitting a Generalized Extreme Value distribution of a local time series with a smoothed western European summer temperature (to derive a long-term trend that is assumed to describe the long-term climate change) or by comparing model simulations of a present-day climate with simulations of the past (preindustrial) climate or an "artificial" climate without anthropogenic forcing (see Vautard et al. 2019 for more details).

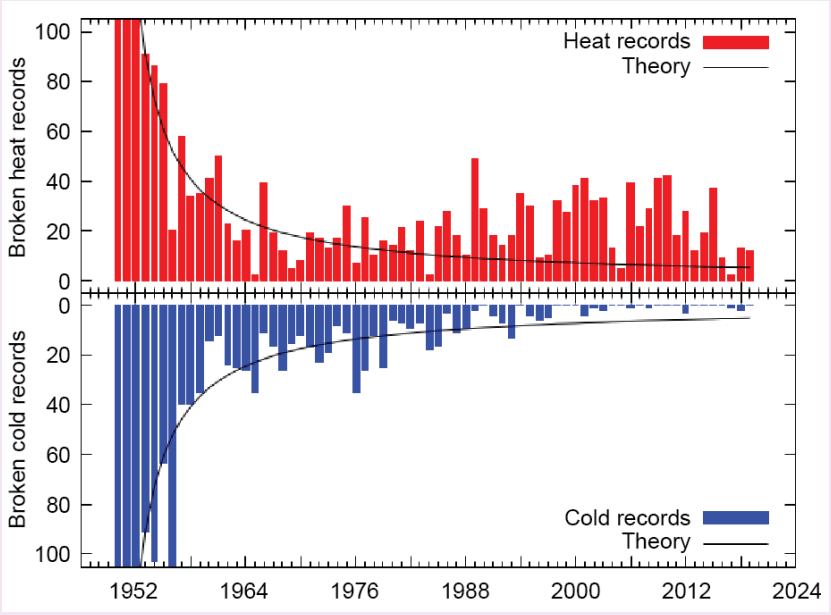

Fig. SB7.8. Number of daily heat and cold records per year for the European averaged temperature since 1950. The black lines indicate the expected numbers in the absence of climate change. Data are based on the E-OBS daily gridded dataset; underlying station data are daily maximum temperatures from ECA&D (www.ecad.eu/). (Source: KNMI/E-OBS, van der Schrier et al. 2013.) The number of underlying stations varies with time but is around 4000 since 1960 and lower prior to that.

Another approach to evaluate the effect of climate change is to analyze whether the number of new records in a specific year is particularly high or low, compared with the theoretical value in the absence of climate change. The theoretical construction (Benestad 2004) is the following: in the first year of a time series, all days break a record (because there are no previous values), so the number of records is 365. In the second year, the theoretical number of records is 365/2 (one-half occurring in the first year, the other half in the second year, assuming records have an equal distribution over the years without climate change). In the third year, one in three days sets a record: the theoretical number is 365/3, etc. For a series starting in 1950, the theoretical number of records in year Y, in the absence of climate change, is 365/(Y – 1949). Figure SB7.8 provides this theoretical number and the observed number of heat and cold records since 1950. In the last 30 years, the number of daily high temperature records is much larger than the theoretical value (more than twice, partly multiples), and the number of daily low temperature records is much smaller. This clearly highlights the warming of Europe in recent decades and its effect on the frequency of broken daily heat records.

Benestad (2004) analyzed the statistical significance of the number of record values in long time series and found that the mean number of records from 17 climate stations spread around the globe was significantly higher than the expected theoretical value by the end of the twentieth century, which is in line with Fig. SB7.8. Since then, in the twenty-first century, the number of European daily records per year has remained relatively steady, although the theoretical value decreases with time, suggesting it is significant that the values remain steady. This does not exclude the fact that there are a couple of years since 2000 with fewer records compared to the theoretical expectation. Notably, this is a regional time series; warming with new heat records has occurred elsewhere around the globe. Additionally, the long-term warming is superposed by shorter-scale climate variability due to circulation changes (e.g., El Niño–Southern Oscillation).

A record sunny year

Overall, the year was also very sunny in Europe. The sunshine duration in 2019 was longer than the European 1983–2017 average of 2293 hours across almost all of Europe (Fig. SB7.9). The widespread positive anomalies of +150 hours to +250 hours caused the average annual sunshine duration over Europe to reach a new record with 2348 hours in 2019 (Fig. SB7.10). The increased duration of sunshine and hence direct solar radiation, with the enhanced advection of warm subtropical air and increased subsidence associated with persistent high-pressure conditions during the heat waves, contributed further to the warm year 2019.

A recent analysis by Imbery at al. (2020) shows an increase of anticyclonic weather types over central Europe since 1980, especially in April. This implies that long-term circulation changes may have contributed to the positive trend of sunshine duration in recent years and decades. However, longer time series of surface solar radiation (e.g., since 1937 in Potsdam, Germany) show a decrease in surface solar radiation (dimming) from 1950 to 1980 and an increase (brightening) since then (Wild 2016). These results suggest that there are multidecadal variations in surface solar radiation, likely caused by aerosols. Related climate model studies are still in progress.

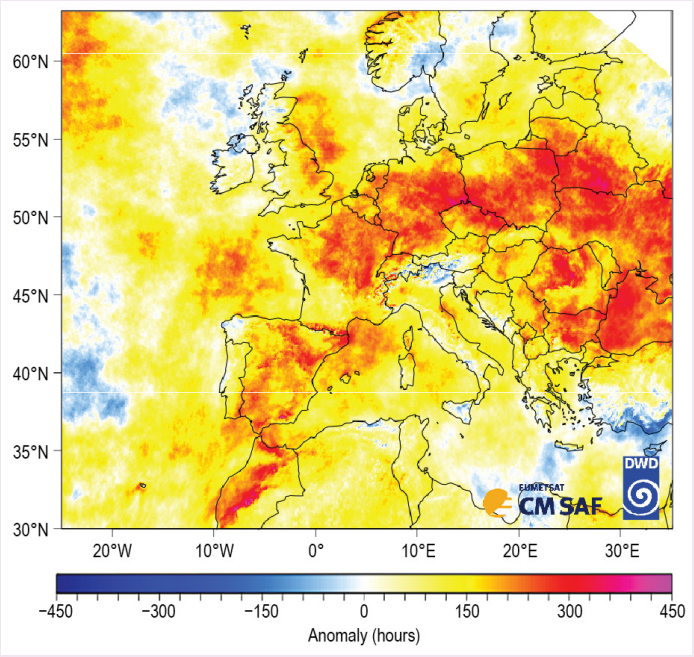

Fig. SB7.9. 2019 anomaly map of sunshine duration (hours) over Europe relative to 1983–2017, derived from EUMETSAT Meteosat satellite observations. (Data source: CM SAF SARAH-2.1 and ICDR, Kothe et al. 2017, Pfeifroth et al. 2019.)

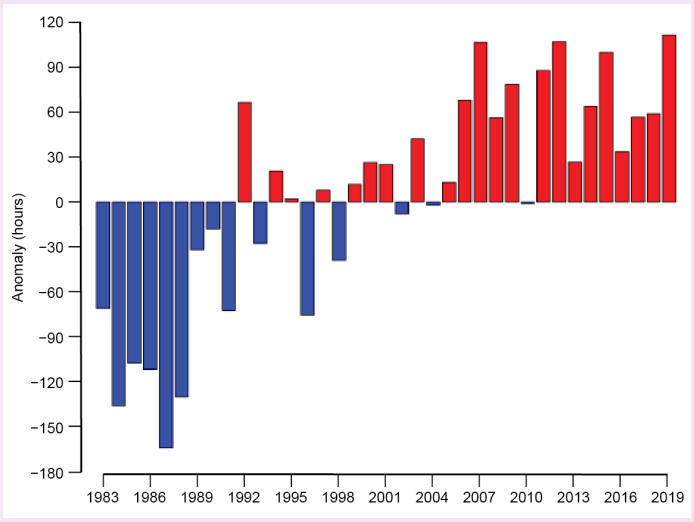

Fig. SB7.10. Annual average anomalies of sunshine duration (hours) over Europe for 1983–2019. The highest value 2019 corresponds to an absolute sunshine duration of 2348 hours. The astronomically maximum possible annual sunshine duration averaged over Europe, defined as the period when the sun is located completely above the horizon (topography neglected), is 4426 hours. (Same domain and data source as Fig. SB7.9.)

4) The Nordic and Baltic countries

This section includes Iceland, Norway, Denmark, Sweden, Finland, Estonia, Latvia, and Lithuania.

(I) TEMPERATURE

The year was slightly warmer than normal with anomalies around +0.7°C in Norway, Sweden, and Finland. However, in the Baltic States, it was among the five warmest years with temperatures more than +1.0°C above average.

Winter had well-above-normal temperatures. Denmark reported its seventh-warmest winter on record with an anomaly of +2.9°C. January, however, was colder than normal in most of the region, especially in northern Finland where temperatures were –3.0° to –4.0°C below normal. February, in contrast, was very mild with anomalies of +4.0°C to +5.0°C in the Baltic States and Finland, resulting in many new monthly records of maximum temperature. On 26 February, 15.8°C was measured at Tirstrup in Djursland (eastern Denmark mainland), tying the previous record at Copenhagen on 24 February 1990. On the same day, a new Swedish record was measured at Karlshamn with 16.7°C. In Latvia, at Kolka, a new record of 13.4°C was set on 16 February for the highest winter maximum temperature. Estonia reported its seventh-warmest February on record with an anomaly of +4.3°C, Latvia its eighth warmest (+4.5°C above normal), and Lithuania its sixth warmest (+3.9°C above normal).

Spring temperatures were above normal by more than +1.0°C in the whole region (Finland +1.2°C, Norway +0.8°C, Denmark +1.5°C, and Latvia +1.5°C above normal). April was especially warm, with Finland and Norway each reporting its second-warmest April on record (+2.5°C and +2.4 °C above normal, respectively) and Latvia its third warmest (+2.1°C above normal). May was the only spring month colder than normal in the whole region except for Lithuania and Latvia, where May was slightly warmer than usual.

Summer temperatures were more than +1.0°C above normal in most of the northern countries: Estonia +1.6°C (tied with 2015 for warmest of the 1961–2019 period), Denmark +1.6°C and Latvia +1.0°C; only Norway and Finland had lesser anomalies of +0.8°C and +0.3°C, respectively. Some new records were set, including a new Norwegian national record high minimum temperature of 26.1°C observed at station Sømna – Kvaløyfjellet (Nordland, central Norway) on 28 July. At the northeastern Swedish station Markusvinsa, a new record maximum temperature of 34.8°C was measured on 26 July. This was the highest temperature ever reported north of the Arctic Circle in Sweden. On 13 June, a new seasonal record with a temperature of 33.0°C was set in Riga, Latvia. Many other stations broke their monthly maximum temperature record during June. In contrast to the warm June, July was colder than normal in the Baltic countries and Finland with anomalies slightly below –1.0°C (Finland –1.1°C, Latvia –1.2°C, Lithuania –1.2°C, Estonia –1.0°C).

Autumn was colder than normal in Norway (–1.0°C below normal), Sweden, and Finland (–0.2°C below normal), while the Baltic states and Denmark reported above-normal temperatures (Latvia +1.6°C anomaly, eighth warmest together with 1949; Lithuania +1.9°C; Estonia +1.1°C; Denmark +0.7°C). On 14 November, daily maximum temperature records were broken at many stations in Estonia; for example, at coastal station Kunda the temperature rose to 12.5°C (the previous record was recorded on 14 November 1938). December 2019 was generally mild, with anomalies ranging from below +1°C in Iceland to above +5°C in easternmost parts of the region.

(II) PRECIPITATION

Overall, 2019 had close-to-normal precipitation in most of the Nordic countries, while some places in southeastern Norway recorded more than 120% of normal precipitation (fifth wettest on record in these areas). Southeastern Norway is normally less exposed to westerlies, but in 2019 it was temporarily affected by a southerly flow of moist air, particularly notable in autumn. Iceland was remarkably dry with some locations observing around 40% of normal precipitation.

Consequently, snow occurred slightly less frequently in the country (e.g., three days fewer than the 1971–2000 average in Reykjavik and five days fewer in Akureyri). The Baltic states also reported below-normal precipitation, particularly Estonia with 60%–80% of normal.

Winter was wetter than normal in Denmark with 105% and Norway with 120% of normal precipitation. Precipitation in Norway, however, was distributed inhomogeneously. While some stations in the east received 200%–300% of normal, several stations in the west received only about 50% of normal. Finland was close to normal with countrywide precipitation of 102% of normal. Estonia and Latvia were drier than normal with about 60%–80% of normal precipitation; western Iceland was even drier. Southern Lithuania recorded locally above 125% due do some low-pressure systems coming from central Europe. In late January, snow cover with depths up to 33 cm developed in eastern Lithuania and locally in western areas. A thin snow cover was observed in March.

Spring again was wetter than normal for the Nordic countries except Iceland (Norway 120%, Denmark 130%, Finland 118% of normal), while the Baltic States reported below-normal precipitation (Latvia 82%, Lithuania 75% of normal). April was extremely dry in the whole region. Latvia reported only 9% of normal precipitation, its driest April on record. Finland received 42.8% of normal, ranking fourth driest, and Denmark reported only 36% of normal precipitation.

The summer season was drier than normal for all countries of the region except for Denmark (115% of normal) and Norway (105% of normal). Finland received only 67%, Latvia and Lithuania 83%, and Estonia 78% of normal precipitation. June was very dry in Estonia. Countrywide, only 30% or less of the monthly normal precipitation was received. The monthly total for Kihnu (island southwest of Estonia), was only 0.3 mm, which is 1% of the month's normal and a record low in a series starting in 1932. July was drier than normal in Finland (48% of normal, its fifth driest on record), Sweden (52% of normal), most of Norway (70% of normal), and Estonia (78% of normal).

Autumn was rather wet in southern Finland and Sweden, southeastern Norway, and Denmark. Denmark reported its wettest autumn on record with 153% of normal precipitation. While some stations in eastern Norway received 150%–200% of normal, several in the western parts reported less than 50% of normal. Sweden received 141%, Finland 124%, Estonia 123%, Latvia 118%, and Lithuania 98%. The first snow fell earlier than usual in Lithuania in early October.

December 2019 was again a wet month for much of the Nordic countries (locally above 250% of normal in northern Finland), but closer to normal or drier in the Baltic countries with a scarcity of snow. Iceland was mainly snow-covered in December, with the greatest depth of 130 cm reported in the north of the country on 23–25 December.

(III) NOTABLE EVENTS AND IMPACTS

Between 1 and 2 January, an extratropical cyclone led to storms and extensive damage to forests north of Stockholm. Up to one million cubic meters of wood were felled by the storm. In Finland, a record 10-min average wind speed of 32.5 m s^{-1} was measured in the Gulf of Bothnia, and wave heights up to 8.1 m at the Sea of Bothnia buoy were close to previous records (just 0.1 m short of the record for any Finnish buoy; the northern Baltic Sea buoy records date to 1996). The storm caused an estimated damage of 10–20 million Euros ($11–22 million U.S. dollars).

In June, Lithuania saw back-to-back temperature and rainfall extremes. A three-day heat wave starting on 11 June brought an absolute maximum temperature record of 35.7°C in the city of Kaisiadorys (southern Lithuania). Days later, on 22 June, an extreme rain event brought 94.4 mm of precipitation in only 1.5 hours in Ustukiai (northern Lithuania). Many local crops were damaged as a result.

Western Norway experienced intense storms in mid-September, with uprooted trees, downed power lines, floods, landslides, and several road closures. Ships had to stay in harbor in Ålesund, stranding 3400 passengers.

5) Iberian Peninsula

This region includes Spain and Portugal mainland. The base period for Spain is 1981–2010, while the base period for Portugal is 1971–2000.

(I) TEMPERATURE

The yearly mean temperature on the Iberian Peninsula was mostly between 0.0°C and +1.0°C above normal. Spain reported a countrywide anomaly of +0.8°C, its sixth-warmest year since records began in 1965. Anomalies in some parts of Spain exceeded +1.0°C. The annual mean anomaly for the Portuguese mainland was +0.3°C. Overall, winter was warmer than normal. Spain reported an anomaly of +0.8°C and Portugal +0.4°C. After the year started with colder-than-normal temperatures in January (−0.1°C anomaly), a very warm February followed, ending the season with temperatures +1.2°C above normal in Spain. In northern Portugal, about 30% of the stations registered new maximum temperature records for February.

Spring started with a warmer-than-usual March, with anomalies of around +0.7°C. While April was close to normal, May proved to be warm again, especially in southern Spain and Portugal, the latter reporting its seventh-warmest May since 1931. Overall spring anomalies were +0.5°C for Spain and +1.0°C for Portugal.

The summer was warmer than normal by +0.8°C for Spain, contrary to Portugal where temperatures were below normal by −0.3°C. During a heat wave from 26 June to 1 July, the highest measured temperatures in Spain reached well above 40.0°C, including 43.4°C in Lleida and 43.2°C at Zaragoza Airport, each on 29 June, and 43°C at Girona Airport on 28 June (all located in northeastern Spain). Seven primary stations in Spain recorded new seasonal daily maximum temperature records during this heat wave.

With an anomaly of +0.7°C, Spain had a warm autumn. Only November (anomaly +0.1°C) had close-to-normal temperatures, while September and October were warmer than usual with anomalies of +0.7°C and +1.3°C. December, too, was a mild month with anomalies above +2°C in central parts of Spain.

(II) PRECIPITATION

Overall, Spain and Portugal reported a close-to-normal year with countrywide precipitation at 97% of normal in Spain and 86% in Portugal (1971–2000 base period for Portugal); however, there were spatial and temporal differences. Although precipitation was above 125% of normal locally in parts of southeastern Spain, most of Iberia had below-normal precipitation, dropping below 60% of normal in the southwest. Episodes of intense and persistent precipitation occurred often during the year, sometimes causing flooding. Multiple stations reported new local records of daily maximum precipitation.

It was the fifth-driest winter in Spain with 49% of normal rainfall. Portugal had 42% of normal precipitation, its fourth-driest winter since 2000. Only in January did northern parts of Spain receive above-normal precipitation. In February, precipitation across the entire Iberian Peninsula was widely 20%–60% of normal. With a countrywide average of 28% of normal precipitation, Spain recorded its fourth-driest February since 1965 and driest of the twenty-first century.

Spring started with a very dry March when precipitation ranged from 20% to 80% of normal in most parts of the Iberian Peninsula. After a very wet April with 148% of normal precipitation, the fourth wettest for Spain, the season ended with an extremely dry May. Nearly the whole Iberian Peninsula received 20%–60% of normal precipitation, with large parts of Spain below even that, making it the fourth- and sixth-driest May on record for Spain and Portugal, respectively.

The summer started with a dry June, ranking seventh driest for Spain (58% of normal) and Portugal reporting that 98% of its territory was under meteorological drought, with 30% categorized in severe or extreme drought. While July brought above-normal precipitation of 120% to Spain, the drought situation in Portugal worsened with precipitation of only 20%–80% of normal in the south

and locally even less. In August, precipitation was distributed heterogeneously in Iberia. Local precipitation totals were more than 250% of normal due to heavy rain. The drought was slightly relieved in northern and central Portugal by above-normal precipitation while the south stayed dry. Overall, Portugal ended the season with 77% of normal precipitation and Spain with 86%.

In autumn, Spain reported a countrywide average of 115% of normal precipitation. Double the normal precipitation was registered in some areas in Spain, such as between Granada and Murcia, while southwestern parts of Iberia were drier than normal with around 60% of normal precipitation. December was mainly wetter than normal, with 150% of the long-term average falling in places. Southern Spain recorded monthly totals below 80% of normal.

(III) NOTABLE EVENTS AND IMPACTS

In mid-May, a heat wave occurred across southern and western parts of the Iberian Peninsula. Alcácer do Sal, Barrosinha in southern Portugal reached 38.1°C on 13 May. Daily maxima at many stations in Portugal and western and southern Spain exceeded 30°C, more than 10°C higher than average daily maxima in places in Portugal.

Torrential rainfall and strong winds in southeastern Spain were observed during 10–15 September due to an almost stationary cut-off low. The most affected areas included Valencia, Alicante, Murcia, Albacete, Almería, and Malaga provinces. Some areas in Alicante and Murcia received more than 400 mm of rain over 48 hours. The highest total was 521 mm, measured in Orihuela (Alicante province). Six stations reported new 24-hour precipitation records. At Ontinyent, 296.4 mm of rain was recorded in 24 hours, about half its average annual total. This was the station's second-highest daily rainfall total on record, behind the 316.0 mm which fell on 4 November 1987. On average for the affected area, the equivalent of a year's rain accumulated in just one 24-hour period—from the morning of 12 September to the morning of the 13th. The storm was exceptional; there are no similar precedents in at least the last 100 years in the Vega Baja del Segura (Murcia province). Consequently, rivers broke their banks in several locations, flash floods damaged several roads, and cars were swept away. Flights, railway, and ship traffic were disrupted, and at least six people died and around 3500 were displaced, including 2000 residents of the town of Santomera (near Murcia).

6) Central Mediterranean region and Turkey

This region includes Italy (anomalies relative to 1961–90), Malta, Slovenia, Croatia, Serbia, Montenegro, Bosnia and Herzegovina, Albania, North Macedonia, Greece, Bulgaria, and Turkey.

(I) TEMPERATURE

The year was warmer than normal for the Mediterranean and the Balkan states. Serbia reported its warmest year on record, and Slovenia its second warmest since 1961, both with temperatures +1.7°C above normal. Italy observed its third-warmest year (+1.6°C), Turkey its fourth warmest (+1.2°C), and Greece its seventh warmest (+0.9°C).

Except for Greece (anomaly −0.2°C), winter was warmer than normal for the region, from +0.6°C above normal for Italy and Serbia to +1.3°C above normal for Slovenia and Turkey. January was colder than normal for some western parts of the region. Serbia and Greece reported January anomalies of −0.9°C and Italy −0.7°C. The season ended with a warmer-than-normal February, except for Sicily and Malta, the latter reporting its second-coldest February on record. Slovenia reported +3.1°C, Serbia +2.1°C, Italy +1.4°C, and Greece +0.7°C above normal.

Spring was warmer than normal for almost the entire region. Anomalies mainly ranged from +0.2°C to +0.7°C above normal. The end of the season, due to northwesterly flow and below-average solar radiation, was unusually cold in Italy and the Balkans. Slovenia reported one of its coldest Mays on record (anomaly –2.8°C), Italy its sixth coldest (anomaly –1.5°C), Serbia its eighth coldest (anomaly –2.1°C), and Malta and Greece reported anomalies of –1.5°C and –0.5°C respectively.

During the summer season, especially the Balkan states experienced widespread temperatures of more than +2.0°C above normal. Slovenia and Italy reported their second-warmest summer on record with anomalies of +2.5°C and +2.9°C, respectively, Greece its fourth warmest (+1.3°C above normal), and Serbia its fifth warmest (+1.8°C). June and August featured very high temperatures. It was the hottest June on record for Malta (+2.5°C), the second warmest for Slovenia (+4.2°C) and Italy (+3.9°C), and the fourth warmest for Greece (+1.5°C). August was the fourth (+1.7°C) and fifth (+2.7°C) warmest on record, respectively, for Greece and Italy.

For the Balkan states, an extremely warm autumn followed. For Croatia (+2.1°C), Serbia (+2.9°C), and Greece (+1.9°C), it was their warmest autumn on record, and Slovenia's second warmest with +1.9°C above normal. Turkey and Italy reported their third-warmest autumn, at +1.9°C above normal. December was also very mild with anomalies mostly between +1°C and +3°C, highest in northeastern Balkans and eastern Turkey.

(II) PRECIPITATION

Annual precipitation was mostly near-normal in the region, but locally well above average due to some heavy precipitation events, resulting in mostly above-normal country averages. Italy reported 113% of its normal precipitation and Slovenia 109%. In Serbia, precipitation was around normal.

Winter was drier than normal in Italy (63% of normal), Slovenia (68%), and Croatia (77%), while it was wetter for Serbia (120%) and Turkey (146%). It was the fifth-wettest winter on record (155%) for Greece. January was particularly wet across almost all the region; Greece reported its wettest January on record with 244% of normal precipitation. In Serbia, snow depths up to 39 cm were observed in the lowlands in mid-January.

Most of the region experienced a wetter-than-normal spring, with Turkey close to normal and Greece reporting slightly-below-normal precipitation of 93%. May was very wet in most of the region with the exception of Greece and Turkey. Croatia and Slovenia reported 195% of normal precipitation, Slovenia's wettest May on record. For Serbia, May was the sixth wettest since records began in 1951 (192% of normal), while Italy reported 185% of normal precipitation.

In summer, it was wetter than normal around the Aegean Sea and in Turkey, while Italy and the Balkans had near- or less-than-normal precipitation. Serbia was slightly wetter with 102% of normal. Turkey and Greece reported 136% and 131% of normal precipitation, respectively. For Italy, Slovenia, and Croatia, precipitation was between 77% and 84% of normal. June was notably dry for these countries with only 34% of normal in Italy, 50% of normal in Slovenia, 67% of normal in Croatia, and Malta reporting no June precipitation for only the fourth time in the last 70 years.

For Serbia, it was the sixth-driest autumn on record with 55% of normal precipitation. Turkey also reported well-below-normal precipitation for autumn (63% of normal). All other countries of the region received above-normal precipitation, except for Malta, which was near normal. For Italy and the Balkan states only, November brought a surplus of precipitation, while for Turkey, only September was wetter than normal in the southwestern and northeastern parts. December had a very heterogeneous distribution of precipitation. It was particularly dry in Sicily, North Macedonia, and Bulgaria (40%–80% of normal in parts), but very wet in southern Turkey, with above 250% of normal in places.

(III) NOTABLE EVENTS AND IMPACTS

Due to heavy snowfall during 3–5 January, many towns and villages were isolated from traffic connections in the central mainland of Greece. Electricity outages occurred mainly in the Thessaly region and Thessaloniki.

In Italy, during an unusual 32-day heat wave from 8 June to 9 July, maximum temperatures exceeded 30°C across wide areas and 40°C in places. At some locations, new records were set for the highest June minimum temperature (e.g., 27.5°C on 27 June in Milan). In Florence, the

maximum temperature exceeded the 90th percentile on 12 consecutive days, the second-longest heat wave since 1955.

Throughout May, the Emilia Romagna region in Italy experienced an exceptional wet spell. Due to heavy precipitation, severe thunderstorms, hail, and snowfalls, total monthly precipitation (average over Emilia Romagna) reached 228 mm, 40% higher than the previous record (164 mm in 1984) and three times higher than the 1961–90 climatological average of 73 mm. Consequently, flooding and landslides occurred, and 100 people were displaced.

On 23 September, two days after the strongest earthquakes to strike Albania in 30 years, severe thunderstorms and heavy rain caused flash flooding in some earthquake-affected areas. According to initial assessments, 1550 houses, two health centers, five bridges, and four power facilities were damaged in the floods. The European Civil Protection Mechanism was activated on 24 September following a request for assistance from the Albanian government.

7) Eastern Europe

This region includes European Russia, Belarus, Ukraine, Moldova, Romania, and West Kazakhstan.

(I) TEMPERATURE

Eastern Europe had an overall warm year. Romania (+1.7°C anomaly), the Ukraine (+1.9°C), Moldova (+2.1°C), and Belarus (+2.0°C) each reported their warmest year on record.

January featured an NAO index value of −0.4 that contributed to below-normal temperatures across most of eastern Europe, with anomalies of −1.0°C in Belarus, −0.7°C in Moldova, and −0.5°C in Ukraine. February (NAO of +1.9) was extremely mild, with anomalies ranging from +3.2°C above normal to more than +4.0°C in European Russia (+4.1°C) and Ukraine (+4.4°C). A negative NAO phase is often related to a meridional circulation pattern over Europe, causing the advection of cold continental air to eastern Europe, while a positive NAO is generally related to a more intense westerly flow from the North Atlantic Ocean bringing mild air to Europe in winter. Thus, January and February 2019 were very contrasting months in atmospheric circulation, which contributed to correspondingly different temperature anomalies.

Well-above-normal temperatures continued in spring. European Russia and Ukraine reported their eighth- and seventh-warmest spring, respectively, each with an anomaly of +2.3°C. Belarus and Moldova reported their fourth- and fifth-warmest spring (anomalies of +1.7°C and +1.4°C, respectively). March (NAO of +2.39) was especially warm, with anomalies of +2.9°C in both Belarus and Romania to +3.9°C in Ukraine, ranking among the top-10 warmest March months for all countries of the region (see Table A7.3 for temperature record lengths of each country).

June was exceptional. Belarus, Ukraine, and Moldova each reported their warmest June on record with anomalies of +4.5°C, +4.7°C, and +3.6°C above normal, respectively. Romania also reported its warmest June on record at +2.5°C above normal. Records were broken at several stations. In Belarus, daytime temperatures up to 34.7°C were recorded while nighttime temperatures often did not fall below 21.0°C between 11 and 26 June.

All three autumn months were warmer than normal for all eastern European countries except West Kazakhstan, which was repeatedly impacted by a northerly inflow of cold air. Belarus reported its second-warmest (+2.2°C), Moldova its third-warmest (+2.6°C), and Ukraine its eighth-warmest (+2.4°C) autumn. It was the warmest October (+2.87°C) in Belarus since records began. Abnormally warm weather between 14 and 22 October, with anomalies up to +10.0°C, was observed across Belarus. The season ended with a warmer-than-normal November, ranking the warmest for Romania (+4.9°C) and fifth warmest for Belarus (+3.2°C) and Moldova (+3.8°C), while for the Ukraine it was only the 12th warmest (+3.1°C).

December 2019 was extremely mild with highest monthly anomalies between +8°C and +10°C in the Arkhangelsk region in northwestern European Russia, with many new records of daily

maximum temperature, especially during 18–23 December. It was the second-warmest December averaged across European Russia (+5.3°C).

(II) PRECIPITATION

Annual precipitation was below normal for all of eastern Europe except for the northern parts of European Russia. Belarus reported 91% of normal precipitation, Ukraine 82% (fifth-driest year), and Moldova 73% of normal precipitation. Eastern Romania and West Kazakhstan received 60%–80% of their normal precipitation.

Overall, the winter was wetter than normal with up to 126% of normal precipitation in parts of the region. January brought a precipitation surplus and was the fifth wettest for European Russia (132% of normal) and Moldova (231%). February, on the other hand, was the fourth driest in Belarus with locally just 20% of normal precipitation. Ukraine reported 46% of normal precipitation, Moldova was close to normal (94%), and European Russia reported above-normal precipitation, up to 267% of normal in the northwest. Snow cover mostly persisted during winter, but in Moldova, February had only some days of snow. In Romania, February snow cover persisted in the mountains throughout the month and even into March above 1200 m a.s.l. European Russia also reported snowfall in March, even in the south (Krasnodar region, North Caucasus). In the Ukraine, record high snow depths (ranging from 40–50 cm, records dating to 1961) were measured at some stations in January.

Spring was wetter than normal in European Russia and Ukraine while Belarus and Moldova received below-normal precipitation. March was rather dry in Romania, Moldova, and Ukraine. Moldova reported its second-driest March on record with a countrywide average of only 1 mm, 3% of normal, and Ukraine received 64% of normal precipitation. In Belarus, it was slightly drier than normal (91% of normal), and European Russia reported a precipitation surplus of 115%. April was drier than normal across all of the region but was driest in European Russia, which reported its sixth-driest April with 66% of normal precipitation and Belarus recording its driest April on record with only 18% of normal precipitation. The season ended wet for the whole region with precipitation of 124%–161% of normal May precipitation, the latter being reported by Ukraine as its sixth-wettest May.

Summer precipitation was below normal except for European Russia with 108% of normal, mainly in the northeast. It was close to normal (97%) in Belarus. Ukraine and Moldova reported just 68% and 87% of their normal precipitation, respectively. Precipitation was distributed inhomogeneously in the summer months as locally extreme amounts were observed.

Autumn was drier than normal in the southern parts and wetter than normal in northern parts. Belarus reported 79%, Ukraine 67%, and Moldova only 27% (sixth driest) of normal precipitation for the season. For Ukraine and Moldova, all autumn months were drier than normal. In Moldova, September (19% of normal, 11th driest) and November (only 15% of normal, fifth driest) were outstanding. December had a similar distribution with above-normal precipitation in northern European Russia (up to 250% of normal), but drier than normal in the south (40%–80% of normal in large parts); however, heavy showers were observed at the Black Sea coast on individual days.

(III) NOTABLE EVENTS AND IMPACTS

On 11 and 12 January, Moldova experienced a cold spell with extreme precipitation totals of 30–190 mm in 48 hours, fallen as snow. Most fell in central and northern parts of the Republic. The snow depth reached up to 40 cm at meteorological stations. Roads were closed temporarily, and 14 communities in five districts were left without electricity for one day. Temperatures continued to be below normal in Moldova until the end of January. These cold spells also affected central European Russia where daily minima of around –20°C were measured in and around Moscow on 23 January, with some places below –25°C. Anomalies fell below –5°C. In northern European Russia (near Arkhangelsk), temperatures dropped to around –40°C on 26 January.

Freezing rain lasted from 2 to 5 February in the Rostov region in the European part of Russia. This damaged the region's electricity supply system and left 2144 buildings without electricity.

Due to the inflow of moist, warm air from the south, heavy thunderstorms developed in late April along a cold front over Romania. On 30 April, a large tornado about 110 km east of Bucharest damaged homes, agricultural fields, and vehicles. At least seven people were injured, most of them after the twister overturned a bus with 39 people inside. Ten houses were left without their roofs.

At several stations in southern and central Ukraine, new records of daily maximum precipitation totals were set on 3–5 June with 76–104 mm, representing 150%–200% of their monthly normal.

A heat wave in the Ukraine lasting from 6 June to 10 July brought record high temperatures and Ukraine's hottest June since records began in 1961, with an average monthly temperature +4.5° to +5.5°C above normal. Maximum air temperatures exceeded 30°C in most parts of the country, and for up to a week, 35°C was exceeded. Locally, anomalies reached up to +7.0°C. On 2 July, the highest maximum temperature record, in place since 1929, was broken at Voznesensk in the Ukraine with a temperature of 39.0°C.

8) Middle East

This region includes Israel, Cyprus, Jordan, Lebanon, and Syria.

(I) TEMPERATURE

The year was more than +1.0°C warmer than normal in most of the region. Temperature anomalies below +1.0°C were recorded only in Syria and northern parts of Jordan. It was the seventh-warmest year in the 69-year record for Israel, but also the coolest since 2013.

The Middle East experienced a warmer-than-normal winter, and anomalies in January and February exceeded +1.0°C locally. After a slightly colder-than-normal March, with anomalies down to –1.0°C for most of the region, April brought even stronger anomalies (below –1.0°C) to the Middle East, except in coastal areas and Cyprus. A warmer-than-normal May followed, with anomalies above +2.0°C in parts of Israel and Jordan. Israel reported its warmest May for at least 50 years. During a prolonged heat spell starting in mid-May, multiple Sharav events (hot and dry winds coming from desert regions) brought very high temperatures to Israel, most notably from 22–24 May when maxima of 43°–45°C were reached in the coastal plain and up to 47°C in the Dead Sea region. Overall, spring was closer to normal except for Cyprus where temperatures were +0.7°C above normal.

Summer was warmer than normal by more than +1.0°C. In June, anomalies in the Middle East were close to +2.0°C and exceeded this in Jordan, placing summer 2019 among the warmest five summers for all countries in the region. The warmth continued in autumn and December with anomalies of well above +1.0°C in much of the Middle East in all four months of September–December.

(II) PRECIPITATION

Overall, the year was drier than normal in southern parts of the Middle East with precipitation 80%–100% of normal in Israel and Jordan, but above normal (above 150% locally) in Syria, Lebanon, and Cyprus.

During January, Cyprus, Lebanon, and the western parts of Syria received above-normal precipitation, while in Israel and Jordan, precipitation was below normal. February was wet again except for some parts in the east of Syria.

In spring, above-normal precipitation (>125% of normal) was received in northern and western Syria and in Lebanon. Southeastern Syria and eastern Jordan had an early start to the dry season, receiving less than 10 mm in the whole spring. In May, precipitation was scarce across the entire region. The dry season continued until September.

In October, the rainy season started in Cyprus, western Syria, Lebanon, and northern Israel, with generally normal rainfall. Rainfall did not increase much in November except some locally heavy showers along the Syrian coast; monthly totals did not exceed 20%–80% of normal. Hence, the whole autumn season was drier than normal. December brought above-normal precipitation in most of the region, except southern Israel and southern and eastern Jordan. Monthly totals exceeding 250% of normal were recorded in parts of Syria and Israel.

Snow was recorded over the Troodos Mountains in Cyprus from January to April and in December 2019. In Israel, Jerusalem (800 m a.s.l.) had a thin layer of snow in mid-January; snow fell in February in the northern parts of the Golan Heights and the peaks of the Galilee Mountains, and even in April on Mount Hermon (2814 m a.s.l.) for several successive days, which is unusual for this time of year.

(III) NOTABLE EVENTS AND IMPACTS

On 8 January, storm Norma brought strong winds, heavy rains and flooding, snowfall, and freezing temperatures in Lebanon and Syria, affecting over 11 300 Syrian refugees at more than 360 settlement sites, mainly in the Beqaa valley. The station Houche-Al-Oumara in Lebanon (920 m a.s.l.) recorded gusts up to 76 km h^{-1}, thunderstorms, 94 mm of precipitation in 48 hours, and a snow depth of 3 cm on the morning of 9 January. Although such storms are not rare in the eastern Mediterranean, the region was vulnerable due to the high number of refugees living in difficult housing conditions.

Between 29 and 31 March, 6500 families in a refugee camp in northern Syria were affected by flooding after torrential rainfall. Tents and personal belongings were destroyed or swept away. As a further consequence, the risk of spreading of illnesses was increased.

During an extreme Sharav event on 17 July, a daily maximum temperature of 49.9°C was measured in Sedom (southern Dead Sea region). This was the highest temperature recorded in Israel in more than 70 years. (The highest temperature ever measured in Israel was 54°C in Tirat Tzvi on 21 June 1942.)

Starting on 13 October, more than 100 forest fires broke out across central-western and northern Lebanon. Over 1200 hectares of land were burned. At least 72 people were injured. In the districts of Chouf and Nakkar, people were displaced after fires extended to populated areas. Twenty landmines exploded because of the fires. On 15 October, Lebanon requested assistance through the EU Civil Protection Mechanism for aerial forest firefighting capacities.

9) South Caucasus

This region includes Armenia, Georgia, and Azerbaijan.

(I) TEMPERATURE

The South Caucasus was warmer than normal by more than +1.0°C in 2019. It was the fourth-warmest year in Georgia since 1960, with an anomaly around +1.5°C. In the capital, Tbilisi, it was the second-warmest year (after 2018) since records began in 1881.

Winter was exceptionally mild. The whole region experienced anomalies above +2.0°C and nearly +3.0°C in Armenia. During all winter months, anomalies were above +2.0°C.

Spring started with a near-normal March in the South Caucasus followed by a colder-than-normal April with anomalies below –1.0°C in Armenia. However, due to well-above-normal temperatures in May, with anomalies above +2.0°C in the whole region, the season overall was warmer than normal.

Summer was characterized by a record warm June (in Georgia, the warmest since 1960) with anomalies of +3.0°C to +5.0°C for the whole region. In July, the western parts of Georgia were slightly colder than normal, and the other parts of South Caucasus had slightly above-normal

temperatures. This reversed in August when anomalies were below normal in Azerbaijan and above normal in Georgia and Armenia.

Autumn was warmer than usual in Georgia and Armenia, while temperatures in Azerbaijan were close to normal. Temperatures were unusually high in October with anomalies above +2.0°C across the region (third-warmest October since 1960 in Georgia), but cold air in the east caused a drop to slightly below-normal values in November in its eastern parts. Warm air came again in December, and anomalies increased notably to around +3°C.

(II) PRECIPITATION

Overall, the year was drier than normal in Armenia and Georgia, particularly in the east where precipitation was only 50%–60% of normal, while it was close to normal in Azerbaijan on average.

The winter season was wet in Azerbaijan and Armenia, which received 125%–250% of normal precipitation and more than 250% in places. Georgia received below-normal precipitation, below 80% of normal in places.

During spring, Azerbaijan again recorded above-normal precipitation of 125% or more while precipitation in Georgia and Armenia was closer to normal. Summer was drier than normal, with the highest deficits in eastern Azerbaijan and totals of only 40% of normal. The dryness persisted more or less during all three summer months; only Georgia received above-average rain in June and particularly July.

Autumn started with a wet September with heavy rain in places, particularly central Georgia and eastern Armenia. Locally, monthly totals exceeded 125% of normal, especially in Armenia. October and November, on the other hand, were drier than normal across the region with only 20%–60% of normal precipitation, and below 20% in places. The deficit continued in December, with a few exceptions; Armenia in particular experienced heavy rain. Due to abnormally dry conditions in December, snow cover in Georgia persisted 18–20 days only in the high-mountainous zone with recorded maximum snow depths up to 10–15 cm. The average snow depths at winter resorts (Bakuriani, Gudauri) were two to three times lower than in previous years.

(III) NOTABLE EVENTS AND IMPACTS

On 4–5 May, heavy rain and hail affected Georgia's eastern region of Kakheti. Heavy rain up to 150 mm day^{-1} in Lagodekhi (near the border to Azerbaijan) flooded entrances, basements, and first floors of many buildings. Infrastructure, such as roads and bridges connecting the villages, as well as riverbank protections, agricultural lands, vineyards, and fruit trees were destroyed. Supplies of drinking water and electricity were interrupted for a short period. In total, more than 5000 people were affected by this disaster.

On 5 August, heavy rain accompanied by a sea storm occurred in Adjara-Guria (southwestern part of Georgia) causing infrastructure damage. One person died.

g. Asia—T. Li, Ed.

Throughout this section the base periods used vary by region. The current standard is the 1981–2010 average for both temperature and precipitation, but earlier base periods are still used in several countries. All seasons mentioned in this section refer to those of the Northern Hemisphere (NH), with winter referring to December–February 2018/19, unless otherwise noted.

1) Overview—T. Li, Z. Zhu, P. Zhang, T. C. Lee, I. Gustari, Y. Mochizuki, C.-W. Choi, L. Oyunjargal, A. Moise, M.-V. Khiem, and H.-P. Lam

Annual mean surface air temperatures during January–December 2019 were above normal across most of Asia, with the temperature anomaly exceeding 1.5°C from Siberia to northeast Asia and from southwestern China to the Indochina Peninsula (Fig. 7.37). Annual precipitation amounts were above normal (>120%) from the southeastern side of the Caspian Sea to India; in northern China, from central to western Siberia; and in the southwestern part of eastern Siberia. Annual precipitation amounts were below normal (<80%) in the northern part of eastern Siberia, the eastern part of East Asia, northwestern China, and all of Southeast Asia (Fig. 7.38).

In winter, negative temperature anomalies were observed from the southern part of western Siberia to central India; positive temperature anomalies occurred from central Siberia to northeast Asia (Fig. 7.39a). In spring, positive temperature anomalies larger than 3.0°C dominated high-latitude Asia (north of 60°N, Fig. 7.39c). In summer, above-average temperatures continued in Siberia, except in the southern part of eastern Siberia (Fig. 7.39e). In autumn, negative temperature anomalies dominated from central Asia to the southern part of central Siberia (Fig. 7.39g).

Seasonal precipitation amounts varied across the region (Figs. 7.39b,d,f,h). Notably, India experienced positive precipitation anomalies in autumn due to the monsoon season ending late; negative precipitation anomalies occurred in Southeast Asia from spring to autumn due to the combined effects of El Niño in spring and a positive Indian Ocean dipole (IOD) in subsequent seasons.

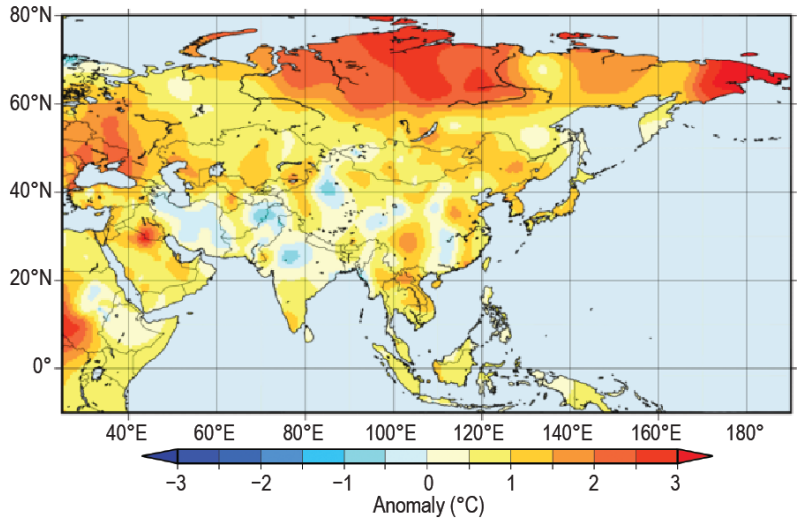

Fig. 7.37. Annual mean surface temperature anomalies (°C; 1981–2010 base period) over Asia in 2019. (Source: Japan Meteorological Agency.)

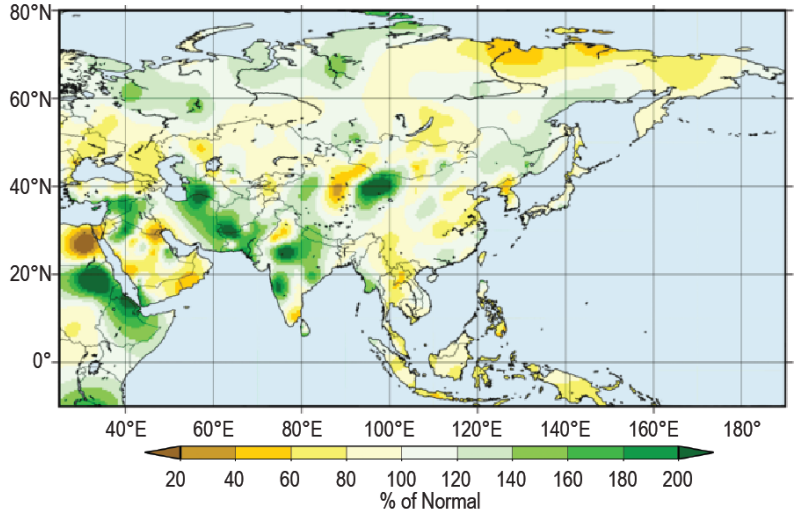

Fig. 7.38. Annual precipitation (% of normal; 1981–2010 base period) over Asia in 2019. (Source: Japan Meteorological Agency.)

In winter, the East Asia trough weakened and withdrew northward while the subtropical jet stream over Japan shifted northward. Positive anomalies of 500-hPa geopotential height and 850-hPa temperature occurred over the East China Sea (Fig. 7.40a). In spring, low-level cyclonic circulation anomalies straddling the equator over the western tropical Pacific were associated with enhanced convective activity in the western equatorial Pacific (Fig. 7.41b). In summer, negative 500-hPa height anomalies over northeast Asia (Fig. 7.40c), which were associated with the southward shift of the subtropical jet stream, brought below-normal precipitation over northeast Asia. In autumn, low-level anticyclonic anomalies straddling the equator were observed over the tropical Indian Ocean in association with suppressed convective activity over the Maritime Continent and southern tropical central and eastern Indian Ocean (Fig. 7.41d). A positive 500-hPa geopotential height anomaly was observed over Japan (Fig. 7.40d), accompanied by the northward shift of the westerly jet stream.

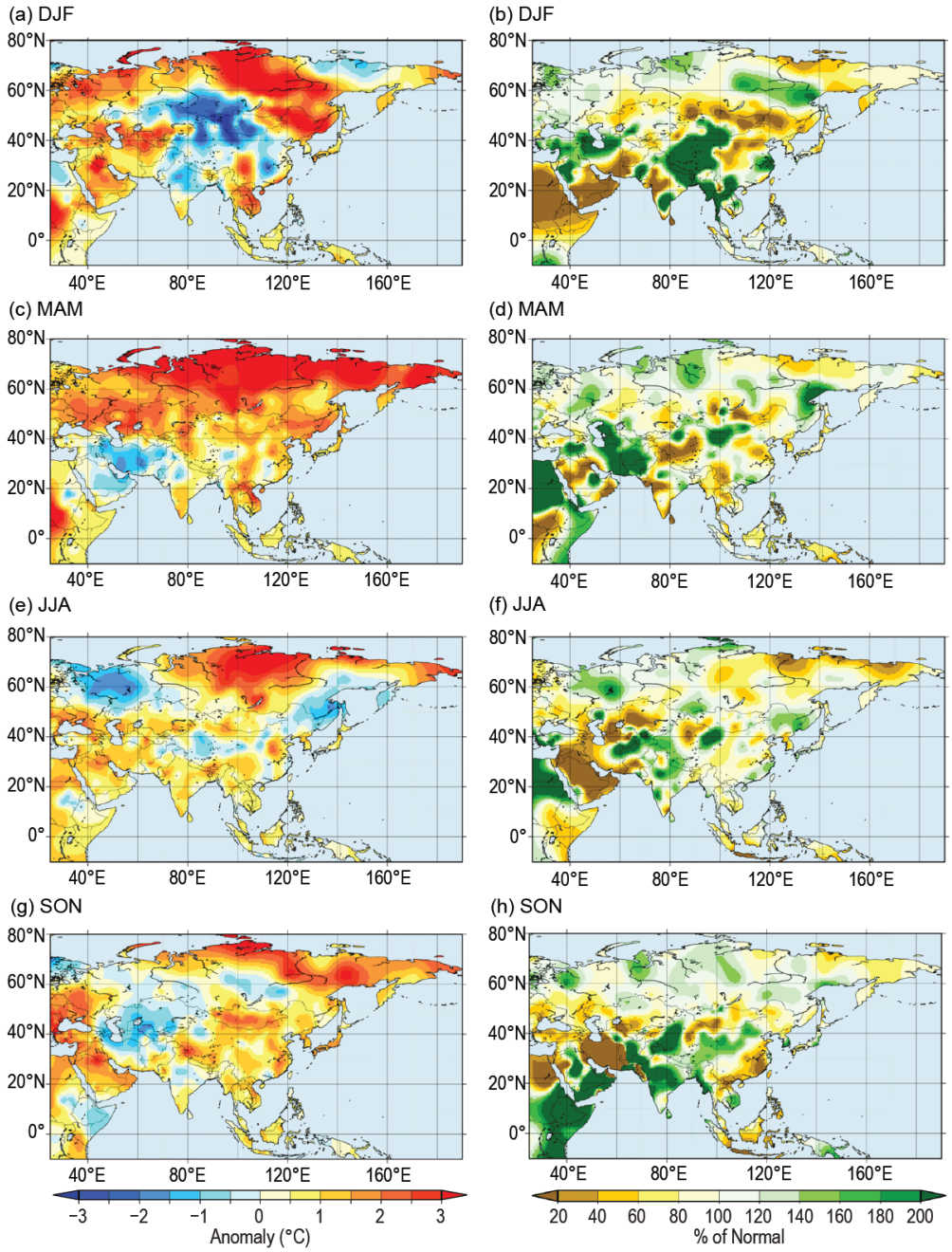

Fig. 7.39. Seasonal mean surface temperature anomalies (°C, left column) and seasonal precipitation (% of normal, right column) over Asia in 2019 for (a),(b) winter; (c),(d) spring; (e),(f) summer; and (g),(h) autumn. Base period: 1981–2010. (Source: Japan Meteorological Agency.)

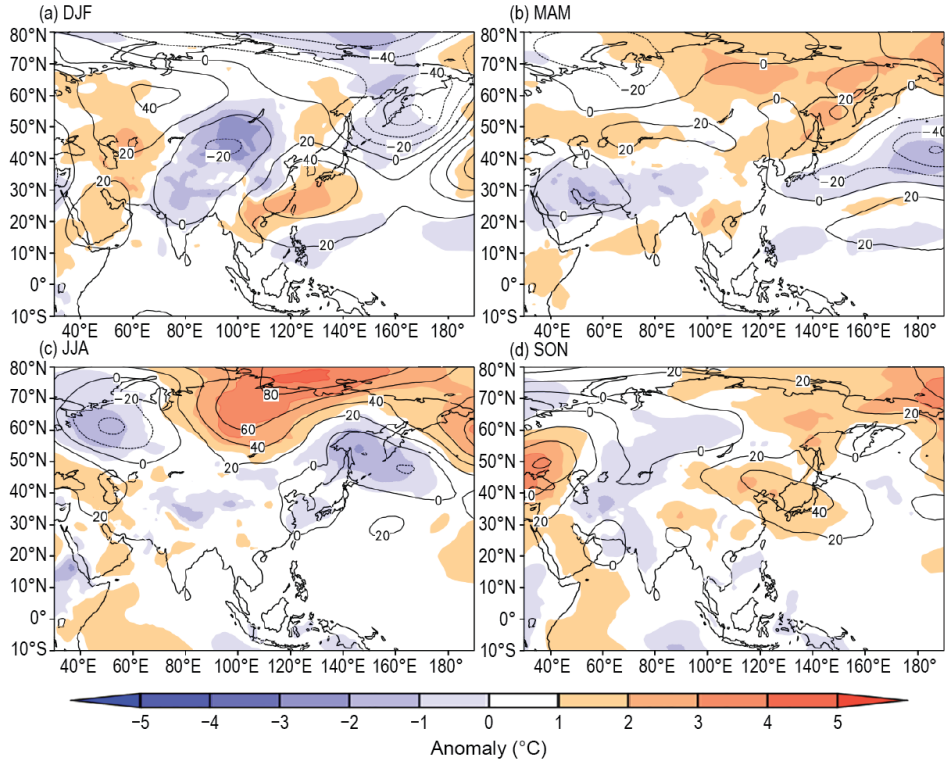

Fig. 7.40. Seasonal mean anomalies of 500-hPa geopotential height (contour; gpm) and 850-hPa temperature (shading; °C) in 2019 for (a) winter, (b) spring, (c) summer, and (d) autumn. Base period: 1981–2010. (Source: JRA-55 reanalysis, Japan Meteorological Agency.)

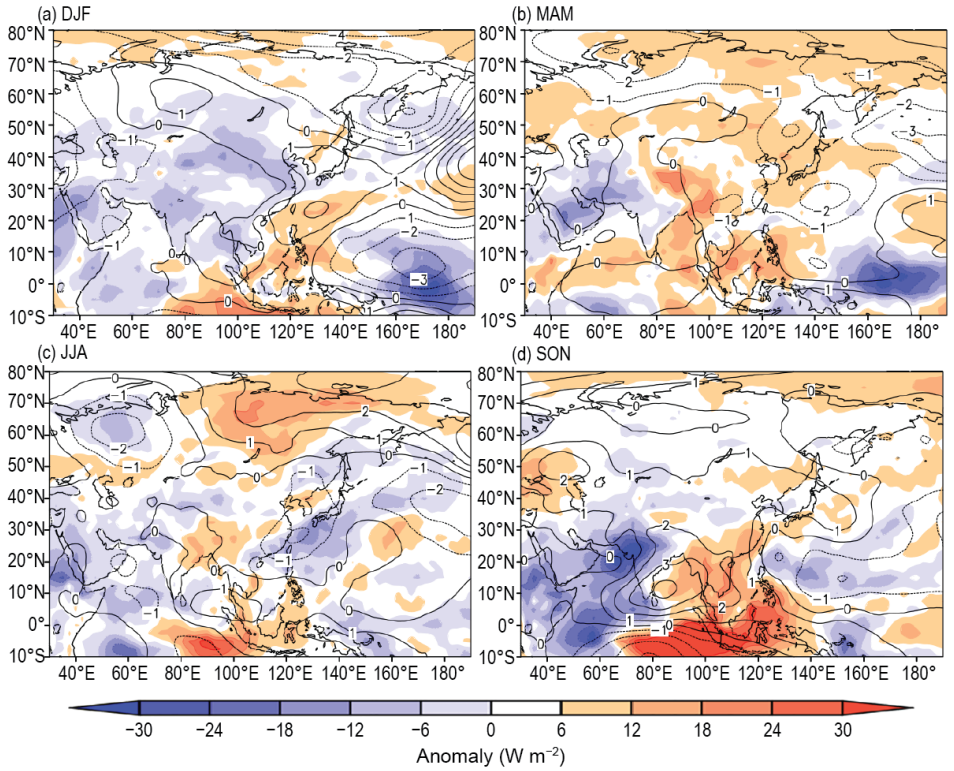

Fig. 7.41. Seasonal mean anomalies of 850-hPa stream function (contour; × 10^6 m^2 s^{-1}) using data from the JRA-55 reanalysis and OLR (shading; W m^{-2}) using data originally provided by NOAA in 2019 for (a) winter, (b) spring, (c) summer, and (d) autumn. Base period: 1981–2010. (Source: Japan Meteorological Agency.)

2) Russia—M. Yu. Bardin and N. N. Korshunova

Estimates of climate features for Russia are obtained from hydrometeorological observations of the Roshydromet Observation Network. Anomalies are relative to the 1961–90 base period, and national rankings and percentiles reflect the 1936–2019 period of record. The boundary between Asian Russia and European Russia is considered to be 60°E. Notable events and impacts (including damage and losses) are reviewed based on operational teletype reports and outlooks prepared by regional hydrometeorological service offices and collected and processed at the All-Russian Research Institute for Hydrometeorological Information–World Data Center (ARIHMI-WDC), Obninsk.

(I) TEMPERATURE

The 2019 mean temperature in Russia was 2.07°C above normal (Fig. 7.42), the fourth highest on record and almost 0.5°C higher than 2018 (the highest temperature on record [2.16°C above normal] was reported in 2015). Anomalies above the 95th percentile were observed at most central and southern European Russia stations and over vast territories in Siberia and the northern Far East, where annual mean temperatures exceeded the climatology by 3.5°–4°C. The highest annual temperature anomaly ever recorded, +2.51°C, was observed in the Central Federal district (part of western European Russia approximately over 50°–57°N, 32°–43°E; Fig. 7.37).

All seasons in Russia have warmed since the mid-1970s. Annual and seasonal trends are statistically significant at 99%, except for winter when the trend (insignificant even at 95%) is accompanied by a strong interdecadal variation. Winters were cooling after the mid-1990s and then started to warm again after 2010 (Fig. 7.42).

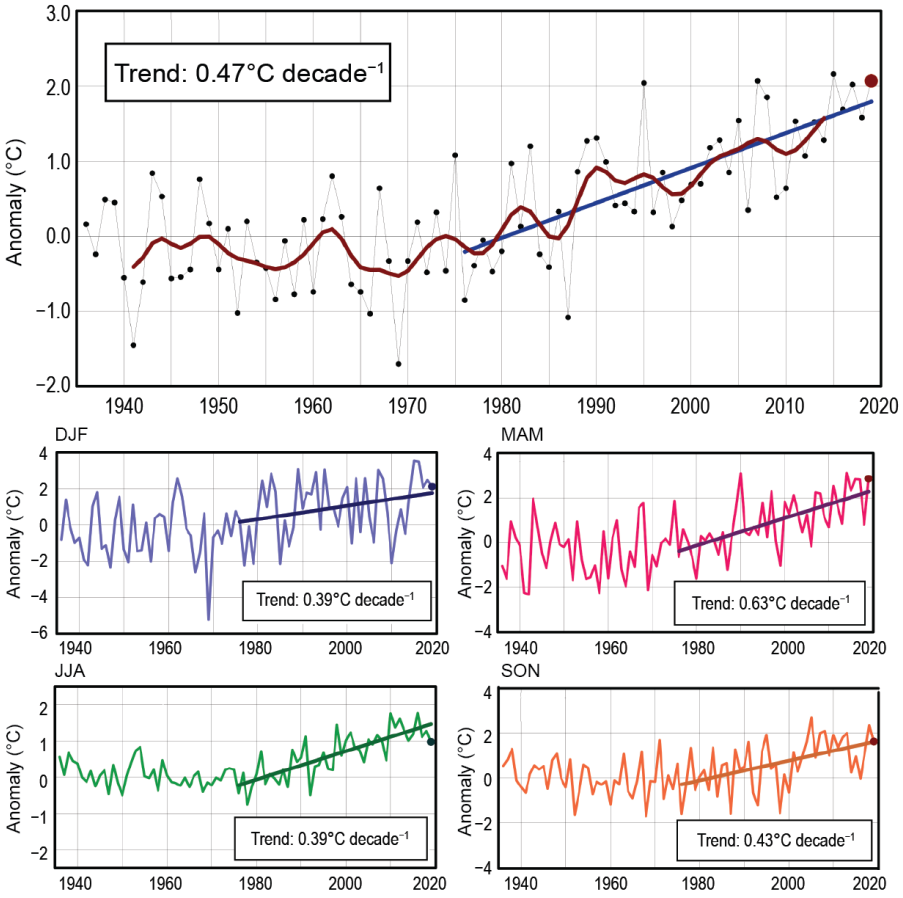

Fig. 7.42. Mean annual and seasonal temperature anomalies (°C; 1961–90 base period) averaged over the territory of Russia for the period 1936–2019. The bold red line on the annual mean time series is an 11-point binomial filter. Linear trend (°C decade^{-1}) is calculated for the period 1976–2019.

With a mean temperature 2.12°C above normal, winter 2018/19 was only the 15th warmest on record but still warmer than expected considering the recent linear trend. Winter was colder than normal in the south of western Siberia (Fig. 7.39a), especially in December 2018, when station temperatures were as much as –7°C below normal.

Spring was very warm: 2.86°C above normal, Russia's fourth-warmest spring on record. In March, the temperature was 4.30°C above normal, making it the fourth-warmest March on record. It was record warm in western Siberia: 6.30°C above normal. The weakened quasi-permanent Siberian anticyclone allowed numerous warm Atlantic cyclones to invade northern Siberia, forming a large warm anomaly in the region: +10° to +12°C above normal (Fig. 7.43). Many stations reported above-average temperatures throughout most of March. Uelen (66°36'N, 169°48'W, the easternmost settlement in Russia) reported a record high monthly temperature during two heat waves that occurred at the beginning of the month and at the end of the month. These heat waves were associated with strong cyclonic activity in the north Pacific.

Summer was moderately warmer than normal, with an overall temperature anomaly of +0.98°C (17th highest). Although Asian Russia was much warmer than normal, with a temperature anomaly of +1.32°C (seventh highest), European Russia observed a temperature anomaly of just +0.07°C

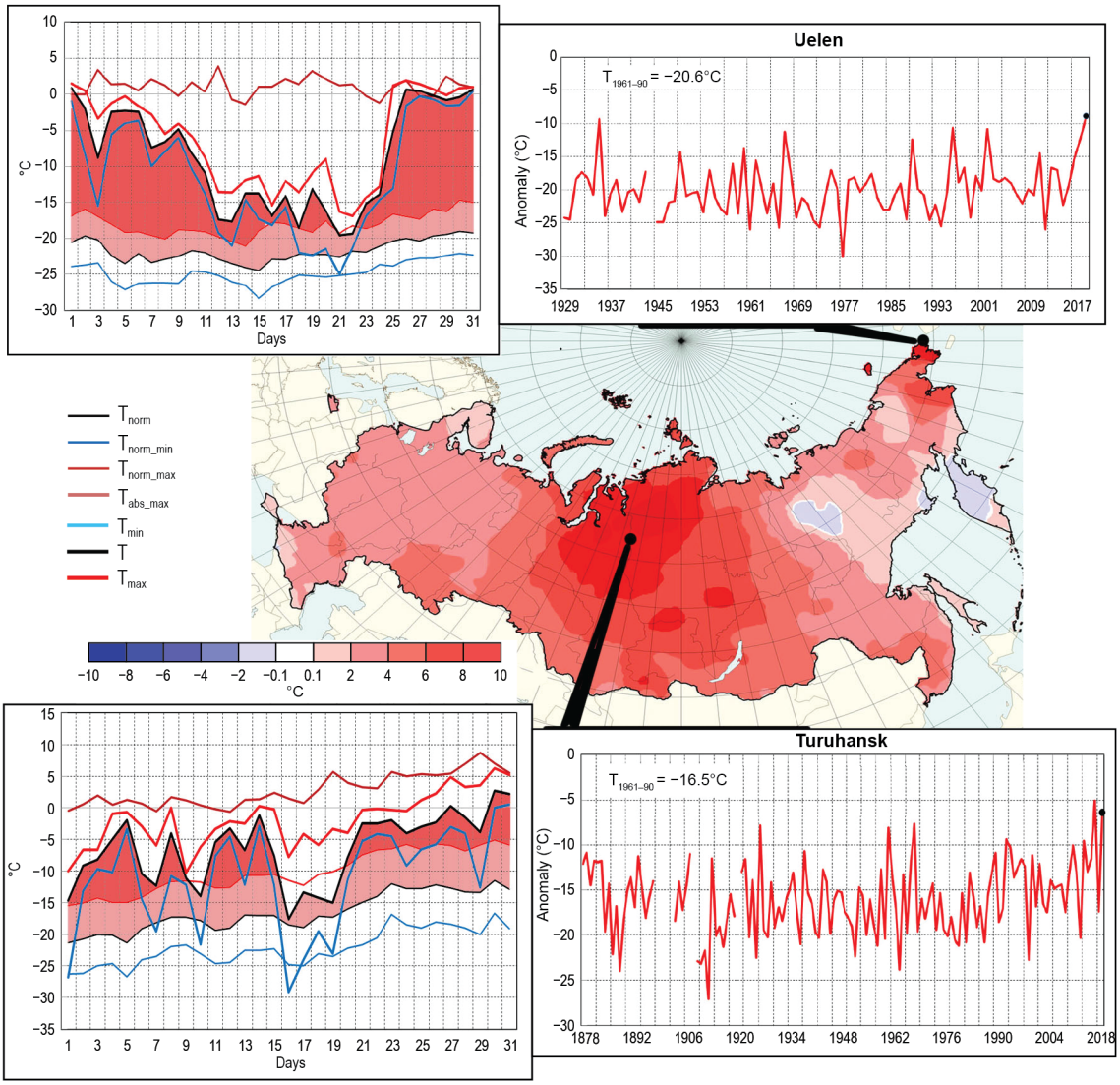

Fig. 7.43. Air temperature anomalies (°C; shaded) in Mar 2019. Insets: Mean monthly and mean daily air temperatures (°C) in Mar 2019 at meteorological stations Turuhansk and Uelen. Plots of daily temperature show observed daily mean (black), minimum (blue), and maximum (red) temperatures along with their climatological normals and absolute maximum temperature; the area between daily mean values above normal and the normal daily mean curve is shaded pink, and where values are above normal daily maximum, shading is red. Periods of record vary.

(51st-warmest summer, significantly lower than its median). This contrast was even more pronounced in August when Asian Russia experienced its third-warmest August on record (+1.47°C), while European Russia experienced an August among its 20 coolest (−0.47°C). June was record warm in the Far Eastern Federal district (Asian Russia east of 110°E) at 2.09°C above normal; European Russia south of 50°N was more than 4°C above normal.

Autumn was moderately warm in Russia as a whole and in Asian Russia, with an area-averaged anomaly of +1.60°C (10th highest). Separately, Asian Russia and European Russia reported seasonal anomalies of +1.76°C (10th highest) and +1.20°C (21st highest), respectively.

(II) PRECIPITATION

Total precipitation across Russia on average was about 108% of normal (sixth wettest; Fig. 7.44). The two wettest years occurred in the last decade (2013 and 2017: the only two years with precipitation more than 110% of normal). European Russia was wetter (110%, eighth wettest) than Asian Russia (106%, sharing 13th–15th in the record).

It was the 22nd-wettest winter since 1936 for the country as a whole, with precipitation 107% of normal. European Russia was wetter (114%, 14th wettest) than Asian Russia (100%, 31st wettest) due to excessive precipitation in European Russia north of 57°N in January and February (146%, fourth wettest; 185%, third wettest). This pattern is explained by the higher activity of North Atlantic cyclones, while strong anticyclonic circulation was observed in southern Siberia. In February, extreme precipitation (more than 200% of normal) was observed in parts of Asian Russia between 58°–65°N, 115°–130°E, and east of 165°E. February precipitation was much below normal in Siberia south of 50°N (<40% of normal) and in European Russia south of 50°N (49%, among the seven driest Februaries on record).

Spring was moderately wet for Russia as a whole, with 112% of normal precipitation (18th wettest). European Russia was extremely wet in March (161%; second wettest on record), with the area north of 57°N (the Northwestern Federal District) being the wettest on record with 173% of normal precipitation but dry in April, at 66% of normal (sixth driest on record for European Russia). In May, the Far Eastern Federal district (Asian Russia east of 110°E) received 146% of normal precipitation, its third-wettest May on record.

In summer, Asian Russia received 100% of its normal precipitation. European Russia was wetter than normal (108%, 19th wettest), with July precipitation 127% of normal (fourth wettest). Notably, the Northwestern Federal district received record high precipitation during July: 157% of normal. There was a significant deficit of precipitation in June in southern European Russia, particularly south of 50°N, except the North Caucasus (46%). Along with record high temperatures, this deficit contributed to severe drought in June in this important agricultural region.

Autumn precipitation in Russia was 109% of normal, sharing 11th on record. Asian Russia was wet with 114% of normal precipitation (fifth wettest), while European Russia received normal precipitation. In October, precipitation amounts varied widely between northern and southern European Russia. The Northwestern Federal District reported record high precipitation that was 172% of normal. Conversely, the Southern Federal District (European Russia south

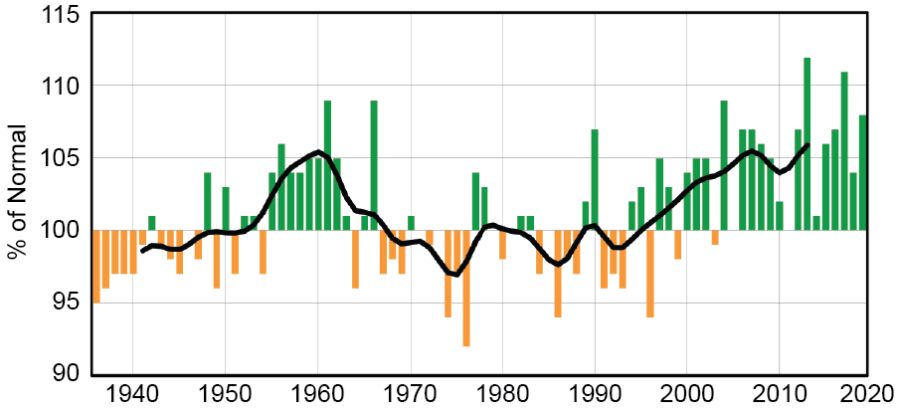

Fig. 7.44. Annual precipitation (% of normal; 1961–90 base period) averaged over the Russian territory for 1936–2019. The smoothed time series (11-point binomial filter) is shown as a bold line.

of 50°N) received only 58% of its normal precipitation, making October 2019 its fifth-driest October on record. November in the Southern Federal district was also dry: 58% of normal precipitation was observed, its third-driest November on record.

(III) NOTABLE EVENTS AND IMPACTS

On 5 June, hail in the Simferopol (44°57'N, 34°06'E) region (20–30 mm, with some hailstones reaching 40 mm in diameter) damaged cars and greenhouses. In addition, 2055 ha of crops including pea, barley, and wheat were damaged. Damages were estimated to be 156 million rubles ($2.15 million U.S. dollars).

On 25 June, heavy precipitation in the Irkutsk region in southeastern Siberia caused water levels to rise on the Biryusa, Uda, Iya, Ikeika, and Kirei Rivers. Four regions, 31 settlements, ~3700 residential buildings (with more than 9000 residents), 32 social facilities, and over 3700 household plots were inundated. Thirteen highway bridges were damaged and many local roadways were impacted. The flooding killed 26 people and injured 1400.

During 26–29 July, heavy, continuous rains in the Irkutsk region (Sayansk: 103 mm in 35 hours; Baikalsk: 123 mm in 24 hours) inundated 20 settlements (475 houses) and three sections of highways. A highway bridge over the Solzan River in Baikalsk was destroyed. The Siberian highway in Tulun was closed, with one bridge destroyed and traffic relocated.

Heavy rains during 1–10 November (109 mm, 220% of the climatological November value) caused flooding on the Yavon, Pola, Uver, Kholova, and Polist Rivers in the Novgorod Oblast region of northwestern Russia. Thirty-five settlements were inundated, with lines of communication cut off to some. Nineteen road sections were damaged and two wooden bridges were destroyed.

3) East and Southeast Asia—P. Zhang, T. C. Lee, I. Gustari, Y. Mochizuki, C.-W. Choi, L. Oyunjargal, A. Moise, M.-V. Khiem, and H.-P. Lam

Countries considered in this section include China, Hong Kong (China), Indonesia, Japan, South Korea, Mongolia, Singapore, and Vietnam. Unless otherwise noted, anomalies refer to the base period of 1981–2010.

(I) TEMPERATURE

Above-normal temperatures prevailed throughout the year across most of China (Fig. 7.37), with an annual mean temperature anomaly of +0.79°C (fifth highest since 1951), which includes an April mean temperature anomaly of +1.8°C (second highest for April since 1951). Hong Kong reported an annual mean temperature of 24.5°C, which is 1.2°C above the 1981–2010 normal and the highest since records began in 1884. Seasonally, Hong Kong experienced its warmest winter and autumn on record since 1884, with mean temperatures reaching 19.1°C and 26.1°C, respectively. There was only one cold day (daily minimum temperature ≤ 12.0°C) in 2019, which is 16.1 days fewer than normal and the fewest number reported since records began in 1884. The annual number of hot nights (with daily minimum temperature ≥ 28.0°C) was 46, which is 28.2 days above average and the most reported since 1884.

Annual mean temperatures were significantly above normal across Japan, with an annual temperature anomaly of +0.92°C, which is the highest since records began in 1898. South Korea's annual mean temperature was 13.5°C (+1.0°C; second highest since national records began in 1973). In May, the monthly mean temperature in South Korea was 18.7°C (second only to 2014 since records began in 1973). The annual mean temperature over Mongolia was 1.5°C (+1.0°C above normal); the country observed its warmest September on record with an average temperature 3.8°C above normal. Mongolia experienced the greatest negative anomaly of the year in February, with a mean temperature of –19.1°C (–2.5°C below normal).

The mean annual temperature of Indonesia was 0.56°C above normal. The highest anomaly recorded was +1.13°C in Kupang, East Nusa Tenggara Province. Singapore's annual mean

temperature was 28.4°C, 0.9°C higher than average and tied with 2016 as the warmest year on record. Four of the past five years are among the country's 10 warmest years since 1929, when records began. Above-average monthly temperatures were recorded every month of 2019, with August (29.1°C) and September (29.0°C) each record warm, with anomalies of +1.2°C and +1.4°C, respectively. November 2019 (28.0°C) tied the record with 2015 and 1998 for warmest November, at +1.4°C above average.

The annual mean temperature for most regions of Vietnam was 1° to 2°C above normal. On 20 April, the temperature in Huong Khe (Ha Tinh) reached 43.4°C, the highest temperature ever observed in the country. There were also two extended heat waves in north and central Vietnam, lasting 27 days in June and 25 days in July, respectively.

(II) PRECIPITATION

Figure 7.38 shows the 2019 annual precipitation as a percentage of normal over East and Southeast Asia. China's annual mean precipitation was 645.5 mm (102.5% of normal; eighth wettest since records began in 1951). The annual total precipitation over river basins was above normal in the Songhua River (132% of normal) and below normal in the Huaihe River (76% of normal) and Haihe River (87%) basins, while near normal in the Yangtze River basin. In 2019, the annual total precipitation in Hong Kong was near normal at 2396.2 mm.

In Japan, annual precipitation amounts were below normal on the Sea of Japan side of northern and eastern Japan, and above normal on the Pacific side of eastern and western Japan and in Okinawa/Amami. Annual total precipitation in South Korea was 1184.3 mm, which is 90.5% of the normal precipitation amount of 1307.7 mm. Although Mongolia's annual precipitation was near normal at 193.4 mm, January was the driest month since records began in 1981 at 32.2% of normal.

In Indonesia, annual rainfall was generally below normal, with a national average (from 104 meteorological stations) of 1920 mm. This is about 81% of normal, making 2019 the fourth-driest year since records began in 1981, behind 1997, 1982, and 2015, all of which are years with strong El Niño events. The largest rainfall deficit, approximately 50% of normal, was recorded at Tretes Station (East Java Province). The year was particularly dry in Singapore, where the Changi climate station recorded an annual rainfall amount of 1368 mm, 63% of normal, making 2019 the third-driest year for Singapore since records began in 1869.

Annual rainfall for most of Vietnam was 80% to 90% of normal, which contributed to widespread drought, water shortages in the south-central and highland regions, and saltwater intrusion in the Me Kong delta region. However, Nghe An to Thua Thien Hue experienced torrential rainfall. From 1 to 5 September, rainfall totals broke precipitation records in Vinh (Nghe An): 878 mm; Huong Khe (Ha Tinh): 933 mm; and Ha Tinh (Ha Tinh): 952 mm.

(III) NOTABLE EVENTS AND IMPACTS

In 2019, five tropical cyclones (TCs) made landfall in China. Tropical Cyclone Lekima was the fifth-strongest TC to make landfall since 1949 and remained inland for 44 hours. Seventy-four people perished or were missing, and there was approximately $8.5 billion (U.S. dollars) of direct economic losses. In early September, Typhoon Faxai made landfall in the Kanto region in eastern Japan, and a record maximum wind gust speed of 57.5 m s^{-1} was observed at Chiba in the Chiba Prefecture. In mid-October, Typhoon Hagibis made landfall on the Izu Peninsula and moved northward to northern Japan. Record heavy rainfall was observed across a wide area, causing severe damage that included flooding from multiple rivers. Seven typhoons affected South Korea during the season, tying with 1950 and 1959 for the most on record. In the South China Sea, six tropical cyclones hit Vietnam directly. Please refer to Chapter 4 for more details about the western North Pacific TC season.

In total, China experienced more high-temperature days (defined as the number of days with daily maximum temperature exceeding 35°C) than normal, with most occurring in the Yunnan

province of China from mid-spring to early summer, in the Shandong province from early to mid-summer, and in the southern part of China from mid-summer to mid-autumn. Northern China experienced 10 sandstorms in the spring, significantly fewer than normal (17).

In winter, a weak Siberian High due to above-normal surface temperatures over Eurasia prevented cold air from reaching the Korean Peninsula. This resulted in an above-normal (+1.3°C) monthly mean temperature in December, which in turn contributed to record low snowfall amounts in many regions in the country.

In Mongolia, 99 hydro-meteorological extreme events were reported; during the summer, occurrences of convection with accompanying extreme events such as flood, hail, and lightning were comparatively higher than in recent years. In particular, lightning frequency was the highest on record. Together, these extreme events caused 22 fatalities and about $5.6 million (U.S. dollars) in economic losses.

In Indonesia, 2019 was marked by severe drought. The longest dry spell (i.e., no observed rainfall), which occurred in the East Sumba District of the East Nusa Tenggara Province, lasted 263 days. Meanwhile, in June, a rare frost reported in the mountainous region of Dieng, Central Java Province (around 2000 m above mean sea level), damaged agricultural crops such as potatoes and carrots.

Sidebar 7.5: **An unusually cool summer in East Asia and a positive Indian Ocean dipole event**—W. WANG, T. LI, F. XIN, AND A. SHIMPO

In 2019, an unusually cool summer, particularly in June–July, occurred over a vast region of East Asia and expanded from central China to Japan (Fig. SB7.11). In fact, the mean June–July 1000-hPa temperature over the region was among three lowest in the past 20 years (Fig. SB7.11a).

The cause of this extremely cool early summer was attributed to an anomalous low-level cyclone centered over southwest Japan (Fig. SB7.11b). Northeasterly anomalies to the northwest of the cyclone advected drier and cooler air from higher latitudes, leading to large-scale negative temperature and specific humidity anomalies, expanding from central China to southern Japan (Figs. SB7.11b,c). The cold and dry advection led to the decrease of low-level moist static energy (MSE) north of 30°N (Fig. SB7.11d), which further reduced local convective instability and caused a precipitation deficit there (Wu et al. 2017; Li et al. 2017). Meanwhile, southwesterly anomalies to the south of the cyclonic center advected higher mean MSE northeastward, increasing the convective instability south of 30°N (Fig. SB7.11d). Such a meridional contrast caused a dipole pattern of the rainfall anomaly over East Asia (Fig. SB7.11c).

A further examination of temperature, precipitation, and wind anomalies over a larger domain reveals that a positive 1000-hPa temperature anomaly appeared over the eastern equatorial Pacific (Fig. SB7.12a). In response to this temperature forcing, westerly anomalies occurred in the central equatorial Pacific, and rainfall deficits appeared over the Maritime Continent (Figs. SB7.12a,b). A negative precipitation anomaly also appeared over the Indian subcontinent (from 10° to 30°N, Fig. SB7.12b). Meanwhile, a zonally oriented upper-level wave train, characterized by an alternating anomalous low–high–low or cyclone–anticyclone–cyclone pattern, occurred along 38°N (Figs. SB7.12b,c). It is speculated that this upper-tropospheric wave train (sometimes called a Silk Road pattern) was triggered by the negative heating anomaly over the Indian subcontinent. According to Gill (1980), a negative heating anomaly could induce a low-pressure anomaly in the upper troposphere, which could perturb the subtropical westerly jet, leading to the downstream development of a synoptic wave train along the jet axis. The wave train had a typical quasi-barotropic vertical structure and a zonal wavelength of about 4000–5000 km. As the wave energy propagated eastward along the jet, a cyclonic anomaly appeared over East Asia (Figs. SB7.12b,c). Note that compared to the location of the upper-level cyclone, the low-level cyclonic center shifted slightly southward (Figs. SB7.11b, 7.12b). The cause of this shift is attributed to the advection of low (high) MSE air to the north (south) of the cyclonic center,

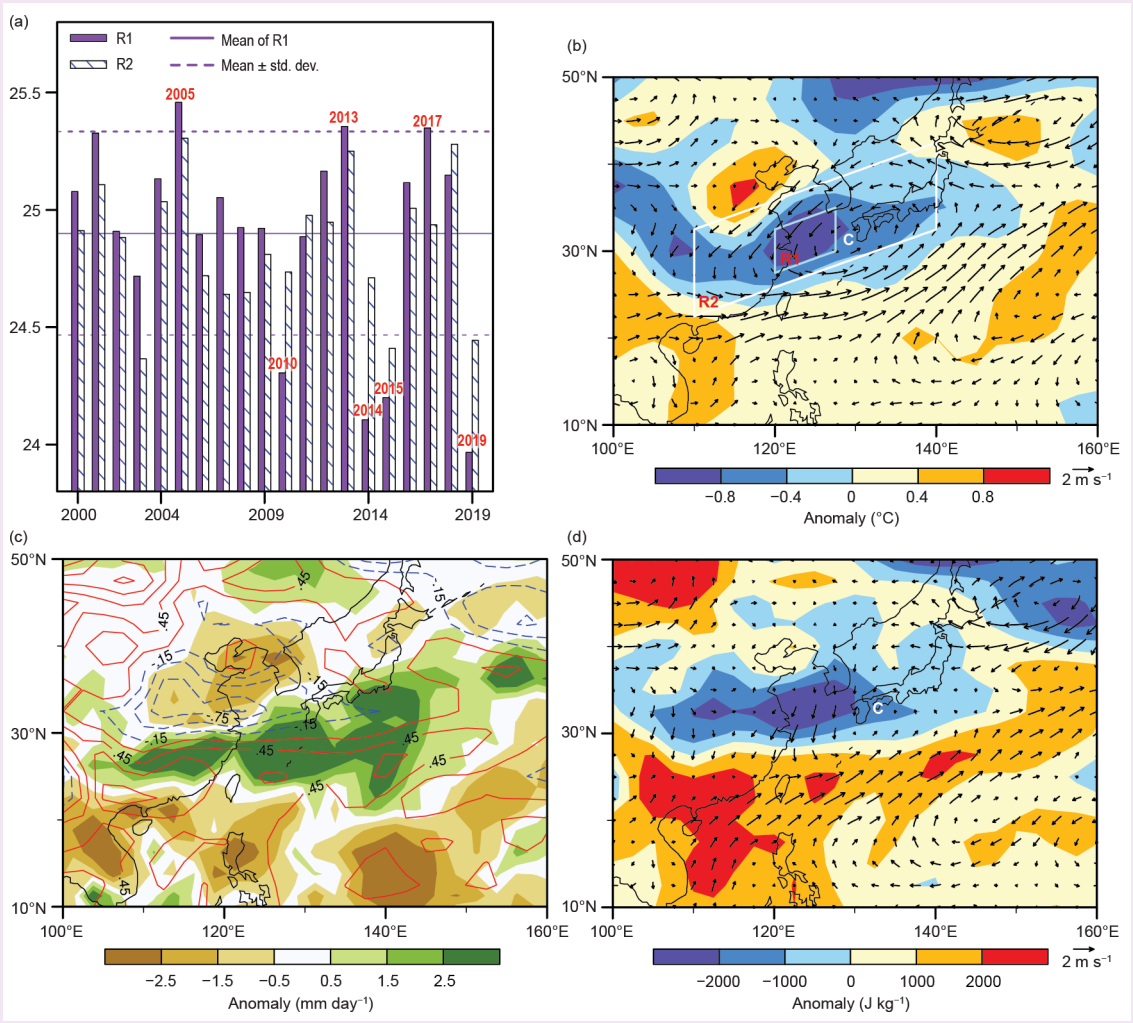

Fig. SB7.11. (a) Time evolution of area-averaged Jun–Jul mean air temperature at 1000 hPa during the past 20 years (2000–19) over the R1 and R2 regions (shown in the white boxes in b). (b) The horizontal patterns of 1000-hPa air temperature (shaded; °C) and 850-hPa wind (vector; m s^{-1}) anomalies. (c) The horizontal patterns of precipitation (shaded; mm day^{-1}) and 1000–850 hPa averaged specific humidity (g kg^{-1}) anomalies. (d) The horizontal patterns of 1000–850 hPa averaged MSE (shaded; J kg^{-1}) and 1000-hPa wind (vector; m s^{-1}) anomaly fields. (Sources: NOAA CMAP precipitation and NCEP/DOE Reanalysis II.)

which caused the southward shift of a positive rainfall anomaly response away from the original cyclonic center. The shifted rainfall response further affected the low-level circulation through a positive convection–circulation feedback. As a result, the low-level cyclone eventually settled at 33°N, shifting slightly southward relative to the upper-level cyclonic center.

In the Indian Ocean, positive (negative) sea surface temperature (SST) anomalies were observed in the western (eastern) tropical Indian Ocean, indicating a positive Indian Ocean dipole (IOD; Saji et al. 1999; Saji and Yamagata 2003) during boreal summer 2019, which in fact evolved into one of the strongest positive IOD events of the past three decades by late autumn (see section 4h). In association with positive IOD events, convective activity is generally enhanced over the western Indian Ocean and suppressed over the eastern tropical Indian Ocean and the Maritime Continent with lower-tropospheric easterly wind anomalies over the tropical Indian Ocean—these characteristic conditions were seen in this 2019 event (see section 4h). Figure SB7.13a shows a time–longitude cross section of outgoing longwave radiation (OLR) anomaly along the equator averaged over 5°N–5°S from July to December 2019, indicating a pair of persistent, enhanced convective activities over the western Indian Ocean and a suppressed one over the eastern tropical Indian Ocean and the Maritime Continent. The time–longitude cross section of equatorial 850-hPa zonal wind anomalies (Fig. SB7.13b) indicates easterly wind anomalies in the lower troposphere at the same time, especially in October and November, which can be attributed to the enhanced and

suppressed convective activities in and around the Indian Ocean. It is noted that the intensity of the 850-hPa easterly wind anomalies over the equatorial Indian Ocean (5°N–5°S, 60°–90°E) during the boreal autumn (September –November) in 2019 was one of the three strongest since 1958, using the Japanese 55-year Reanalysis (JRA-55; Kobayashi et al. 2015; not shown). This highlights one of the important features of this 2019 event.

In summary, an extremely cool summer occurred over a vast region of East Asia in 2019. This cooling stemmed from an upper-level wave train induced by an anomalous cyclone over southern Japan. Meanwhile, an independent phenomenon—a strong positive IOD event—occurred in the tropical Indian Ocean during boreal summer and autumn 2019.

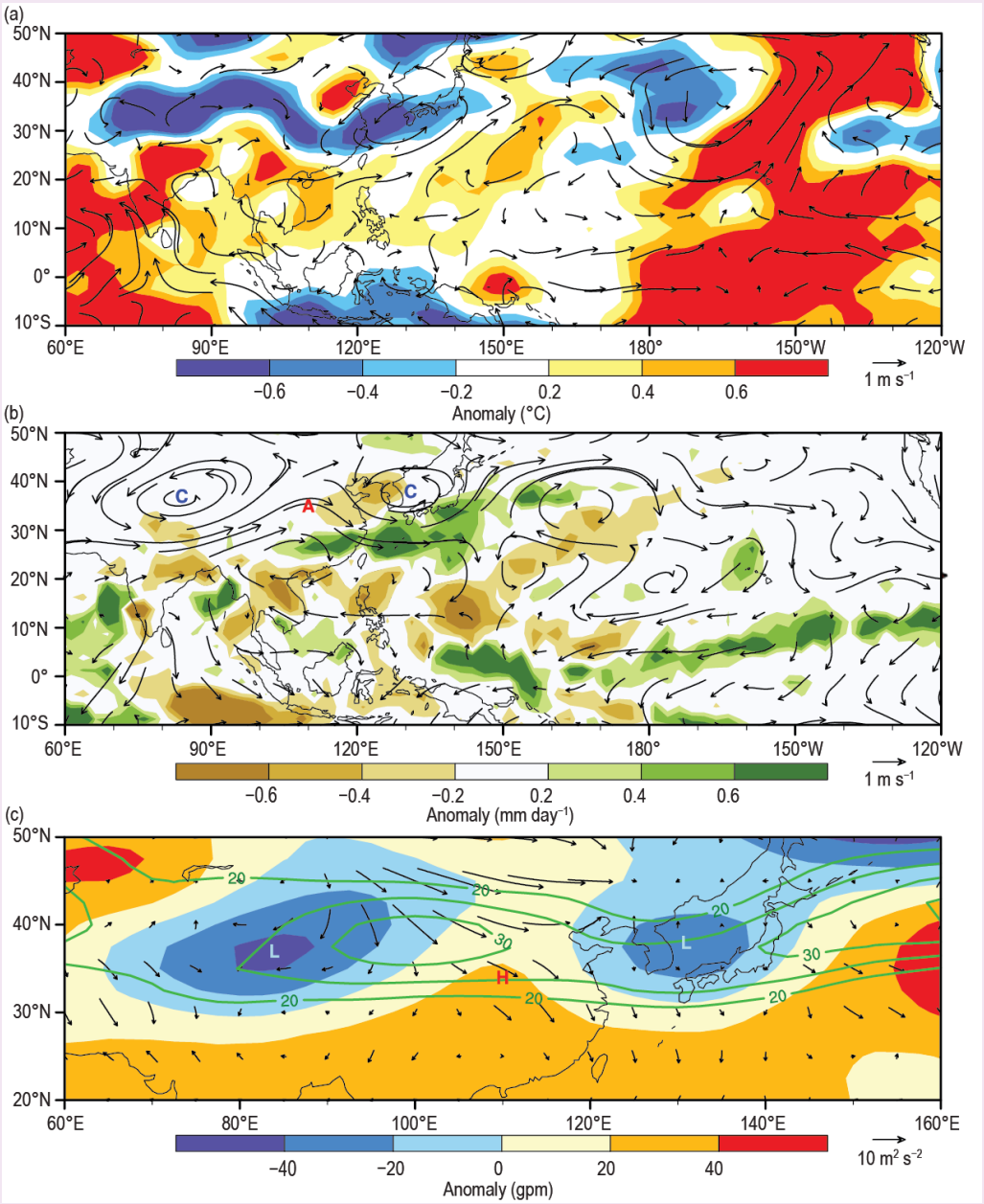

Fig. SB7.12. Horizontal patterns of (a) 1000-hPa temperature (shaded; °C) and 850-hPa wind (vector; m s^{-1}) anomalies; (b) precipitation (shaded; mm day^{-1}) and 200-hPa wind anomaly fields; and (c) wave activity flux (Takaya and Nakamura, 2001; vector; m^2 s^{-2}) and geopotential height (shaded; gpm) anomaly fields at 200 hPa averaged during Jun–Jul 2019 (Base period: 2000–19). Green contours in (c) denote the climatological zonal wind at 200 hPa.

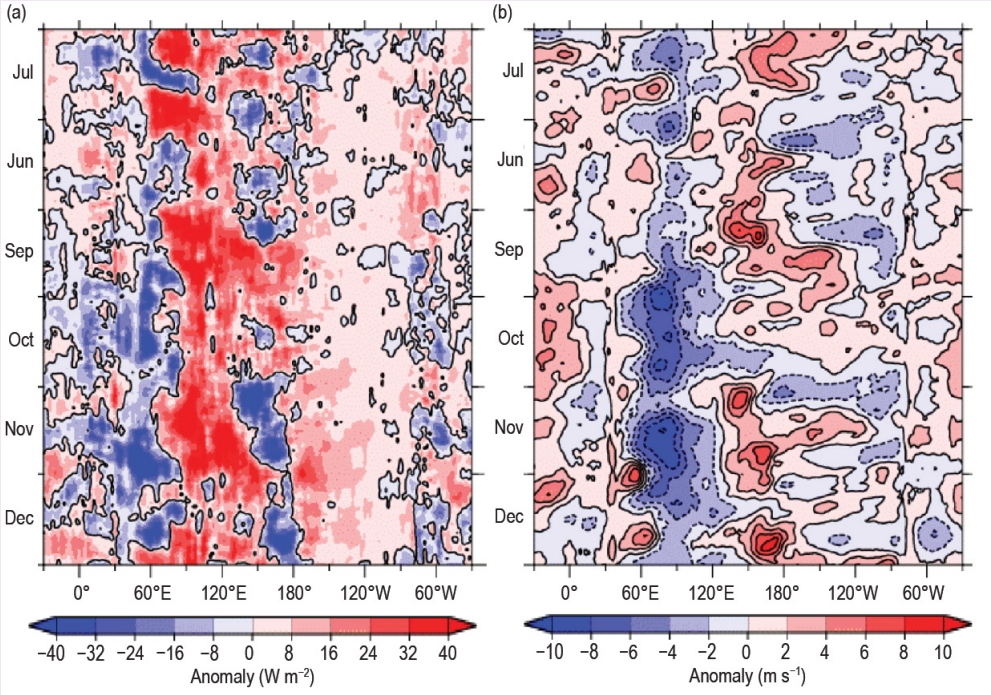

Fig. SB7.13. Time–longitude cross section (5°N–5°S) of 7-day running mean (a) OLR anomaly and (b) 850-hPa zonal wind anomaly for Jul–Dec 2019. Intervals are (a) 8 W m^{-2} and (b) 2 m s^{-1}, respectively (see color bars). Base period is 1981–2010. (Sources: Tokyo Climate Center; https://ds.data.jma.go.jp/tcc/tcc/products/clisys/ASIA_TCC/mjo_cross.html.)

4) South Asia—A. K. Srivastava, J. V. Revadekar, and M. Rajeevan

Countries in this section include Bangladesh, India, Pakistan, and Sri Lanka. Unless otherwise noted, climate anomalies are relative to the 1981–2010 base period.

(I) TEMPERATURE

In 2019, South Asia experienced above-normal temperatures. The annual mean surface air temperature averaged over India was 0.36°C above average, making 2019 its seventh-warmest year on record since nationwide records began in 1901 (Fig. 7.45). India's seasonal mean temperatures were above normal for all four seasons. Higher-than-normal temperatures during the

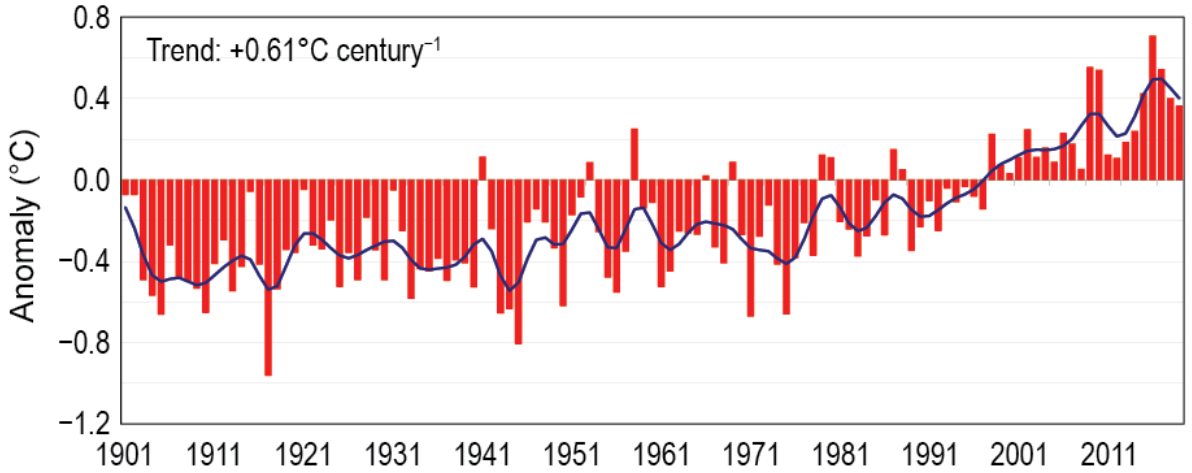

Fig. 7.45. Annual mean temperature anomalies (°C; 1981–2010 base period) averaged over India for the period 1901–2019. The smoothed time series (9-point binomial filter) is shown as a continuous black line.

pre-monsoon season (March–May; +0.39°C) and the monsoon season (June–September; +0.58°C, warmest since 1901) largely accounted for the above-normal annual temperature for the year. The 10 warmest years on record are: 2016 (+0.71°C); 2009 (+0.55); 2017 (+0.54); 2010 (+0.53); 2015 (+0.42); 2018 (+0.40); 2019 (+0.36); 1958 (+0.25); 2002 (+0.25); and 2014 (+0.24).

(II) PRECIPITATION

Summer monsoon season (June–September) rainfall contributes about 75% of the annual precipitation over South Asia. In 2019, the summer monsoon season set in over Kerala in southern peninsular India on 8 June, seven days later than its climatological normal date (1 June). The monsoon covered the entire country on 19 July, four days later than its climatological normal date (15 July).

The long-term average (LTA) value of the summer monsoon rainfall, calculated using all the data from 1961–2010, is 880 mm. The standard deviation of Indian summer monsoon rainfall (ISMR) is around 10% of the LTA value. However, over smaller regions, the natural variability of the monsoon is larger (std. dev. around 19%). During 2019, India as a whole experienced one of its heaviest summer monsoon rains since 1995 despite a delayed and suppressed monsoon during June. The ISMR averaged over the country as a whole was 110% of its LTA; however, seasonal rainfall was not evenly distributed over the country (Fig. 7.46).

The 2019 ISMR was also characterized by large temporal variability within the season (Fig. 7.47). Table 7.2 lists 24-hour rainfall records during the 2019 ISMR. Seasonal rainfall over the homogeneous regions of central India was 129% of its LTA; it was 116% of its LTA over the south peninsula. Northwest India and east and northeast India received 98% and 88% of their LTA, respectively. On a monthly scale, rainfall for the country as a whole was significantly below normal during June (57% of its LTA); near normal during July (105% of its LTA); and above normal during August (115% of its LTA). It was substantially above normal during September (152% of its LTA). During the season, out of 36 meteorological subdivisions, two subdivisions (Saurashtra and Kutch and West Madhya Pradesh) received large excess rainfall (more than 159% of their LTA), 10 received excess, 19 received normal, and the remaining five subdivisions received deficient rainfall.

During the remainder of the year, precipitation across India was above normal (148% of LTA) during winter (January–February); below normal (75% of LTA) during the pre-monsoon season (March–May); and above normal (129% of LTA) during the post-monsoon season (October–December).

Pakistan, which is at the western edge of the pluvial region of the south Asian monsoon, receives 60%–70% of its annual rainfall during its summer monsoon season (July–September). The summer monsoon sets in over eastern parts of Pakistan around 1 July with a standard deviation of five days. In 2019, summer monsoon rainfall over Pakistan was normal (99% of the LTA value). The country received near-normal rains during July (92% of

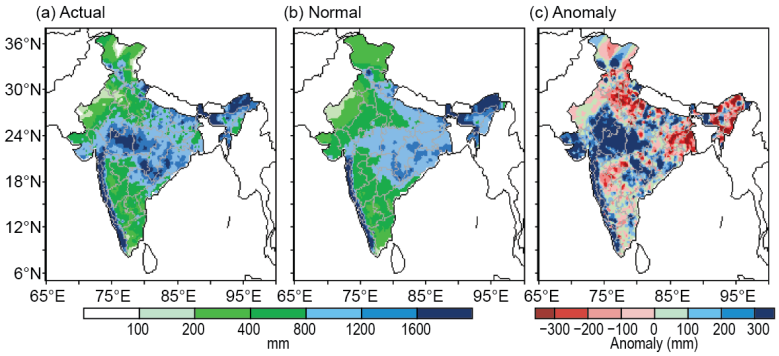

Fig. 7.46. Spatial distribution of (a) actual, (b) normal, and (c) anomalous monsoon seasonal (Jun–Sep) rainfall (mm) over India in 2019.

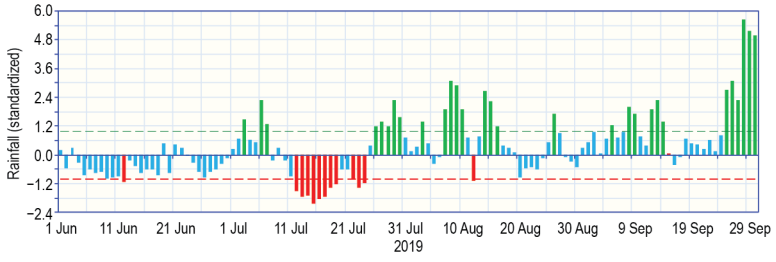

Fig. 7.47. Daily standardized rainfall time series averaged over the core monsoon zone of India (1 Jun–30 Sep 2019).

Table 7.2. Record 24-hour rainfall during the 2019 monsoon season.

Number	Station	Rainfall total (mm)	Date	Previous record (mm)	Date of record	Year of record
			Jun 2019			
1	Long Islands	308.0	13	281.9	7	1957
2	Raisen	115.6	30	110	24	1970
3	Kodaikanal	63.0	6	61.1	1	1986
			Jul 2019			
1	Shajapur	177.0	28	174.8	12	1998
2	Jagdalpur	201.8	29	180.9	7	1934
			Aug 2019			
1	Baroda City	556.8	1	277.1	5	1956
2	Alibag	410.9	4	311.2	19	1970
3	Coimbatore	120.0	9	60.8	6	1964
4	Vellore	165.7	17	106.2	8	1909
5	Tuticorin	30.5	18	30.2	12	1972
6	Uthagamandalam	183.6	9	84.2	20	1971
7	Coimbatore AP	106.4	9	83.7	24	1988
8	Belgaum (Sambra) AP	148.2	8	101.1	17	1978
9	Hassan	134.0	9	110	28	2008
10	Karipur	170.8	10	153.4	7	1997
11	Cial Cochi	212.7	9	66.5	12	2008
			Sep 2019			
1	Pant Nagar	129.4	1	105	10	1967
2	Seoni	313.4	9	208	1	1947
3	Jagdalpur	288.5	6	163.8	24	1911
4	Nandyal	125.8	16	97.8	25	1990
5	Medikeri	136.4	5	110.4	1	1995

its LTA) and August (103%), and above-normal rains during September (121%). Geographically, rainfall was generally normal except over northwestern Pakistan. Bangladesh received normal rainfall during its 2019 summer monsoon season. Sri Lanka also received normal rainfall during its summer monsoon season (May–September).

The northeast monsoon (NEM) normally sets in over southern peninsular India during October and over Sri Lanka in late November. The NEM contributes 30%–50% of annual rainfall over southern peninsular India and Sri Lanka as a whole. In 2019, the NEM onset over southern peninsular India occurred on 16 October, four days earlier than its normal onset date. NEM seasonal rainfall over southern peninsular India was normal (109% of its LTA value). The NEM rainfall activity over Sri Lanka was also normal.

(III) NOTABLE EVENTS AND IMPACTS

Heavy rain and flood-related incidents claimed over 850 lives in different parts of India during the pre-monsoon, monsoon, and post-monsoon seasons. Of these, 306 casualties were reported from the state of Bihar alone. From Maharashtra, 136 casualties were reported. From the southern Indian state of Kerala, 88 deaths due to heavy rains and landslides were reported during the second week of August. The cyclonic storm Fani, which crossed the Odisha coast on 3 May, claimed around 80 lives in the eastern coastal state of Orissa and neighboring Bangladesh.

During the first three weeks of July, severe flooding in Bangladesh affected 21 districts, resulting in 120 deaths and causing landslides and widespread destruction of properties and agricultural crops.

Heat wave conditions, which prevailed over northeastern and central India during March–June, claimed about 350 lives. Of these, 292 deaths were reported during 15–18 June from the state of Bihar. Many cities in northern and central India were abnormally warmer in the first three weeks of June, with temperatures surpassing 45°C for several days. Some unusually high temperatures observed on 3 June were Churu (50.3°C), Bikaner (48.4°C), and Ganganagar (48.8°C), all of which are in the state of Rajasthan. Temperatures over the capital city of Delhi remained above 45°C for 12 days and reached 48.0°C on 10 June, an all-time high for the month of June in the city.

Lightning associated with thunderstorm activity reportedly claimed over 380 lives in central, northeastern, northwestern, and the peninsular parts of India during the pre-monsoon, monsoon, and post-monsoon seasons. Snowfall- and avalanche-related incidents claimed 33 lives from Jammu and Kashmir, and 18 lives from Leh (18 January). A cold wave claimed 28 lives from different parts of Uttar Pradesh during the last week of December 2019.

Due to heavy summer monsoon rainfall, Sri Lanka experienced floods in September, which is rare for this month. The floods engulfed 13 districts, affecting about 120 000 people. In December, 14 districts across the country were flooded due to heavy northeast monsoon rains.

At least 24 people died and more than 2 million were displaced after Tropical Cyclone (TC) Bulbul hit the coastal areas of Bangladesh on 9 November.

5) Southwest Asia—A. Fazl-Kazem and A. Vazifeh

This section covers only Iran. Turkey is included in the Europe subsection, 7f. Climate anomalies are relative to a 1997–2017 base period for temperature and 1985–2019 base period for precipitation.

(I) TEMPERATURE

All seasons in 2019 experienced above-average temperatures (Fig. 7.48), with the greatest anomaly of +3°C in summer, leading to an annual anomaly of +1.6°C. The highest temperature anomalies in winter were recorded in northwest to northeast Iran (Ardabil, Gilan, and northern Khorasan-Razavi Provinces). In spring, with daily temperatures ranging from 0° to 20°C in most areas, the average temperature anomaly was +0.8°C for the country (Fig. 7.47b). The hottest areas in spring were the Dashte-Lut Desert, parts of Sistan and Baluchestan, and some regions of the Kerman Province where average temperatures ranged from 35° to 40°C. Average temperatures in the Alborz highlands (the climatological coldest area) ranged from –10° to –5°C.

The summer temperature anomaly was the highest among the four seasons and more spatially uniform (Fig. 7.48c). In parts of the northern provinces, as well as Isfahan, Khorasan Razavi, Yazd, Sistan and Baluchestan, Hormozgan, Fars, Bushehr, Khuzestan, and western Iran, the average temperature was between 30° and 40°C. Eastern and central Iran experienced average temperatures of 25°–30°C.

In autumn the average national temperature was +0.4°C above average. Except for Khorasan Razavi, all provinces experienced above-average temperatures for the season, with most anomalies ranging from +0.1° to +3.0°C (Fig. 7.48d). The highest anomalies were over western and southeastern Iran, Semnan and Isfahan Provinces, and a small part of northern Mazandaran.

(II) PRECIPITATION

Iran received an average of 309 mm of precipitation in 2019, which is 112% of normal. Spring and autumn were wetter than normal, while winter and summer were drier than normal in 2019 (Fig. 7.49). The highest mean monthly accumulated precipitation occurred at the following stations: Kalaleh airport in north (257.4 mm) in April; Kooh-Rang station (621.5 mm) in March; and Kia-Shahr port city in north (398.5 mm) in November.

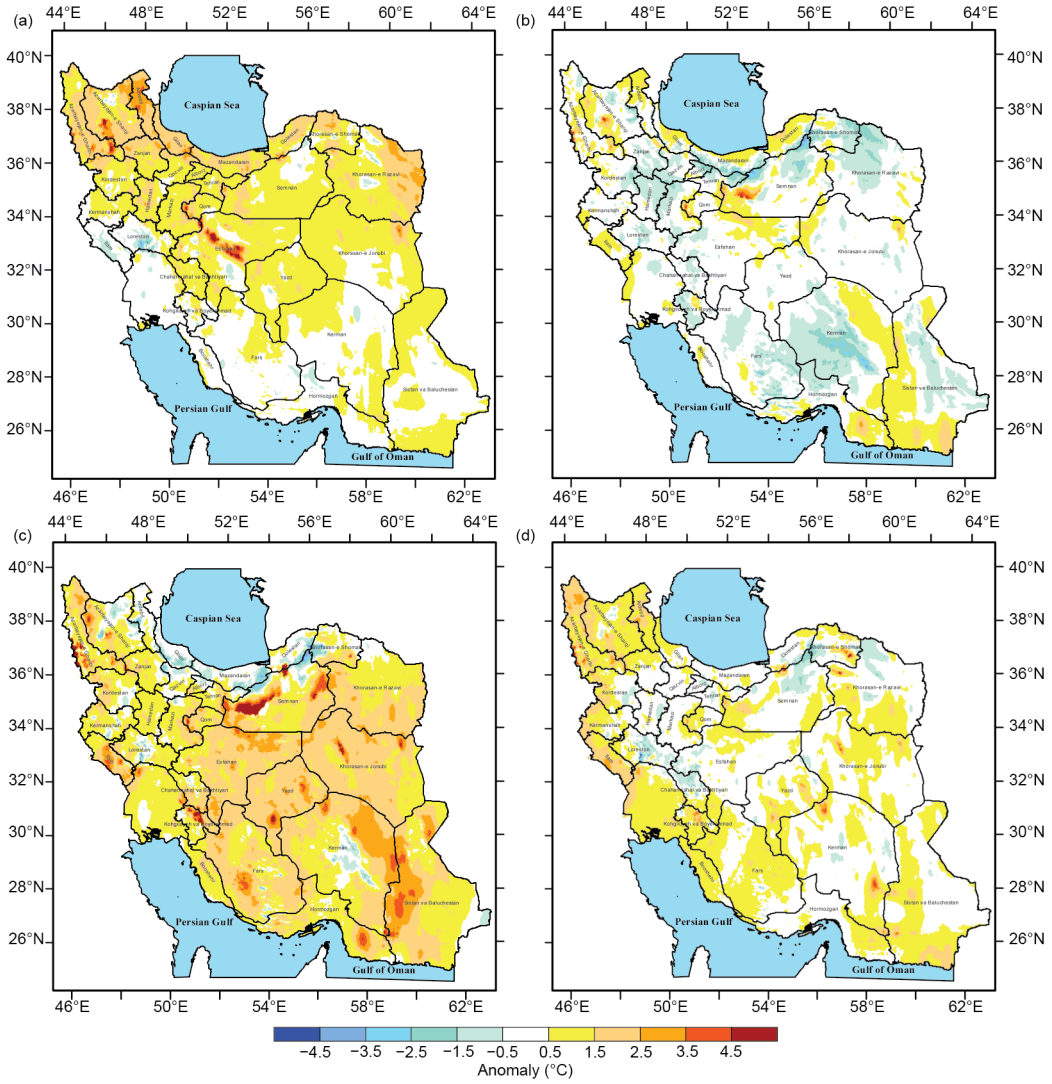

Fig. 7.48. Seasonal mean surface temperature anomalies (°C; 1997–2017 base period) over Iran in (a) winter, (b) spring, (c) summer, and (d) autumn 2019. (Source: I. R. of Iran Meteorological Organization.)

During winter, Iran received 64.7 mm of precipitation, which is about 33% of its average. Geographically, precipitation was below average across most of the country except northwestern Iran and some small parts of northern and western Iran.

In spring, the average rainfall across the country was 70.8 mm, which was 227% of normal. Heavy precipitation from frontal systems mixed with convective instability caused severe floods in the north and from the southwest to the west of the country.

In autumn, total average precipitation was 91.4 mm, which is about 150% of normal. A new 24-hour record of 300.6 mm was observed at RoodSar station in Gilan Province, which borders the Caspian Sea in northern Iran. Accumulated precipitation in the southwest, west, north, northeast, and parts of Kerman and Fars Provinces was more than 150% of normal. However, areas over the southeast and the central desert were drier than normal.

(III) NOTABLE EVENTS

A maximum temperature of 53°C was observed in Shahdad of Kerman province in southeast Iran on 2 July. A minimum temperature of –20.3 °C occurred in Shahre-Kord station on 1 March, and a minimum temperature of –20.5 °C was reported at Kooh-Rang station in the Chahar-Mahal province in western Iran on 20 December 2019. The highest summer minimum daily temperature

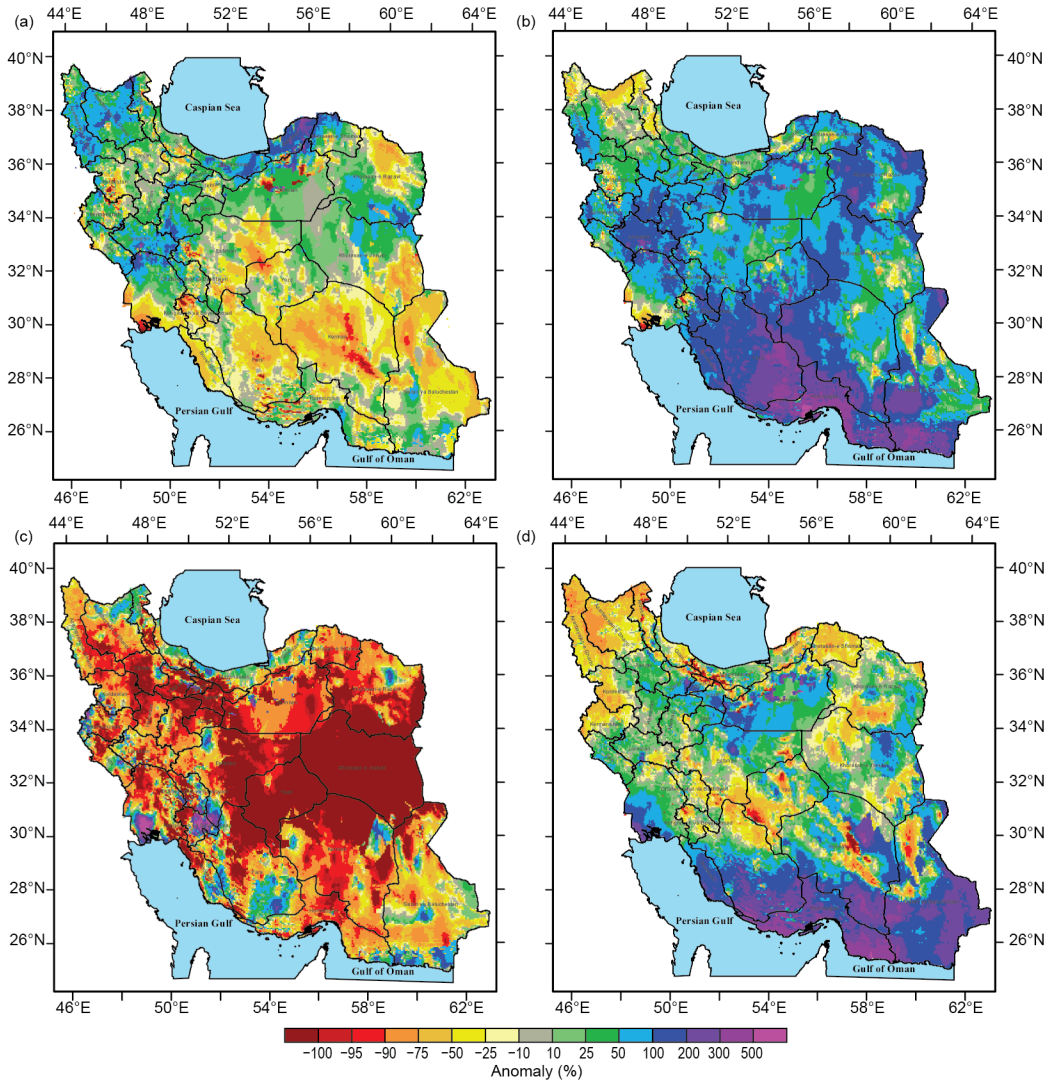

Fig. 7.49. Observed precipitation anomaly percentage (relative to the 1985–2019 base period) over Iran in (a) winter, (b) spring, (c) summer, and (d) autumn 2019. (Source: I. R. of Iran Meteorological Organization.)

(33.8°C) in Tehran was recorded on 17 July. This new record was 1.2°C higher than the original record of 32.6°C.

In March–April, heavy and record-breaking accumulated precipitation in north and southwest Iran caused devastating disasters with severe life, property, and agricultural damages in the regions.

h. Oceania—C. Ganter, Ed.

1) Overview—C. Ganter

Oceania was under the influence of El Niño-like conditions early in 2019, although these were weak. In fact, not all countries considered El Niño to be present. Regardless, by mid-year, clear-cut neutral El Niño-Southern Oscillation (ENSO) conditions were in place. The pattern of sea surface temperatures (SSTs) in the Indian Ocean was generally consistent with a positive Indian Ocean dipole (IOD) from late May, with the IOD index firmly in positive territory between August and the end of the year. The 2019 IOD was the strongest in the observational record since 1997 (see section 4h for details). During the second half of the year, a rare sudden stratospheric warming (SSW) event also influenced the southern countries of Oceania: Australia and New Zealand. The combination of the positive IOD and negative Southern Annular Mode (SAM) contributed toward Australia's exceptional fire season in the second half of 2019 (see Sidebar 7.6).

2) Northwest Pacific and Micronesia—M. A. Lander, C. P. Guard, and B. Bukunt

This assessment covers the area from the date line west to 130°E, between the equator and 20°N. It includes the U.S.-Affiliated Islands of Micronesia but excludes the western islands of Kiribati and nearby northeastern islands of Indonesia. The reference period used for this assessment is 1981–2010.

For much of Micronesia, the weather and climate of 2019 will be remembered—or largely forgotten—as a quiet year relatively free of extremes of wind, waves, or rainfall. It was somewhat dry in the first half. Several typhoons passed through the region but largely avoided populated islands. Most locations were cooler and/or drier than during 2018.

(I) TEMPERATURE

Approximately twice as many locations in Micronesia experienced above-average annual mean temperatures as those that experienced below-average annual mean temperatures during 2019 (see Table 7.3 for temperature anomalies for selected locations across Micronesia). Abnormally sunny and dry conditions in the first half of the year likely contributed to the above-average temperatures seen in some of the westernmost islands of Micronesia (Yap, Guam, and Saipan), while cloudy wet weather at some of the easternmost islands (Pohnpei, Kosrae, and Majuro) contributed to some below-average temperatures. During the second half of 2019, the situation reversed with Guam and Saipan becoming cloudy, wet, and cooler.

Table 7.3. Average 6-month temperature anomalies, with 6-month and annual rainfall (totals and percent of average) for selected Micronesia locations during 2019. Averages quoted are for the 1981–2010 base period. Latitudes and longitudes are approximate. "Kapinga" stands for Kapingamarangi Atoll in Pohnpei State, Federated States of Micronesia. The color fills of the boxes indicate: pink for above-average temperature and blue for below-average temperature; green for above-average rainfall and yellow for below-average rainfall.

Location	Max Temp Min Temp		Rainfall (mm)							
	Jan–Jun	Jul–Dec	Jan–Jun	Jan–Jun	Jan–Jun	Jul–Dec	Jul–Dec	Jul–Dec	Jan–Dec	Jan–Dec
	°C	°C	AVG	2019	%	AVG	2019	%	2019	%
Saipan 15°N, 146°E	+1.20 +0.21	+0.10 −0.70	449.1	322.3	71.8	1322.8	1921.8	145.3	2244.1	126.7
Guam 13°N, 145°E	+0.79 +0.46	+0.44 +0.27	691.6	471.4	68.2	1788.4	1864.4	104.2	2335.8	94.2
Yap 9°N, 138°E	+0.24 +0.67	−0.29 +0.42	1169.7	1157.2	98.9	1902.0	1533.6	80.6	2690.9	87.6
Palau 7°N, 134°E	−0.55 −0.49	−0.13 −0.63	1798.1	1256.0	69.8	2279.4	1975.6	86.7	3231.6	79.3
Chuuk 7°N, 152°E	+0.36 +1.31	+0.35 +1.05	1584.2	1708.9	107.9	1833.1	1989.1	108.5	3698.0	108.2
Pohnpei 7°N, 158°E	−0.68 +1.95	−0.35 +1.53	2266.4	2256.0	99.5	2336.6	2995.7	128.2	5251.7	114.1
Kapinga 1°N, 155°E	n/a	n/a	1750.8	2691.4	153.7	1510.5	1793.8	118.8	4485.1	137.5
Kosrae 5°N, 163°E	−0.25 −0.35	+0.03 +0.33	2567.9	3112.5	121.2	2342.5	1775.0	75.8	4887.5	99.5
Majuro 7°N, 171°E	−0.27 +0.93	+0.38 +1.05	1368.3	1266.2	92.5	1868.2	1888.5	101.1	3154.7	97.5
Kwajalein 9°N, 168°E	+0.44 +0.51	+0.82 +0.62	801.4	614.43	76.7	1579.1	1382.5	87.6	1997.0	83.9

(II) PRECIPITATION

Widespread dry conditions were present across much of Micronesia during the first half of 2019 (Table 7.3), likely a typical response to the waning of El Niño conditions. According to NOAA's Oceanic Niño Index (ONI), the El Niño threshold was met in the 3-month period of September–November 2018 (see section 4b). The ONI continued above the El Niño threshold through June 2019 and thereafter faded to ENSO-neutral. Dry conditions across most of Micronesia typically occur in the first half of any year during which the ONI begins the year above the +0.5°C El Niño threshold and then steadily decreases over the course of the year (Ropelewski and Halpert 1987).

Rainfall deficits on Guam and Saipan exacerbated their respective wildfire seasons, with Guam in particular experiencing more area burned in the first half of 2019 than during the extreme post-El Niño drought of early 2016. A majority of locations were drier during 2019 than in 2018, for the entire year and also for its first and second halves.

(III) NOTABLE EVENTS AND IMPACTS

While 2018 saw nearly all of the islands of Micronesia experience at least some moderate impacts from tropical cyclones, 2019 was relatively quiet for the populated islands. However, several significant systems occurred in the region during 2019.

Super Typhoon Wutip (the second tropical cyclone [TC] of 2019) reached its peak intensity of 140 kt (72 m s^{-1}) on 25 February, west of Guam. It became the most powerful February typhoon on record, surpassing Typhoon Higos of 2015. The Mariana Islands were spared the wrath of Wutip, with the typhoon passing just far enough west of Guam and Saipan to avoid problematic rains and high winds. Guam did receive 100–150 mm of beneficial dry season rainfall.

Super Typhoon Hagibis passed directly over the uninhabited island of Anatahan (16.3°N, 145.6°E) on the night of 7 October. At that time, its intensity was 140 kt, but less than 24 hours earlier it had been only a tropical storm (24–63 kt or 12.3–32.4 m s^{-1}). Hagibis exhibited "...the most intensification by a tropical cyclone in the western North Pacific in 18 hours since Yates in 1996," (Philip Klotzbach, pers. comm.). Hagibis also possessed a very small eye—small enough to qualify as a "pinhole" eye (i.e., any eye diameter less than 10 nautical miles, representing less than 10% of the storm size measurements made by aircraft [Musgrave et al. 2008]). After passing Anatahan, Hagibis underwent an eyewall replacement cycle in which the pinhole eye was surrounded and replaced by a new, much larger eye (Fig. 7.50).

Typhoon Kammuri passed westward to the south of Guam on 25 November, bringing gales and heavy rainfall to the island. Kammuri had an unusual structure for a developing tropical cyclone, known as a central cold cover (CCC; Dvorak 1984). At 0420 UTC on 30 November, the NOAA-20 satellite detected a cloud-top infrared brightness temperature of –109.4°C just west of Kammuri's center. This qualifies as the coldest cloud-top temperature on record observed by a meteorological satellite (CIMSS 2019). The previous record for coldest documented brightness temperature of –102.2°C was observed during TC Hilda in 1990 (Ebert and Holland 1992). The

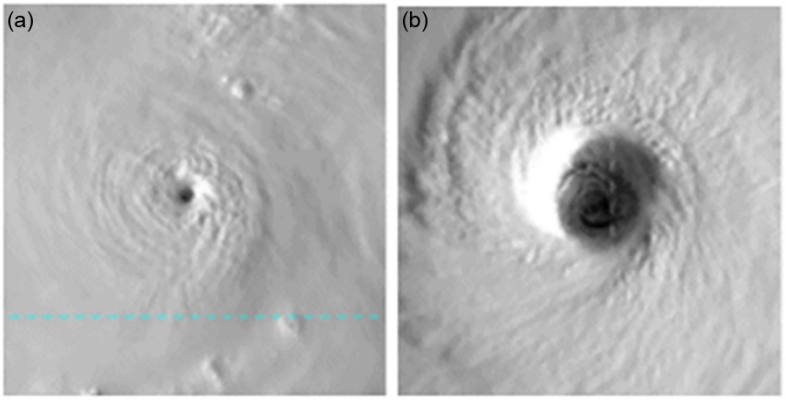

Fig. 7.50. The pinhole eye of Super Typhoon Hagibis on the evening of 7 Oct (left), and with a much larger eye as seen 63 hours later on the morning of 9 Oct (right). The images are at the same scale (220 km × 220 km).

enormous CCC cloud pattern was described by Dvorak (1984) to be indicative of stalled development, and indeed, during the 3-day time period of Kammuri's possession of a CCC, its intensity held steady at or just below typhoon force.

Please refer to section 4f6 for additional details and statistics on these tropical cyclones.

3) Southwest Pacific—E. Chandler

Countries considered in this section include American Samoa, Cook Islands, Fiji, French Polynesia, Kiribati, New Caledonia, Niue, Papua New Guinea (PNG), Samoa, Solomon Islands, Tonga, Tuvalu, Vanuatu, and Wallis and Futuna (see Fig. 7.51). The temperature analysis is based on the Climate Anomaly Monitoring System (CAMS) Monthly Surface Air Temperature Anomalies (https://iridl.ldeo.columbia.edu/maproom/Global/Atm_Temp/Anomaly.html). Anomalies are with respect to the 1971–2000 base period. The precipitation analysis is based on monthly analyses presented in the Climate and Oceans Support Program in the Pacific (COSPPac) Monthly Bulletin (www.pacificmet.net/products-and-services/climate-bulletin) and COSPPac Online Climate Outlook Forum (www.pacificmet.net/products-and-services/online-climate-outlook-forum). The base period for precipitation is 1979–95.

The year began with a borderline neutral to weak El Niño event. Both atmospheric and oceanic indicators remained at El Niño thresholds until the middle of 2019, before giving way to neutral-ENSO conditions thereafter. SSTs were persistently above-normal across the Pacific equator through 2019, with a pool of warm water evident on and to the west of the date line for most of the second half of the year. In contrast, atmospheric indicators remained close to neutral with normal rainfall patterns prevailing toward the end of the year.

(I) TEMPERATURE

Air temperatures were near normal across most of the southwest Pacific during the first quarter of 2019 (Fig. 7.52a), with the exception of +1° to +2°C anomalies in a region centered on the date line. By March, the warm anomalies stretched eastward along the equator, covering Nauru, Kiribati, and the northern Cook Islands. This region of above-normal air temperatures was associated with the above-normal equatorial SSTs.

Fig. 7.51. Map of the Southwest Pacific showing the countries considered in this section. (Source: www.geographicguide.com/oceania-map.htm.)

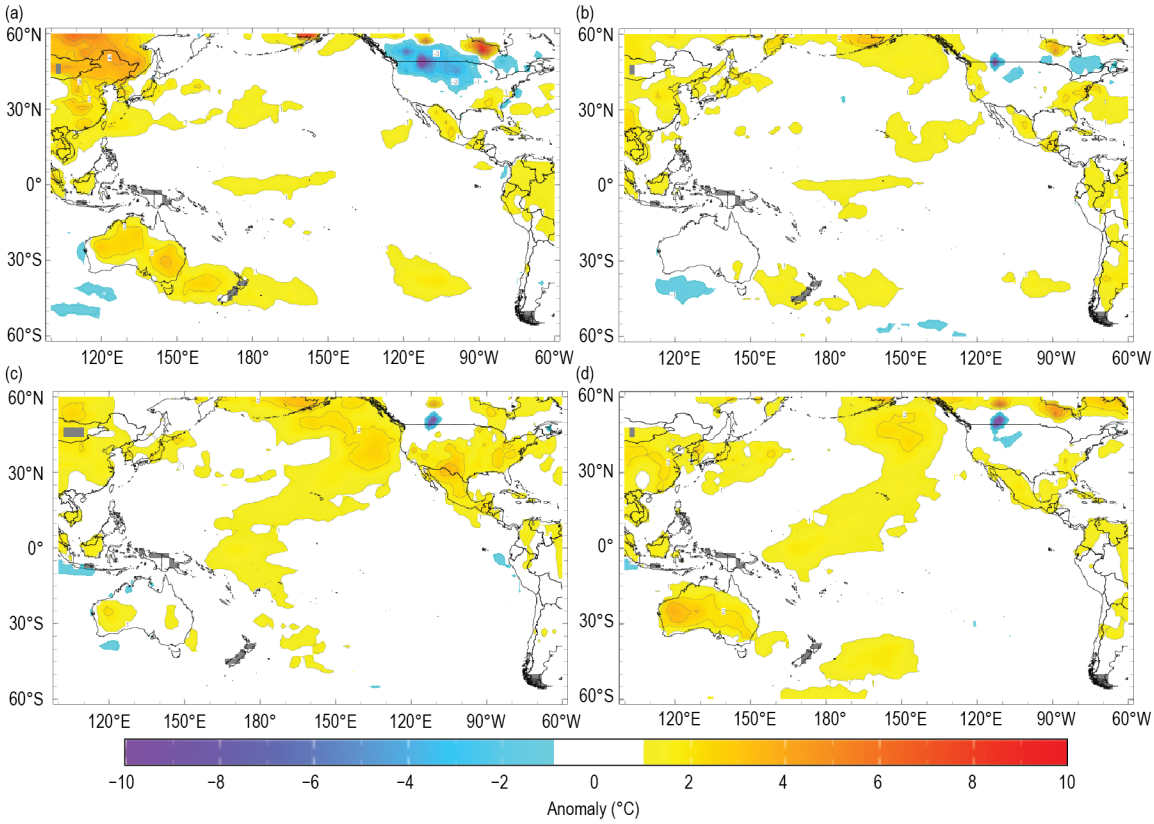

Fig. 7.52. Seasonal temperature anomalies (°C) for (a) JFM, (b) AMJ, (c) JAS, and (d) OND. (Source: CAMS.)

The air temperature anomaly pattern in the southwest Pacific persisted into the second quarter of the year (Fig. 7.52b), with temperatures 1° to 2°C above normal remaining along the equator and extending farther south to include Tuvalu, Samoa, American Samoa, the Cook Islands, and French Polynesia.

In July and August, the warm air temperature pattern shifted farther west, with a large region of anomalies 1° to 2°C above normal in the southwest Pacific extending from the eastern Solomon Islands to the northern Cook Islands, with the southern extent of this region including Fiji, Tonga, and Niue (Fig. 7.52c).

The region of warmth, with air temperatures 1° to 2°C above normal, receded in September and became limited to a region around Nauru, western Kiribati, and Tuvalu, as the underlying above-average SSTs were more localized around and to the west of the date line.

During October–December (OND), an area of air temperatures 1° to 2°C above normal occurred around Nauru, Kiribati, and Tuvalu, while a small region of air temperatures 2° to 3°C above normal was centered on the Gilbert Islands group in western Kiribati (Fig. 7.52d). Above-average air temperature anomalies in OND are consistent with the persistent above-average SSTs in the far western Pacific.

In summary, 2019 experienced near-normal temperature patterns across much of the southwest Pacific, with the notable exception of a region of air temperatures 1° to 2°C above normal centered on the date line; this region was largest in extent during the second half of the year.

(II) PRECIPITATION

The region experienced a mixed rainfall pattern in the first quarter of 2019, largely a result of the South Pacific Convergence Zone (SPCZ) being shifted southwest in January before moving to a northeast position through February and becoming largely suppressed in March (Fig. 7.53). Rainfall above the 90th percentile for January–March (JFM) was recorded in eastern Fiji, western Kiribati, eastern PNG, northern Vanuatu, and Tonga. Two stations recorded their wettest JFM on

record: Butaritari in Northern Kiribati (1830.9 mm) had its wettest JFM in 81 years of record, as did Vava'u in northern Tonga (1635.3 mm) for its 73-year record.

The SPCZ was close to its long-term average position during April–June (AMJ), in line with a near-neutral ENSO state. A large region of anomalously high rainfall centered on the equator, on and to the west of the date line, was associated with persistently above-average underlying SSTs. This resulted in rainfall above the 90th percentile in eastern Fiji, western and central Kiribati, Samoa, Tuvalu, and southern Vanuatu. Several places recorded their highest AMJ rainfall on record, including Udu Point in northern Fiji (1234.7 mm, 70 years of record), Tarawa (1516.5 mm, 70 years of record) and Beru (1005.1 mm, 62 years of record) in Kiribati, and Niu in Tuvalu (1211.7 mm, 74 years of record).

Despite continuing ENSO-neutral conditions, the SPCZ became more active than usual as the dry season progressed through July, August, and September (JAS), with the SPCZ largely enhanced in the western region over the PNG Islands and Solomon Islands and over Samoa during September. The enhanced rainfall from earlier in the year that was centered on the equator had largely dissipated, leaving a smaller region of enhanced rainfall covering the Solomon Islands and parts of PNG. Rainfall was above the 90th percentile in southeastern PNG, the Solomon Islands, Niue, and Tonga for the JAS period. Taro in the northern Solomon Islands recorded its wettest JAS in 41 years (1402.5 mm).

There were no large regions of enhanced or decreased rainfall across the region for OND; the SPCZ was somewhat active during this time, sitting south of its climatologically normal position during October and moving northward by December. In northern Fiji, Rotuma was the only station with rainfall above the 90th percentile during OND (1285.8 mm, 11th highest in 104 years of record); conversely, Madang (PNG), Munda (Solomon Islands), and Port Vila (Vanuatu) all received rainfall below their 10th percentiles for this period.

In summary, rainfall in the southwest Pacific in 2019 was dominated by a large region of enhanced rainfall on and to the west of the date line early in the year. This region of enhanced rainfall was reduced both in terms of geographical size and strength through the year, with rainfall patterns later in 2019 being close to the climatological normal.

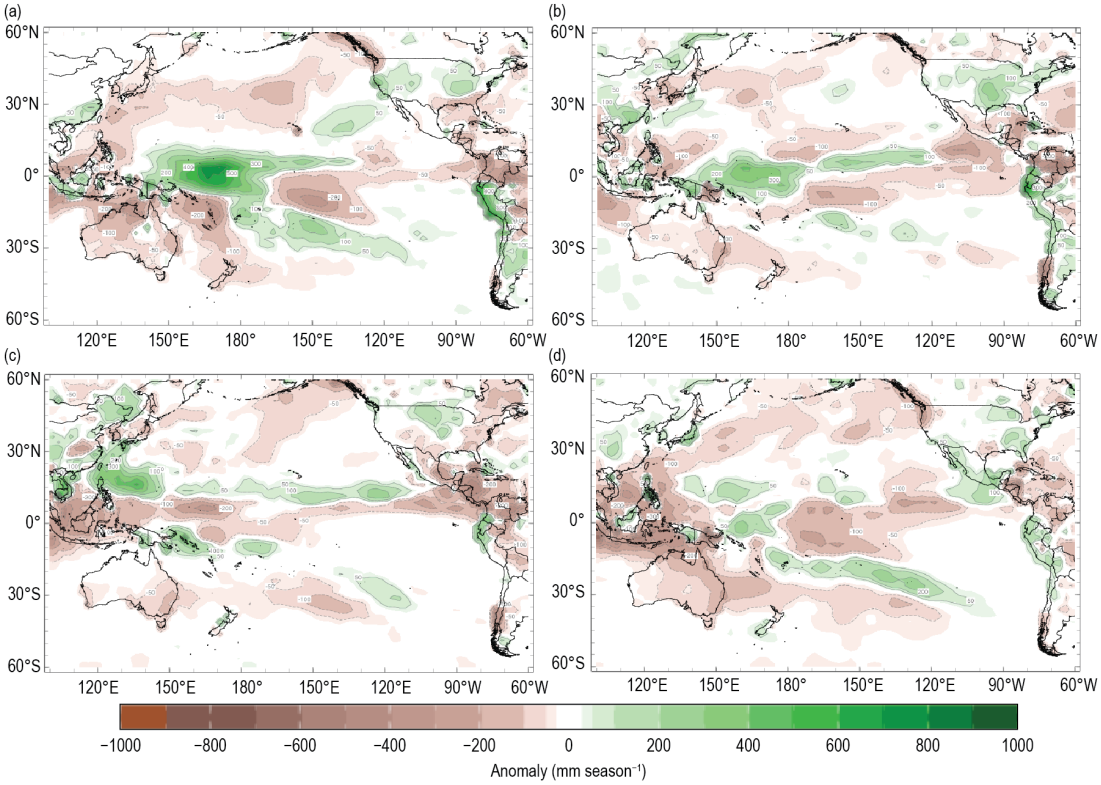

Fig. 7.53. Seasonal precipitation anomalies (mm season^{-1}) for (a) JFM, (b) AMJ, (c) JAS, and (d) OND.

(III) NOTABLE EVENTS AND IMPACTS

On 11 February, TC Oma developed in the Coral Sea, ultimately intensifying to a Category 3 storm as it passed north of New Caledonia. Oma formed northwest of the Solomon Islands and southeast of Vanuatu. The system caused heavy rain, localized flooding, and strong winds in the northern provinces of Vanuatu and Ile Art, the northern archipelago of New Caledonia. Both areas suffered substantial impacts to their agricultural industries. As the system passed near the Solomon Islands, an oil carrier was run aground at Rennell Island, resulting in at least 75 tons of spilled oil, causing reef damage to the world's largest coral atoll.

On 26 February, TC Pola formed to the northeast of Tonga, tracking slowly south over the coming days. It strengthened as it passed between Fiji and Tonga, reaching Category 4 TC status. The storm did not pass over any land areas as it reached its maximum strength with wind gusts over 200 km h^{-1}.

TC Sarai moved southwest toward western Fiji on 26 December, then passed about 100 km south of Kadavu Island (Fiji) and slowly tracked toward Nuku'alofa (Tonga) over coming days. The storm brought damaging winds and rainfall, particularly to the main Fiji Island, Viti Levu, resulting in flooding and two deaths due to drowning. There was also extensive damage to road infrastructure and interruptions to commercial flights and cruises.

Please refer to section 4f6 for additional details of these storms.

4) Australia—S. Tobin and C. Ganter

For this section monthly area-averaged temperatures are based on the ACORN-SAT dataset v2 (Trewin 2018), which begins in 1910. Rainfall and daily temperatures are based on the AWAP dataset (Jones et al. 2009), which begins in 1900 for rainfall and 1910 for temperature.

(I) TEMPERATURE

2019 was Australia's warmest year on record. The area-averaged annual mean temperature was 1.14°C above the 1981–2010 average, well above the previous record of +0.95°C in 2013.

Australian annual mean maximum temperatures (Fig. 7.54) were the highest on record at 1.71°C above average, also well above the previous record of +1.21°C in 2013. Annual mean minimum temperatures (Fig. 7.55) were 0.57°C above average, the sixth highest on record.

Annual mean temperatures were above average across nearly all of Australia and were the highest on record for a large area of northern and eastern New South Wales, southeast Queensland, most of Western Australia away from the coast, and for areas of the Northern Territory.

The annual mean maximum temperatures were in the highest 10% of historical observations for nearly all of Australia and above average for a large area of northern and central Queensland. They were the highest on record for most of Western Australia and

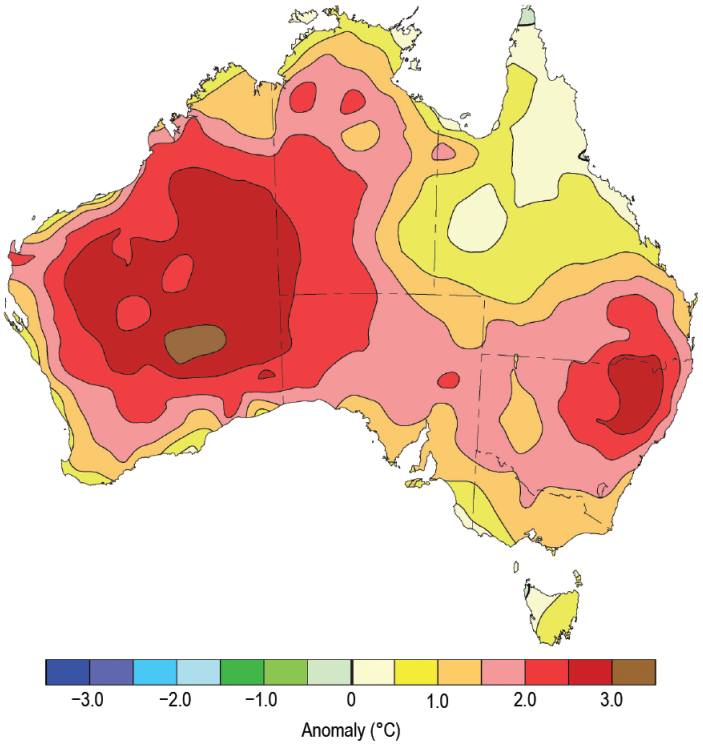

Fig. 7.54. Maximum temperature anomalies (°C) for Australia, averaged over 2019, relative to a 1981–2010 base period. (Source: Australian Bureau of Meteorology.)

South Australia, the western half of the Northern Territory, and from southeast Queensland to Gippsland in eastern Victoria.

Mean minimum temperatures were also above average for much of the country but close to average for some areas, particularly across the north and some parts of the south of Western Australia and South Australia. Annual mean minima were in the highest 10% of historical observations for large parts of the northern inland of the Northern Territory and the east and west of the mainland.

Warmth was widespread and persistent through the year—the national mean temperature was among the 10 highest on record for all months except May, June, August, and September. January, March, and December were each the warmest on record for their respective months.

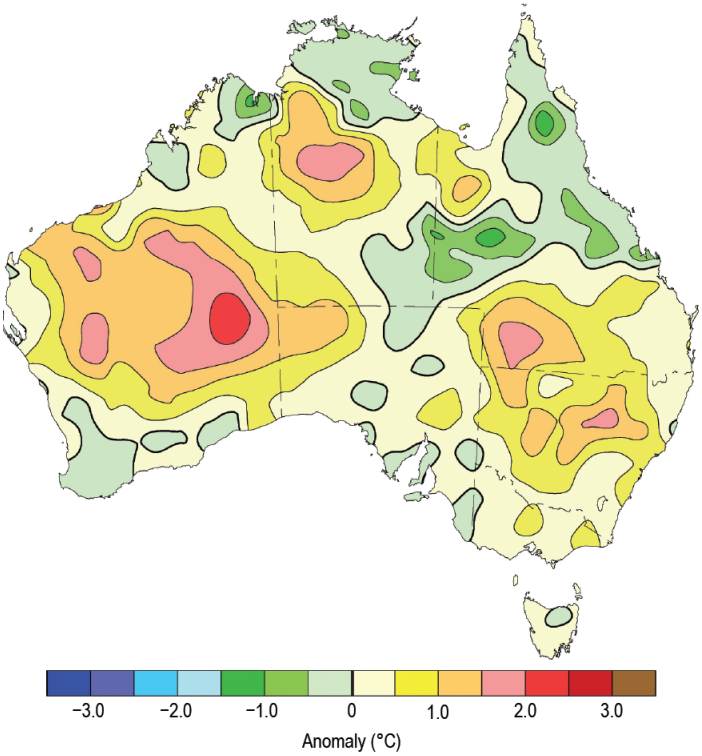

Fig. 7.55. Minimum temperature anomalies (°C) for Australia, averaged over 2019, relative to a 1981–2010 base period. (Source: Australian Bureau of Meteorology.)

Increased diurnal temperature range and increased occurrence of frost are typical of the cool season in inland eastern Australia during drought (which was present in 2019) due to reduced cloud cover, low humidity, and low soil moisture. Areas of the inland southeast observed record low mean monthly minima for August, and nights were also much cooler than average for areas of the mainland southeast and tropics during September, with frost damage in some grain-growing regions.

(II) PRECIPITATION

Averaged across Australia, rainfall for 2019 was the lowest on record at 277.6 mm, well below the previous record low of 314.5 mm set in 1902. Rainfall for 2019 was 57% of the 1981–2010 average.

Rainfall for the year was very much below average over most of Australia and lowest on record for much of northeastern New South Wales and southeastern Queensland, western and northern areas of South Australia, the inland Northern Territory, and southeastern Western Australia (Fig. 7.56). Rainfall had been below average for much of eastern and southwestern Australia since late 2016, with protracted drought affecting large areas and comparable to the driest periods in Australia's recorded history, including the Federation Drought and the Millennium Drought (BoM 2019).

Annual rainfall was above average across parts of Queensland's northwest and northern tropics. This was mostly a result of very much-above-average rainfall during the first quarter of the year.

The monsoon arrived later than usual during 2018/19, with onset at Darwin not occurring until 23 January, tying for the third-latest start since reliable records commenced in 1957. Overall, the northern wet season (October 2018–April 2019) was drier than average for the Northern Territory and Western Australia but wetter than average for parts of Queensland. Monsoon onset was again late in 2019/20, with no monsoonal activity across northern Australia before the end of 2019.

The second half of the year was particularly dry across most of southern Australia. Nationally, each month from August through December was among the 10 driest on record for their respective month, with July ranking 12th driest. The end of the year was especially dry, with November and December the driest on record for their respective months nationally.

A very strong positive IOD (see section 4h) contributed to very low rainfall across Australia during 2019. Additionally, a negative phase of the SAM was present from late October to late December, amplifying the drying effect of the positive IOD in eastern Australia. ENSO, Australia's other main natural climate driver, remained neutral during 2019 by Australian measures (see Sidebar 7.6 for more detailed discussion).

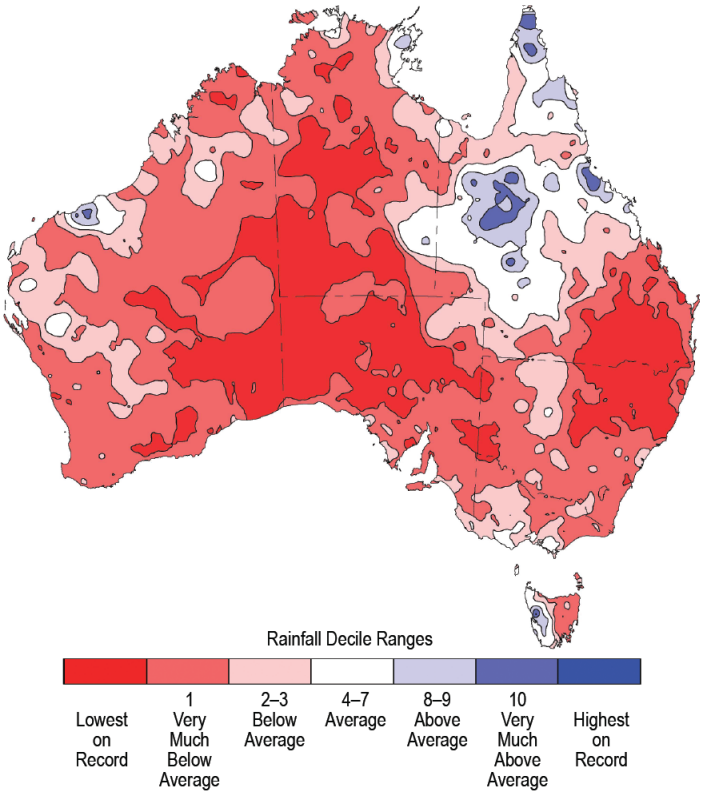

Fig. 7.56. Rainfall deciles for Australia for 2019, based on the 1900–2019 distribution. (Source: Australian Bureau of Meteorology.)

(III) NOTABLE EVENTS AND IMPACTS

An extended period of heat waves affecting much of Australia began in early December 2018 and continued into January 2019, which were exacerbated by antecedent dry conditions. January was Australia's warmest month on record for any time of the year, with severe intensity heat wave conditions extending across southern Australia at times, with numerous temperature records set.

Tropical rainfall during late January and early February led to large areas of flooding in tropical coastal Queensland and parts of the western Peninsula and Gulf Country. Flooding in low-lying regions of western Queensland continued into April, resulting in stock losses and damage to property; the damage was estimated to be near $2 billion Australian dollars (~ $1.3 billion U.S. dollars), according to a local news source. Floodwaters from the north eventually reached Kati Thanda-Lake Eyre, bringing the most significant filling of the lake since 2010–11.

Widespread warm and dry conditions, on top of well-below-average rainfall over a prolonged period, contributed to elevated fire danger over much of southeastern Australia during summer 2018/19. Large fires affected Gippsland in Victoria and parts of Tasmania from summer into autumn 2019.

The Forest Fire Danger Index (FFDI), a measure of fire weather severity, rose early in September 2019 and remained elevated over spring (Fig. SB7.14). The accumulated monthly FFDI for December was the highest on record when averaged over Australia as a whole. Very large bushfires affected eastern Australia from September through year's end, with fires in southeast Queensland, eastern New South Wales, and northeastern Victoria and Gippsland burning around 5 million ha by the end of 2019 (see Sidebar 7.6 for more information).

On 17 November, severe thunderstorms in southeast Queensland produced hail in excess of 4 cm in diameter, with early estimates of insured property damage exceeding $80 million (U.S. dollars). Storms in eastern New South Wales on 26 November caused wind and rain damage across Sydney and the Blue Mountains.

A slow-moving high-pressure system over the Great Australian Bight allowed heat to build over the continent, resulting in record-breaking heat over much of Australia from mid-December 2019. Heat persisted across much of the country with only temporary relief in parts of the south and east, before concluding with extreme heat and dangerous fires in the southeast at the end of the year and lasting into the first days of 2020. Temperature records were set in all states and the Northern Territory but were most numerous in the southeast. These records included Australia's

hottest day on record, 18 December, when the national area-averaged maximum temperature reached 41.88°C, easily exceeding the previous record of 40.30°C set on 7 January 2013. Six other days in December 2019 also exceeded this previous record.

For further detail on these and other significant events, see Special Climate Statements, Monthly Weather Reviews, and the Annual Climate Statement at www.bom.gov.au/climate/current/.

Sidebar 7.6: **An early start to an extreme bushfire season in Australia**—C. GANTER AND S. TOBIN

Southern and eastern Australia experienced a significant bushfire season during the second half of 2019, with conditions gaining global attention. Much of the severity of the bushfire conditions seen in Australia during 2019 can be related to the protracted drought across much of the east coupled with record high temperatures.

The year was influenced by a strong positive Indian Ocean dipole (IOD), the strongest event since 1997 (see section 4h for details). This climate driver was a key contributor to the dry conditions experienced in the second half of 2019 that intensified drought conditions already in place following below-average rainfall in 2017 and 2018. A strong sudden stratospheric warming (SSW) over Antarctica (which is rare for the Southern Hemisphere [SH], with 2002 the only comparable event in the twenty-first century; see Sidebar 6.1 for details) led to a negative phase of the Southern Annular Mode (SAM), with negative SAM in place for much of October–December. At this time of the year, a negative SAM phase is associated with drier-than-average conditions over parts of eastern Australia (Hendon et al. 2007) and increases the likelihood of extreme heat for much of southern and eastern Australia (Marshall et al. 2014).

In addition to the climate drivers in 2019, much of southern and eastern Australia was experiencing rainfall deficiencies at a range of timescales. In particular, parts of the east had been notably dry for 2–3 years, with a weaker positive IOD occurring in 2018 contributing to the dry conditions.

Historically, bushfire activity across the east coast starts in spring (September–November) across Queensland, extending into northeast New South Wales (NSW), and spreads south progressively as the months warm up. However, trends toward a lengthened fire season have been identified across parts of Australia, with the fire season typically starting earlier and ending later in many parts.

For 2019, while there was some fire activity beforehand, the first big flare up began in early spring. Areas of southeast Queensland and northeast NSW had above-average daytime temperatures, very low humidity, and gusty winds leading to dangerous fire weather. By 7 September, more than 50 significant fires were burning across Queensland, increasing to 80 fires by 9 September. In NSW, more than 50 fires were active by 9 September. Losses included the iconic Binna Burra Lodge—a place surrounded by green subtropical rainforest that does not usually burn.

In October and November, days of dangerous fire weather conditions affected all Australian states and territories, with fires breaking out across the southern states of Victoria, Tasmania, South Australia, and Western Australia. By the end

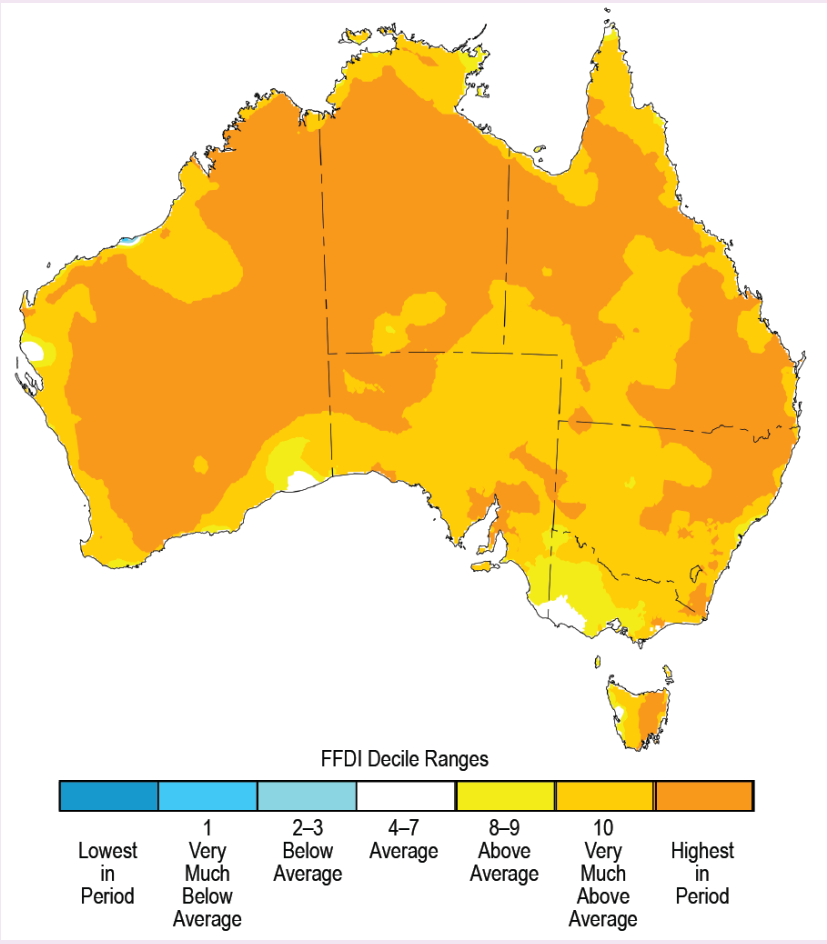

Fig. SB7.14. McArthur Forest Fire Danger Index (FFDI) deciles. Base period 1950–2019.

of spring, catastrophic fire danger was declared in the Greater Sydney region for the first time since the introduction of this level in 2009.

For spring as a whole, the accumulated McArthur Forest Fire Danger Index (FFDI; McArthur 1967) values were more than twice the average in large areas of eastern Australia, with the area-averaged value for Australia the highest in 50 years of record (see Fig. SB7.14 for spring FFDI deciles).

With a delayed onset of the monsoon moving into the SH, heat built across northern and central Australia from the start of December, with heatwaves repeatedly affecting the fire grounds. The hottest temperature recorded was at Nullarbor, South Australia, on 19 December, when it reached 49.9°C, a new December record for Australia and the highest temperature recorded for any month since February 1998.

The December national maximum temperature anomaly was +4.15°C, well above the previous December record of +2.41°C set in 2018. It was also the highest anomaly for any month (i.e., most above-average month) of the 110-year national record. With numerous large fires in the landscape, record heat, and severe drought, the conditions led to major losses of lives, property, and forests.

In December, the NSW government declared a state of emergency to help deal with the bushfires. On 2 January 2020, the Premier of the state of Victoria declared a state of disaster for parts of Victoria.

December accumulated FFDI values were highest on record for Australia as a whole and also for each state and territory, except Tasmania, which was second highest. The large numbers of fires across much of eastern Australia meant that thick smoke covered many areas of coastal NSW, including Sydney, particularly during November and into December. Smoke also significantly affected many areas of eastern Australia at some point during the fire season. At one point, Australia's capital, Canberra, was the city with the worst air quality in the world.

Conditions began to ease somewhat beginning 4 January 2020, although fires continued into the new year. The area burnt in NSW alone has been estimated to be a record 5.46 million ha, while nationally more than 3000 homes were destroyed and conservative estimates of wildlife death are in the order of 1 billion animals (Christopher Dickman, pers. comm. March 2020[1]). While there have been previous seasons (for example, 1974/75) where larger areas have been burnt nationally than in 2019/20, in those seasons the fires were predominantly in remote northern and central grassland and savanna areas, often fueled by excess vegetation growth in normally arid areas following heavy rainfall. No previous season compares with 2019/20 for the amount of area burned in Australia's subtropical and temperate forests, with fires extending even to areas where fires were previously exceptionally rare or unknown, such as the rainforests of southeast Queensland.

[1] Numbers are estimated for terrestrial mammals, birds, and reptiles, and only for the states of New South Wales and Victoria. Bats, frogs, and other fauna were not included, nor were the fire-related effects assessed for South Australia, Queensland, or Western Australia. Background to the estimate can be found here: https://onlinelibrary.wiley.com/doi/full/10.1111/emr.12403.

5) New Zealand—N. Fedaeff

In the following discussion, the base period is 1981–2010, unless otherwise noted. The nationwide average temperature is based upon the National Institute of Water and Atmospheric Research (NIWA)'s seven-station temperature series that began in 1909 (see www.niwa.co.nz/our-science/climate/information-and-resources/nz-temp-record/seven-station-series-temperature-data).

(I) TEMPERATURE

According to NIWA's seven-station temperature series, 2019 was New Zealand's fourth-warmest year since records began in 1909. The nationwide average temperature for 2019 was 13.37°C, 0.76°C above the annual average. Annual mean temperatures were above average (+0.51° to +1.20°C above the annual average) across the majority of New Zealand. Areas of well-above-average (more than 1.20°C above average) temperatures were observed in the Bay of Plenty and Hawke's Bay. Near-average (within −0.50° to +0.50°C of average) temperatures occurred in parts of the Wairarapa, the West Coast, Tasman, Nelson, Marlborough, and coastal Canterbury (Fig. 7.57a).

The year began with New Zealand's third-warmest January on record. Widespread heat wave conditions took hold during the end of the month with several locations experiencing their warmest January day on record. The warmest temperature of 2019 was recorded on 31 January at Hanmer Forest. The high of 38.4°C tied for New Zealand's fourth-highest January temperature and also tied for the 18th-highest temperature on record for all months. A key climate driver and contributor to the hot start to 2019 was the presence of above-average coastal SSTs. Some areas around Hawke's Bay and Canterbury experienced marine heat wave conditions; marine heat wave conditions also persisted in the Tasman Sea to March.

At the start of August, a strongly negative SAM and stronger-than-normal polar and sub-tropical jet streams fueled a more active weather pattern to end winter. Southwesterly winds and several strong cold fronts during this time brought periods of thunderstorms and snow to southern and western parts of the country. The cooler temperatures at the end of winter and start of spring were also influenced by a rare SSW event, which occurred in the polar stratosphere during late August that peaked in mid-September (see Sidebar 6.1 for details). While this event was not classified as a major SSW event (winds at 10 hPa, 60°S saw an unprecedented deceleration but did not reverse to easterlies—a criteria for the classification of a major event), it was the largest warming event observed in the August–September Southern Hemisphere (SH) record extending back to 1980.

Despite several sharp cold snaps, temperatures as a whole were near average for September and October, before prevailing northwesterlies in November brought unseasonably warm weather and New Zealand's warmest November on record. The lowest air temperature of the year was −9.2°C, recorded at Lake Tekapo on 3 June. This was the highest annual minimum temperature recorded in New Zealand this decade.

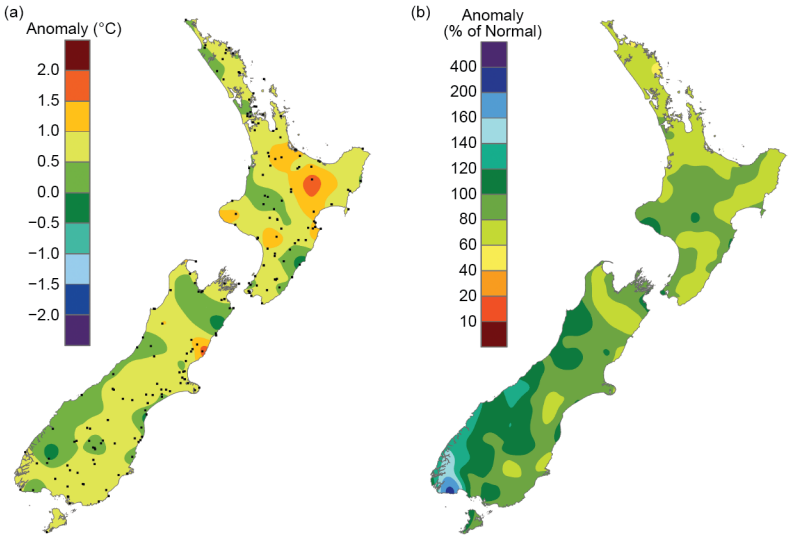

Fig. 7.57. 2019 annual (a) average temperature anomaly (°C) and (b) total rainfall (%), relative to 1981–2010. The dots in panel (a) represent the locations of climate stations used to create both the temperature and rainfall maps. (Source: NIWA.)

(II) PRECIPITATION

Annual rainfall totals for 2019 were below normal (50%–79% of normal) across Northland, Auckland, and the Bay of Plenty as well as parts of

Waikato, Hawke's Bay, the Wairarapa, and Marlborough (Fig. 7.57b). On the North Island, 13 locations observed record or near-record low rainfall amounts. Conversely, rainfall was above normal (120%–149% of normal) in western Southland and parts of Westland, with four locations observing near-record high rainfall. For Hokitika, it was the fourth-wettest year in the record extending back to 1866. Of the regularly reporting rainfall gauges, the wettest location in 2019 was Cropp River, in the Hokitika River catchment (West Coast, South Island, 975 m a.s.l.), with an annual rainfall total of 14 227 mm. The driest of the regularly reporting rainfall sites in 2019 were Clyde and Cromwell (Central Otago), which each recorded 417 mm of rainfall.

(III) NOTABLE EVENTS AND IMPACTS

See Fig. 7.58 for a schematic of notable events. By the end of February, Nelson observed a 40-day dry spell, defined as a period of 15 days or more with less than 1 mm of rain on any one day, its fourth-longest dry spell in the record extending back to 1862. The tinder-dry conditions in the Tasman District fueled a large scrub fire in Pigeon Valley near Wakefield. The fire burned for most of February and into early March, and a Civil Defence State of Emergency was declared. It was reportedly the largest aerial firefight in New Zealand's history, and the cost of the event based on figures from the Insurance Council of New Zealand (ICNZ) was $3.98 million New Zealand dollars (~ $2.47 million U.S. dollars).

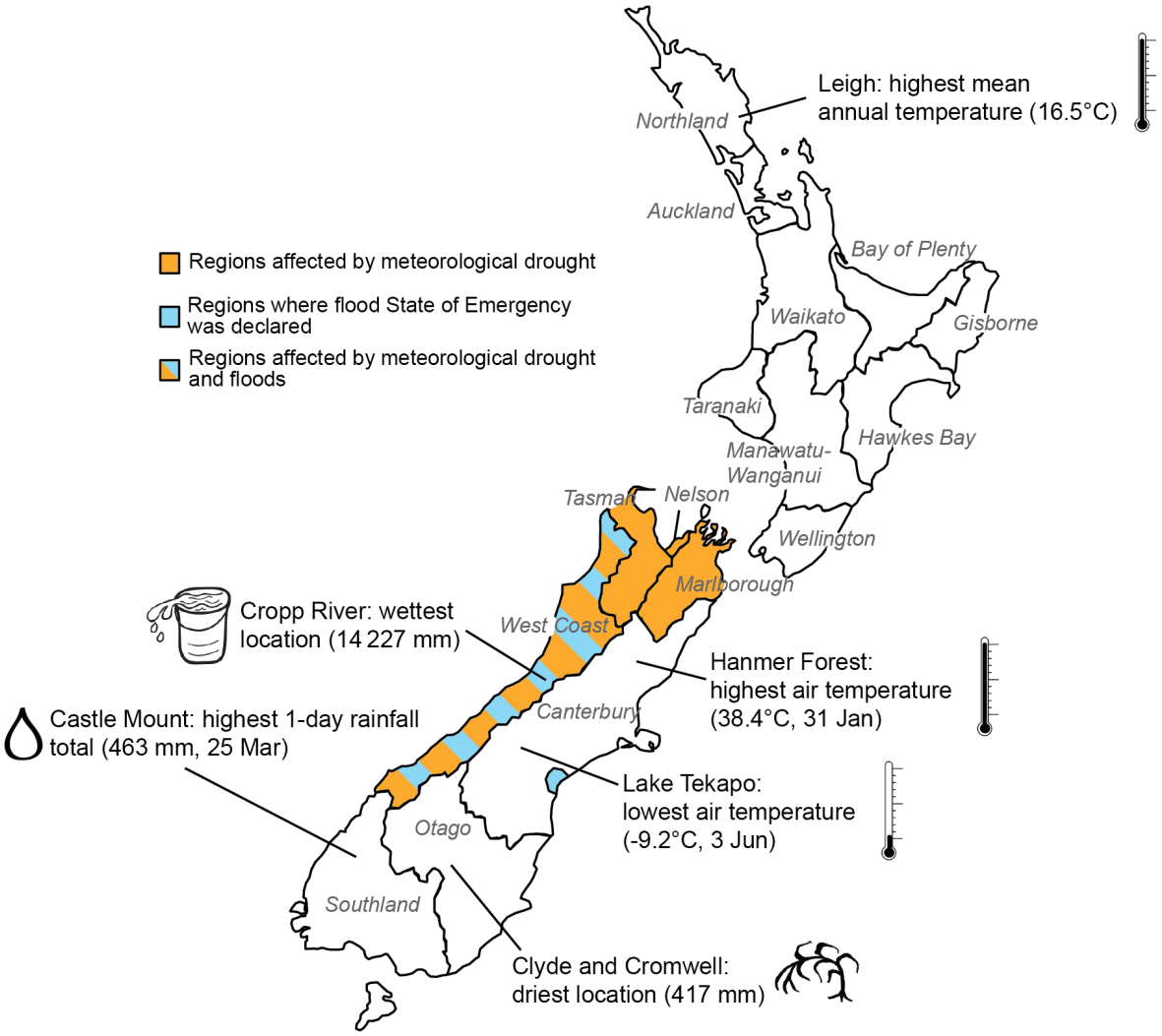

Fig. 7.58. Notable weather events and climate extremes for New Zealand in 2019. (Source: NIWA, https://niwa.co.nz/climate/summaries/annual-climate-summary-2019.)

Extremely heavy rainfall occurred in the western South Island on 25–27 March. The weather event was associated with an atmospheric river extending from Australian cyclones coupled with extra energy from the Tasman Sea marine heat wave, as well as a strong low-pressure system siphoning moisture toward New Zealand. A State of Emergency was declared in Westland, and the Waiho River bridge on State Highway 6 was claimed by raging floodwaters. A New Zealand 48-hour rainfall record of 1086 mm was set at the Hokitika catchment of the Cropp River, surpassing the previous record of 1062 mm at the same site in 2013. The event resulted in $4.09 million New Zealand dollars (~ $2.53 million U.S. dollars) in damages based on figures from ICNZ.

Acknowledgments

e. Africa

Samson Hagos was supported by the National Oceanic and Atmospheric Administration (NOAA) Oceanic and Atmospheric Research, Program Climate Program Office (CPO), under NOAA grant number NA17OAR4310263.

g. Asia

Tim Li wishes to thank all authors in the Asia section for their timely contributions and internal and external reviewers and the document editors for their constructive comments. The following grants (China National Key R&D Program 2018YFC1505806, NSFC grant 41630423, NSF grant AGS-1643297 and NOAA grant NA18OAR4310298) are acknowledged.

APPENDIX 1: Acronym List

AMJ	April–June
CAMS	Climate Anomaly Monitoring System
CONUS	contiguous United States
ENSO	El Niño–Southern Oscillation
ETP	eastern tropical Pacific
FFDI	Forest Fire Danger Index
GHCN	Global Historical Climate Network
ICNZ	Insurance Council of New Zealand
IOD	Indian Ocean dipole
ISMR	Indian summer monsoon rainfall
JAS	July–September
JFM	January–March
JRA-55	Japanese 55-year Reanalysis
JTWC	Joint Typhoon Warning Center
LTA	long-term average
MSE	moist static energy
NAO	North Atlantic Oscillation
NEM	northeast monsoon
NH	Northern Hemisphere
NIWA	National Institute of Water and Atmospheric Research
NSW	New South Wales
OLR	outgoing longwave radiation
OND	October–December
ONI	Oceanic Niño Index
PNG	Papua New Guinea
RSMC	Regional Specialized Meteorological Centre
SAM	Southern Annular Mode
SH	Southern Hemisphere
SPCZ	South Pacific Convergence Zone
SST	sea surface temperature
SSW	sudden stratospheric warming
TC	tropical cyclone
TD	tropical depression
TS	tropical storm
WMO	World Meteorological Organization

APPENDIX 2: Supplemental Materials

Table A7.1. Summary of events and impacts, including number of fatalities (f) and injured people (i) by lightning strikes, by country and specific region. (Data sources: Central American National Weather Services, National Emergency Committees communications and regional newspapers)

Country	Specific Region	Dates (2019)	Impacts
Panamá	Colón province	20 Aug	1f, 1i
	Ngäbe-Buglé Shire	05 Sep	2f
	Chiriquí province	18 Oct	5i
Costa Rica	Zarcero	02 Aug	1f
	Aguas Zarcas, San Carlos	24 Sep	1f, 3i
	Alajuela province	09 Oct	5i
Nicaragua	45 miles east of Bilwi	16 Aug	2f
	Kayaska, Bocay	13 Sep	1f
	Matagalpa department	25 Oct	1f
El Salvador	Sonsonate department	25 Jul	1f
	Usulután department	23 Sep	1f
	El Salvador department	26 Sep	1i
Honduras	Intibucá department	06 May	16i
	Intibucá department	05 Jun	1f
	Yoro department	07 Jul	1f
	Francisco Morazán department	08 Aug	1f
	Valle department	17 Aug	2f, 5i
	Comayagua department	05 Oct	1f
Guatemala	Chimaltenango department	01 Sep	2f
	Antigua Guatemala	02 Sep	1i
	Petén department	04 Sep	1f
	San Marcos department	27 Oct	4i
Belize	Armenia Village	19 Apr	1f
		Total	**21f, 41i**

Table A7.2. Summary of events and impacts, including number of fatalities (f), missing people (m), injured people (i), affected people (a), number of affected families (n), and damaged houses (d), by country and specific region. [Data sources: Central American National Weather Services, National Emergency Committees communications and regional newspapers].

Country	Specific Region	Dates (2019)	Hydrometeorological Condition	Impacts
Guatemala	Alta Verapaz, Chimaltenago and San Marcos departments	02–03 Jun	Heavy rainfall, strong winds and landslides	3057a
	Alta Verapaz, Petén and San Marcos departments	03–04 Jun	Heavy rainfall and landslides	2275a
	Guatemala, Huehuetenango, Sololá and Schitepéquez departments	09 Jun	Heavy rainfall, landslides, and floods	30 086a
	Jutiapa, Huehuetenango, Jalapa, Alta Verapaz and Santa Rosa departments	11–12 Jun	Heavy rainfall and landslides	21 118a
	Suchitepéquez and Guatemala departments	14–15 Jun	Heavy rainfall, landslides and bridge collapse	604a
	Los Naranjales, Colotenango, Huehuetenango	27 Jun	Heavy rainfall and landslides	3f
	Escuintla and Suchitepéquez departments	28 Jul	Heavy rainfall and strong winds	112a
	Guatemala, Quetzaltenango, Retalhuleu and Sacatepéquez departments	03–04 Aug	Heavy rainfall, landslides and floods associated with a low pressure system	412a
	Guatemala, and Santa Rosa	15 Aug	Heavy rainfall, landslides, overflow of rivers and floods	1f, 1m, 5062a
	Alta Verapaz, Sololá, Guatemala, Santa Rosa, Sacatepéquez and Suchitepéquez departments	17–18 Aug	Heavy rainfall, landslides, and floods	25 332a
	Guatemala, Sololá and Suchitepéquez departments	19 Aug	Heavy rainfall, landslides, overflow of rivers and floods	252a
	Chimaltenango, Sacatepéquez, Guatemala, Zacapa and San Marcos departments	20–21 Aug	Heavy rainfall, landslides, and floods	2705a
	Guatemala and Jalapa departments	01 Sep	Rainfall and landslides	1f, 4i, 1037a
	Chiquimula and Guatemala departments	10–11 Sep	Rainfall, strong winds and landslides	3000a
	Guatemala, Quiché and Suchitepéquez deaprtments	16 Sep	Rainfall, floods and landslides	40 065a
	Chiquimula, El Progreso, Guatemala, Quetzaltenango, Sacatepéquez and Santa Rosa	23 Sep	Rainfall, floods and landslides	1f, 1m, 21 275a
	Alta Verapaz, Quiché and Santa Rosa departments	24 Sep	Rainfall and landslides	50 200a
	Alta Verapaz, Guatemala, Quetzaltenango, Quiché, Sacatepéquez, Santa Rosa and Sololá departments	29–30 Sep	Rainfall, floods and landslides	1f, 20 246a
	Petén, Huehuetenango and Santa Rosa departments	01 Oct	Rainfall, floods and landslides	350a, 159d
	Nueva Esperanza, Río Escondido	04 Oct	Rainfall and overflow of rivers	1f
	Linea C4 Sis, San Andres Villa Seca, Retalhule department	16 Oct	Rainfall and floods	122a
	Santa Marta del Mar, Barra Coyolate and Trocha 8, Escuintla department	16 Oct	Rainfall and floods	1500a, 300d
	Quetzaltenango, San Marcos and Huehuetenango departments	30 Oct	Rainfall, floods and landslides	4f, 642a
	Provenir, Sayaxché	08 Nov	Heavy rainfall	210a

(cont) Table A7.2. Summary of events and impacts, including number of fatalities (f), missing people (m), injured people (i), affected people (a), number of affected families (n), and damaged houses (d), by country and specific region. [Data sources: Central American National Weather Services, National Emergency Committees communications and regional newspapers].

Country	Specific Region	Dates (2019)	Hydrometeorological Condition	Impacts
Panamá	Ngäbe-Buglé Shire	30 Sep	Rainfall and overflow of rivers	1f
	Panamá and West Panamá provinces	09 Nov	Heavy rainfall, landslides, overflow of rivers and floods	232a, 99d
	Panamá, Coclé, Colón, and Bocas del Toro province	28 Nov	Rainfall, strong winds, landslides and floods	183a
	Colón Island and Changuinola	25 Dec	Rainfall and floods	1070a, 215n
Costa Rica	Upala, Alajuela province	08 Jul	Heavy rainfall and floods	134a
	La Lucha de Lagarto and Río Claro, Golfito	08 Sep	Heavy rainfall and landslides	117n
	Santa Cruz, Nicoya, Hojancha, Nandayure in Guanacaste, Cobano, Lepanto and Paquera of Puntarenas, Paraíso and Orosí in Cartago	08 Sep	Heavy rainfall, landslides and floods associated with a low pressure system	2815a
Nicaragua	Quezalguaque, León department	19 May	Heavy rainfall and overflow of rivers	1f
	Carazo, Rivas, Managua, and Boaco departments	23 May	Heavy rainfall and floods associated with a low pressure system	344n
	Matagalpa, Nueva Segovia, Madriz, León and Managua departments	01 Oct	Rainfall, strong winds, and floods	300d
	Metagalpa, Madriz, Nueva Segovia, Chontales, Rio San Juan and Managua	14–15 Oct	Heavy rainfall and floods associated with a low pressure system	2f, 534n, 528d
El Salvador	San Salvador department	17 Aug	Heavy rainfall	1i
	La Paz, San Salvador and La Libertad departments	16 Oct	Heavy rainfall, landslides, and floods	4f, 1m, 130n
Honduras	Choluteca department	06–08 Oct	Rainfall and overflow of rivers	2f

Table A7.3. Temporal coverage of nationally averaged temperature and precipitation in-situ observations for Europe/WMO RA VI Region. For some countries, only one station (preferably with long time series) has been used (name of the location in brackets). All records extend to the present.

Nation	Temperature start of record	Precipitation start of record	Source
European average	1950	1950	GHCN[1] data
Albania (Korce)	1963	1963	CLIMAT[2]
Andorra	1950	1950	NMHS[3]
Armenia	1935	1935	NMHS
Austria	1767	1858	NMHS
Azerbaijan (Astara)	1991	1991	CLIMAT
Belarus	1881	1945	NMHS
Belgium	1981	1981	NMHS
Bosnia & Herzegovina (Banja Luka)	1955	1955	CLIMAT
Bulgaria	1930	1954 (Burgas)	NMHS/CLIMAT
Croatia (Split/Marjan)	1949	1949	CLIMAT
Cyprus (Nicosia)	1899	1899	NMHS
Czech Republic	1961	1961	NMHS
Denmark	1873	1874	NMHS
Estonia	1961	1961	NMHS
Finland (Helsinki)	1900	1961	NMHS
France	1900	1959	NMHS
Georgia	1960	1881 (Tbilisi)	NMHS
Germany	1881	1881	NMHS
Greece	1960	1949 (Athens)	NMHS/CLIMAT
Hungary	1901	1901	NMHS
Iceland (Stykkishólmur)	1900	1856	NMHS
Ireland	1900	1900	NMHS
Israel	1951	1935 (Deganya)	NMHS
Italy	1961	1949 (Alghero)	NMHS/CLIMAT
Jordan (Amman)	1981	1981	NMHS
Kazakhstan	1941	1941	NMHS
Latvia	1924	1924	NMHS
Lebanon (Beirut)	1949	1949	CLIMAT
Lithuania	1961	1887 (Vilnius)	NMHS
Luxembourg (Findel)	1947	1947	NMHS
Malta (Luqa)	1923	1949	NMHS/CLIMAT
Moldova (Chisinau)	1886	1891	NMHS
Monaco	not available	not available	—
Montenegro (Plevlja)	1955	1955	CLIMAT
Netherlands	1901	1901	NMHS
North Macedonia (Bitola)	1955	1955	CLIMAT
Norway	1900	1900	NMHS

(cont) Table A7.3. Temporal coverage of nationally-averaged temperature and precipitation in-situ observations for Europe/WMO RA VI Region. For some countries, only one station (preferably with long time series) has been used (name of the location in brackets). All records extend to the present.

Nation	Temperature start of record	Precipitation start of record	Source
Poland	1951	1951	NMHS
Portugal	1931	1931	NMHS
Romania	1961	1954 (Bistrita)	NMHS/CLIMAT
Russia, European part	1936	1936	NMHS
Serbia	1951	1951	NMHS
Slovakia	1951	1961	NMHS
Slovenia	1961	1961	NMHS
Spain	1965	1965	NMHS
Sweden	1860	1860	NMHS
Switzerland	1864	1864	NMHS
Syrian Arab Republic (Aleppo)	1960	1960	CLIMAT
Turkey	1971	1949 (Adana)	NMHS
Ukraine	1891	1891	NMHS
United Kingdom	1884	1862	NMHS

[1]GHCN = Global Historical Climatology Network (Menne et al. 2018)
[2]CLIMAT station data as reported worldwide via the WMO Global Telecommunication System
[3]NMHS = National Meteorological and Hydrological Service; for individual names of NMHSs see https://public.wmo.int/en/about-us/members

References

Amador, J. A., 1998: A climatic feature of the tropical Americas: The trade wind easterly jet. *Top. Meteor. Oceanogr.*, **5** (2), 91–102.

——, 2008: The Intra-Americas Seas Low-Level Jet (IALLJ): Overview and future research. Ann. N. Y. Acad. Sci., 1146, 153–188, https://doi.org/10.1196/annals.1446.012.

——, E. J. Alfaro, H. G. Hidalgo, and B. Calderón, 2011: Central America [in "State of the Climate in 2010"]. *Bull. Amer. Meteor. Soc.*, **92** (6), S182–S183, https://doi.org/10.1175/1520-0477-92.6.S1.

Aragão L. E. O. C., and Coauthors, 2018: 21st century drought-related fires counteract the decline of Amazon deforestation carbon emissions. *Nat. Commun.*, **9**, 536, https://doi.org/10.1038/s41467-017-02771-y.

Bahaga, T. K., A. H. Fink, and P. Knippertz, 2019: Revisiting interannual to decadal teleconnections influencing seasonal rainfall in the Greater Horn of Africa during the 20th century. *Int. J. Climatol.*, **39**, 2765–2785, https://doi.org/10.1002/joc.5986.

Benestad, R. E., 2004: Record-values, nonstationarity tests and extreme value distributions. *Global Planet. Change*, **44**, 11–26, https://doi.org/10.1016/J.GLOPLACHA.2004.06.002.

BoM, 2019: Special Climate Statement 70—Drought conditions in Australia and impact on water resources in the Murray–Darling Basin. Bureau of Meteorology, 39 pp., www.bom.gov.au/climate/current/statements/scs70.pdf

Bosart, L. F., T. C. Leicht, and A. K. Mitchell, 2020: The intense High Plains "bomb" cyclone of 12–14 March 2019. 30th Conf. on Weather Analysis and Forecasting/26th Conf. on Numerical Weather Prediction, Boston, MA, Amer. Meteor. Soc., 5B.4, https://ams.confex.com/ams/2020Annual/webprogram/Paper362748.html.

CIMSS, 2019: Typhoon Kammuri in the West Pacific Ocean, with record cold cloud-top temperatures. CIMSS Satellite Blog, https://cimss.ssec.wisc.edu/satellite-blog/archives/35120.

Cunha, A. P., and Coauthors, 2019: Extreme drought events in over Brazil from 2011 to 2019. *Atmosphere*, **10**, 642, https://doi.org/10.3390/atmos10110642.

Dvorak, V. F., 1984: Tropical cyclone intensity analysis using satellite data. NOAA Tech. Rep. 11, 45 pp.

Ebert, E. E., and G. J. Holland, 1992: Observations of record cold cloud-top temperatures in Tropical Cyclone Hilda (1990). *Mon. Wea. Rev.*, **120**, 2240–2251, https://doi.org/10.1175/1520-0493(1992)120<2240:OORCCT>2.0.CO;2.

FAN, 2019: Incendios forestales en Bolivia 2019. Fundación Amigos de la Naturaleza, accessed 23 January 2020, http://incendios.fan-bo.org/Satrifo/publicaciones/#tab-4.

FloodList, 2019: Thousands affected by flooding in Presidente Hayes, Concepción and Guairá. FloodList, 20 March, accessed 23 January 2020, http://floodlist.com/america/paraguay-flodds-presidente-hayes-concepcion-guaira-march-2019.

Funk, C. C., and Coauthors, 2014, A quasi-global precipitation time series for drought monitoring. USGS Data Series 832, 4 pp., https://doi.org/10.3133/DS832.

Gill, A. E., 1980: Some simple solutions for heat-induced tropical circulation. *Quart. J. Roy. Meteor. Soc.*, **106**, 447–462, https://doi.org/10.1002/qj.49710644905.

Hendon, H. H., D. W. Thompson, and M. C. Wheeler, 2007: Australian rainfall and surface temperature variations associated with the Southern Hemisphere annular mode. *J. Climate*, **20**, 2452–2467, https://doi.org/10.1175/JCLI4134.1.

Hidalgo, H. G., E. J. Alfaro, J. A. Amador, and A. Bastidas, 2019: Precursors of quasi-decadal dry-spells in the Central America dry corridor. *Climate Dyn.*, **53**, 1307–1322, https://doi.org/10.1007/s00382-019-04638-y.

Imbery, F., and Coauthors, 2020: Klimatologische Einordnung des Aprils 2020. DWD, 11 pp., www.dwd.de/DE/leistungen/besondereereignisse/temperatur/20200505_klimatologische_einordnung_april.pdf.

Jones, D. A., W. Wang, and R. Fawcett, 2009: High-quality spatial climate datasets for Australia. *Aust. Meteor. Oceanogr. J.*, **58**, 233–248, https://doi.org/10.22499/2.5804.003.

Jones, P. D., T. Jonsson, and D. Wheeler, 1997: Extension to the North Atlantic oscillation using early instrumental pressure observations from Gibraltar and south-west Iceland. *Int. J. Climatol.*, **17**, 1433–1450, https://doi.org/10.1002/(SICI)1097-0088(19971115)17:13<1433::AID-JOC203>3.0.CO;2-P.

Kobayashi, S., and Coauthors, 2015: The JRA-55 reanalysis: General specifications and basic characteristics. *J. Meteor. Soc. Japan*, **93**, 5–48, https://doi.org/10.2151/jmsj.2015-001.

Kothe, S., U. Pfeifroth, R. Cremer, J. Trentmann, and R. Hollmann, 2017: A satellite-based sunshine duration climate data record for Europe and Africa. *Remote Sens.*, **9**, 429, https://doi.org/10.3390/rs9050429.

Li, T., B. Wang, B. Wu, T. Zhou, C.-P. Chang, and R. Zhang, 2017: Theories on formation of an anomalous anticyclone in western North Pacific during El Niño: A review. *J. Meteor. Res.*, **31**, 987–1006, https://doi.org/10.1007/s13351-017-7147-6.

MAAP, 2019: MAAP#109: Fires and deforestation in the Brazilian Amazon. Monitoring of the Andean Amazon Project, https://maaproject.org/2019/fires-deforestation-brazil-2019/.

Magaña, V., J. A. Amador, and S. Medina, 1999: The midsummer drought over Mexico and Central America. *J. Climate*, **12**, 1577–1588, https://doi.org/10.1175/1520-0442(1999)012<1577:TMDOMA>2.0.CO;2.

Marshall, A. G., D. Hudson, M. C. Wheeler, O. Alves, H. H. Hendon, M. J. Pook, and J. S. Risbey, 2014: Intra-seasonal drivers of extreme heat over Australia in observations and POAMA-2. *Climate Dyn.*, **43**, 1915–1937, https://doi.org/10.1007/s00382-013-2016-1.

McArthur, A. G., 1967: Fire behaviour in eucalyptus forests. Leaflet 107, Department of National Development, Forest and Timber Bureau, Canberra, Australia, 35 pp.

Menne, M. J., C. N. Williams, B. E. Gleason, J. J. Rennie, and R. H. Lawrimore, 2018: The Global Historical Climatology Network monthly temperature dataset, version 4. *J. Climate*, **31**, 9835–9854, https://doi.org/10.1175/JCLI-D-18-0094.1.

Musgrave, K. D., C. A. Davis, and W. H. Schubert, 2008: Pinhole eyes in tropical cyclones. 28th Conf. on Hurricanes and Tropical Meteorology, Orlando, FL, Amer. Meteor. Soc., 17C.1, https://ams.confex.com/ams/28Hurricanes/webprogram/Paper138273.html.

NOAA, 2019: Tropical Storm Karen - 24–25 September 2019. NOAA/National Weather Service, www.weather.gov/sju/karen2019.

Pfeifroth, U., S. Kothe, J. Trentmann, R. Hollmann, P. Fuchs, J. W. Kaiser, and M. Werscheck, 2019: Surface radiation data set - Heliosat (SARAH) - edition 2.1. Satellite Application Facility on Climate Monitoring, accessed 14 February 2020, https://doi.org/10.5676/EUM_SAF_CM/SARAH/V002_01.

Rodríguez-Fonseca, B., and Coauthors, 2015: Variability and predictability of West African droughts: A review of the role of sea surface temperature anomalies. *J. Climate*, **28**, 4034–4060, https://doi.org/10.1175/JCLI-D-14-00130.1.

Rosa, E. B., L. P. Pezzi, M. F. L. de Quadro, and N. Brunsell, 2020: Automated detection algorithm for SACZ, oceanic SACZ, and their climatological features. *Front. Environ. Sci.*, **8**, 18, https://doi.org/10.3389/fenvs.2020.00018.

Saji, N. H., and T. Yamagata, 2003: Structure of SST and surface wind variability during Indian Ocean dipole mode events: COADS observations. *J. Climate*, **16**, 2735–2751, https://doi.org/10.1175/1520-0442(2003)016<2735:SOSASW>2.0.CO;2.

——, B. N. Goswami, P. N. Vinayachandran, and T. Yamagata, 1999: A dipole mode in the tropical Indian Ocean. *Nature*, **401**, 360–363, https://doi.org/10.1038/43854.

Schneider, U., A. Becker, P. Finger, A. Meyer-Christoffer, and M. Ziese, 2018: GPCC monitoring product: Near real-time monthly land-surface precipitation from rain-gauges based on SYNOP and CLIMAT data. DWD, accessed 4 March 2020, https://doi.org/10.5676/DWD_GPCC/MP_M_V6_100.

Smith, A. B., 2020: 2010-2019: A landmark decade of U.S. billion-dollar weather and climate disasters. Climate.gov, www.climate.gov/news-features/blogs/beyond-data/2010-2019-landmark-decade-us-billion-dollar-weather-and-climate.

Spence, J., M. A. Taylor, and A. A. Chen, 2004: The effect of concurrent sea surface temperature anomalies in the tropical Pacific and Atlantic on Caribbean rainfall. *Int. J. Climatol.*, **24**, 1531–1541, https://doi.org/10.1002/joc.1068.

Takaya, K., and H. Nakamura, 2001: A formulation of a phase-independent wave-activity flux for stationary and migratory quasi-geostrophic eddies on a zonally varying basic flow. *J. Atmos. Sci.*, **58**, 608–627, https://doi.org/10.1175/1520-0469(2001)058<0608:AFOAPI>2.0.CO;2.

Todey, D., D. Peck, D. Kluck, and C. Felkley, 2020: Agricultural impacts of the spring and summer extremes of 2019." 25th Conf. on Applied Climatology, Boston, MA, Amer. Meteor. Soc., 7.2, https://ams.confex.com/ams/2020Annual/webprogram/Paper371246.html.

Trewin, B., 2018: The Australian Climate Observations Reference Network – Surface Air Temperature (ACORN-SAT) version 2. Bureau Research Rep. 032, 57 pp., www.bom.gov.au/climate/change/acorn-sat/documents/BRR-032.pdf.

Uvo, C. B., 2003: Analysis and regionalization of Northern European winter precipitation based on its relationship with the North Atlantic Oscillation. *Int. J. Climatol.*, **23**, 1185–1194, https://doi.org/10.1002/joc.930.

van der Schrier, G., E. J. M. van den Besselaar, A. M. G. Klein Tank, and G. Verver, 2013: Monitoring European average temperature based on the E-OBS gridded data set. *J. Geophys. Res. Atmos.*, **118**, 5120–5135, https://doi.org/10.1002/JGRD.50444.

Vautard, R., and Coauthors, 2019: Human contribution to the record-breaking July 2019 heat wave in Western Europe. World Weather Attribution, www.worldweatherattribution.org/human-contribution-to-the-record-breaking-july-2019-heat-wave-in-western-europe/.

Vincent, L. A, D. Phillips, and R. Whitewood, 2015: Canada [in "State of the Climate in 2014"]. *Bull. Amer. Meteor. Soc.*, **96** (7), S169–S171.

Wild, M., 2016: Decadal changes in radiative fluxes at land and ocean surfaces and their relevance for global warming. *Wiley Interdiscip. Rev.: Climate Change*, **7**, 91–107, https://doi.org/10.1002/wcc.372.

Wilks, D., 2011: Statistical Methods in the Atmospheric Sciences. 3rd ed. International Geophysics Series, Vol. 100, Academic Press, 676 pp.

Wu, B., T. Zhou, and T. Li, 2017: Atmospheric dynamic and thermodynamic processes driving the western North Pacific anomalous anticyclone during El Niño. Part I: Maintenance mechanisms. *J. Climate*, **30**, 9621–9635, https://doi.org/10.1175/JCLI-D-16-0489.1.